NONEQUILIBRIUM EFFECTS IN SHOCK TUNNELS

Thesis submitted for the degree of

Doctor of Philosophy

by

Malcolm Kenneth McIntosh

Department of Physics
School of General Studies
Australian National University
Canberra A.C.T.

September, 1971

Title: Nonequilibrium Effects in Shock Tunnels

Candidate: Malcolm Kenneth McIntosh

Supervisors: R.J. Stalker B.Sc., M.Eng.Sc., Ph.D.
R.J. Sandeman B.Sc., M.Sc., Ph.D.

The contents of this thesis, except where indicated in the acknowledgements or by a reference, are entirely my own work.

M. K. McIntosh

(M.K. McIntosh)

TABLE OF CONTENTS

Tables

Figures

Nomenclature

B = magnetic field

c = specific heat

C = $\frac{\mu^* T}{\mu T^*}$

d = distance

E = electric field

F = force

h = enthalpy

j = current density

p = pressure

q = charge

u = velocity

V = voltage

R = Resistance

Re = Reynolds Number = $\frac{\rho u x}{\mu}$

X = mass fraction

x = distance

δ = order function or boundary layer thickness

γ = ratio of specific heats

ρ = density

θ = oblique shock angle to free stream

ϕ = wedge angle to free stream

μ = viscosity

$\bar{\chi}$ = shock wave - boundary layer interaction parameter

Subscripts

f = of formation

i = for the i^{th} species in a mixture

p = at constant pressure

v = at constant volume

s = stagnation conditions

1 = conditions before shock wave

2 = conditions after the shock wave

* = reference quantity

1. INTRODUCTION

Since World War II, the shock tunnel has been developed as a versatile and inexpensive means of investigating high speed gas flows. A very large part of the work in this field has been concerned with bodies moving in air and, specifically, with vehicles re-entering the Earth's atmosphere after flights in space. Figure 1 is a velocity-altitude chart showing a variety of direct-entry flight corridors. Almost all work has concentrated on the manned re-entry corridor at speeds below 8 km/sec. If the speed is given by $\sqrt{2 \times \text{stagnation enthalpy}}$, this corresponds to a stagnation enthalpy of 3.2×10^{11} erg/gm.

This value (3.2×10^{11} erg/gm) is, by a combination of technical and incentive limits, about the highest obtainable in conventionally driven shock tunnels. Figure 2 is a summary of current techniques for laboratory simulation of re-entry type flows. Techniques which give stagnation enthalpies in air in excess of 3.2×10^{11} erg/gm are the arc-heated driver, magnetohydrodynamic augmentation of the flow energy of a conventional shock tunnel and the free piston driver. The test gas produced by the first two of these techniques is often contaminated with metallic material through erosion of the energy-supplying electrodes, making it unsuitable for studies of flow in "atmospheric" gases. The free-piston driver, on which the work in this study is based, is a relatively new technique which has been developed to yield total test flow enthalpies as high as those encountered during entry to planetary atmospheres after deep space or inter-planetary voyages.

The unique ability of the free piston shock tunnel to produce clean test gas at very high enthalpy levels is particularly important in studies of entry to atmospheres consisting of gases other than air. Direct entry speeds on inter-planetary missions are high (see figure 1) because the vehicle must escape the Earth's gravitational field; the compositions of such atmospheres limit the usefulness of trials in air; and actual missions are sufficiently expensive that any theoretical or experimental simulation is of value. Hence, efforts were made in this study to include test gases of similar composition to the atmospheres of Mars and Venus, the Earth's closest neighbours.

Also included on figure 2 are performance levels used in a variety of individual experimental studies (the numbers correspond to references listed on the page following the figure). These are representative of an extensive literature survey and indicate that any work done with tunnel reservoir temperatures above 8000°K will be a useful addition to present knowledge.

The most interesting feature of very high speed re-entry type flows is that the kinetic energy of the gas molecules passing over the body is comparable to the formation energy of chemical bonds. Figure 3 shows the kinetic energy per molecule of ambient air as a function of the flight velocity. Also shown on the energy scale are reaction energies (not to be confused with reaction activation energy, the reaction energy is the net energy yield for the reaction) for a variety of reactions which occur in the "atmospheric" gases. (Note that reaction energies are additive, so that it takes 32.35 eV to form two O^+ ions from one O_2 molecule.) As the molecules have a Maxwell-Boltzman velocity distribution in most of the Earth's re-entry flight corridor, the energy of some molecules is much higher than the mean value shown in figure 3, so that some ionisation occurs below 8 km/sec flight velocity (as evidenced by the communications blackout during re-entry), but dissociation accounts for most of the internal energy increase in the gas as it is heated by the passage of the body. Above 8 km/sec, ionisation has a significant effect on the energy balance.

Although a reaction may be energetically feasible, the formation of products is a function of the frequency with which reactant particles collide and the probability of a collision yielding the reaction products. The former is a function of the number of particles and their velocity distribution and the latter is a function of the energy of the collision, which is also a function of the velocity distribution. The number of product particles depends upon the time the gas spends in the environment, which is a function of the gas velocity and the dimensions of the region.

From these considerations, it is apparent that, for laboratory simulation of the chemical changes which occur in re-entry flows, the free stream velocity and density of the gas, as well as the body size should be reproduced. The last of these is often impractical, but useful results may be obtained using smaller sized models.

Other flow properties such as Mach number and total pressure, which are important if the aerodynamic forces on the body are to be simulated, need not be reproduced if only the chemical properties are to be examined, provided that the Mach number is high enough for the flow to be considered hypersonic.

As described above, the free stream velocity is directly related to the stagnation enthalpy. The density is related less directly to the stagnation or nozzle reservoir pressure. The free piston shock tunnel, as shown in figure 2, has the capability of producing high values of both of these properties.

In a new facility, such as the free piston shock tunnel, it is essential to obtain a thorough understanding of the experimental performance and, if possible, to develop a theoretical model before simulation experiments are made on vehicle models.

Three types of calibration can be considered for a very high enthalpy shock tunnel: "wind tunnel", "shock tunnel" and "chemical". Wind tunnel calibrations are those conducted in continuous, "blow-down" or other facilities in which the reservoir properties may be regarded as steady or only slowly and predictably varying. They concentrate on flow in the nozzle and the determination of such properties as pitot pressure and heat transfer at many positions in the nozzle flow. Their aim is to determine the uniformity of the flow and the effects of the viscous boundary layer on the nozzle walls, as well as to find accurate, absolute values for the flow properties at the nozzle exit. Shock tunnel calibrations are made to assess the effects on flow at the nozzle exit of the large amplitude, short duration transients (shock waves), which generate high enthalpy gas in the nozzle reservoir. They require time-resolving measurements of, for example, the pressure and luminosity of the gas as it forms the nozzle reservoir and of wind tunnel type measurements in the nozzle flow. They have as their primary function the determination of a "useful" test time during which the flow is steady and the properties of the test flow are known. A high enthalpy shock tunnel has an added complication in that the test gas changes its nature and hence its wind- and shock-tunnel properties as a result of reactions among its chemical constituents. Such changes in the nature of the test gas should be accounted for in a chemical calibration as they play an important part in the simulation of re-entry model flows.

A number of wind- and shock-tunnel calibration measurements had been made on the Australian National University (A.N.U.) free piston shock tunnels prior to the commencement of this study. A review is given in chapter 3. The first aim of this study was to extend those calibrations and to chemically calibrate the tunnels. Many techniques commonly used to calibrate shock tunnels for aerodynamic studies give little or no information on the chemical properties of the test gas. Hence, the development of new techniques, the adaptation of old techniques to the high enthalpy environment, and the development of an adequate theoretical model were all required.

To assist in the calibrations and as a first step to the investigation of flows over models of re-entry vehicles, a number of simple model flows were examined. The combination of low free stream density and small model size was such that there were no observable effects of chemical reactions in the model flows and the test gas could be considered, for practical purposes, as a perfect gas. The nozzle reservoir properties shown in figure 2 indicate that the free piston shock tunnels are the most likely to produce model flows with chemical nonequilibrium. Tunnels with lower enthalpy levels than the free piston machines have been used to investigate vibrational relaxation over models, but the author has seen no reference to a hypersonic tunnel capable of producing chemically reacting model flows.

Early in 1970 a new, large, free piston shock tunnel known as T.3 became operative at the A.N.U. Calibrating experiments and calculations indicated that model flows with chemical nonequilibrium could be effectively studied in this tunnel. The results of a preliminary study of chemical nonequilibrium in very high enthalpy model flows form the final chapter of this thesis and they are believed to be the first of their kind.

/6

2. THEORETICAL MODELS

2.1 Chemical Properties of Gases

As indicated in chapter 1, investigations of high enthalpy gas flows should consider the effects of chemical reactions within the flowing test gas. These are expected to occur as the gas is heated by the rapid conversion of large quantities of kinetic energy to thermal energy during compression, for example, on a body nose. The reverse process occurs during expansion, for example, in a body wake.

For the conditions experienced in the flight corridors of figure 1, and unless extremes of density are encountered, a gas may be considered as a mixture of reacting chemical species, each of which behaves as a perfect gas (refs. 18,44). A description of the chemical properties of a gas requires the specification of two sets of properties: namely, of the equilibrium thermodynamic properties of each of the constituent chemical species and of the kinetics of the reactions among the species.

2.1.1 Thermodynamic Properties

The thermodynamic properties of chemical species are determined experimentally from spectroscopic observations of the characteristic frequencies of electromagnetic radiation emitted and/or absorbed by particles (atoms or molecules) of the species. From the observed frequencies, the energy level structure of the particle can be deduced (refs. 1,2). Two sets of tables of energy levels were used in this study (refs. 2,3) and they were found to be adequate for the species and conditions encountered in the free piston shock tunnels.

The energy level structure of a particle can be used to calculate its thermodynamic properties in several ways: (i) Simple models of the behaviour of the particle such as the "rigid rotator" and the "harmonic oscillator" use the energy levels directly (refs. 4,5,52). They are limited in accuracy by the number of energy levels included in each calculation (the time taken for a calculation is proportional to the number of energy levels considered) more often than by inadequacies of the models. Since the number of energy levels required for an accurate numerical description increases with increasing temperature, such models are usually used at low temperatures only (below 5000°K in this work). (ii) A quantum mechanical description of the particle can be obtained by using the energy level structure and a suitable electronic potential energy function with the Schrödinger Wave Equation (ref. 4), but the time taken for such calculations prevents their use in calculations of complex gas flows. (iii) The energy levels can be used to determine the equilibrium partitioning of energy within the particle, which is described mathematically by "partition functions" (refs. 5,18). This method is also too involved to be included in complex gas flow calculations. However, it can be used to give thermodynamic properties with high accuracy and several sets of tabulated properties so derived were used in this study (refs. 6 to 10). Economic use of the tabulated data required that they first be fitted with polynomial functions of temperature; then each subsequent calculation of thermodynamic properties required only the evaluation of the polynomials. Two polynomial forms are in common use; one evolved at the Cornell Aeronautical Laboratories (refs. 44,54) and the other recommended by JANAF (ref. 9). Both give errors of approximately 5%.

During the course of this study, energy level data and polynomial coefficients from "least squares" fits to tabulated data were collected for 26 species: CO_2, N_2, O_2, CO, NO, CN, C, O, N, A, He, N_2^+, O_2^+, CO^+, NO^+, C^+, N^+, A^+, He^+, C^{++}, O^{++}, N^{++}, A^{++}, He^{++}, e^-, C_2.

Thermodynamic properties for each of the above species were determined using methods (i) and (iii) described above, and using tabulated thermodynamic data from at least two sources. Agreement between results using the different methods and data sources was within 5% over the temperature ranges specified by the data sources.

To check the accuracy of the above specifications of thermodynamic properties of species further, gross equilibrium thermodynamic properties (enthalpy, entropy and density as functions of temperature and pressure) were calculated for a number of common gases and gas mixtures. Comparison with published tables (refs. 11 to 16) gave agreement within 5%.

2.1.2 Reaction Kinetics

At the high temperatures used in this study, reactions among the chemical species formed in a gas are commonly investigaged by monitoring the appearance or disappearance of species following a rapid "switching" of the gas from an initial non-reacting state to a reacting state (refs. 17,110). Switching may be achieved by a shock wave (ref. 21) or a flash of electromagnetic radiation (flash-photolysis) (ref. 19). A less transient situation is possible in a flow-discharge system (ref. 20). A high-to-low temperature "switch" may be obtained by a sudden expansion of the gas. Optical and mass spectrometers are the most commonly used monitoring systems.

In heated air below 8000°K, the dominant reactions are (ref. 23 to 27,52):

(1) $N_2 + M \rightleftharpoons 2N + M$

(2) $O_2 + M \rightleftharpoons 2O + M$

(3) $NO + M \rightleftharpoons N + O + M$ where M = a third body

(4) $N_2 + O \rightleftharpoons NO + N$

(5) $O_2 + N \rightleftharpoons NO + O$

(6) $N_2 + O_2 \rightleftharpoons 2NO$

(7) $N + O \rightleftharpoons NO^+ + e^-$

Above 8000°K, ions such as N_2^+, O_2^+, N^+ and O^+ appear in significant quantities and their formation reactions

e.g. $N + M \rightleftharpoons N^+ + e^- + M$

and ion exchange reactions

e.g. $N^+ + O \rightleftharpoons N + O^+$

become significant. At still higher temperatures of approximately

15000°K, and for the densities typical of this study, doubly charged species, N^{++} and O^{++}, are formed and the small quantity of argon in the air becomes partially ionised.

Rate constants for these reactions have been determined by many workers and the work has been reviewed on many occasions. Several review papers were used in this study (refs. 23 to 30). It was noted that almost all work has been done at temperatures below 6000°K and extrapolation to 15000°K was used for this study. For each reaction, the results in the review papers were compared to ensure the best possible accuracy.

For reactions (1) to (7) above, the rate constants were found to have an accuracy of ± 10%. For some of the ion exchange reactions, errors in the rate constants of 2 orders of magnitude were probable. However, the effects of such errors in the ionization reaction rates on the flow properties were small because the species involved only appeared in appreciable concentrations in the hot, high density nozzle reservoir and at the very beginning of the nozzle expansion, where they were very close to equilibrium. Before conditions in the nozzle expansion became favourable for nonequilibrium, their numbers had become negligible.

Recombination reactions are more complicated than dissociation and ionization reactions because the species need not recombine to form molecules or atoms in the ground state, but may form species in excited states. This is most important where the excited level is metastable and decay to the ground state is very slow (LASER action has been achieved in carbon dioxide in a shock tunnel by this process), or for vibrational levels in diatomic and triatomic molecules where the relaxation time is comparable to the characteristic flow time (e.g., the time for the gas to flow over a body or through a shock heated slug of gas). In most applications, recombination to states other than the ground state is ignored and the recombination rate is taken to be an average value computed through the forward rate and the equilibrium constant (which includes contributions from vibrational and other levels because it is calculated from the equilibrium thermodynamic properties of the species involved in the reaction).

The reaction system for air described above (no excited states are considered in the reaction rates) has given good agreement with experiments here (described in subsequent chapters) and elsewhere. This may be due to the rates being determined from experiments similar to those used to verify them, rather than to the insignificance of recombination to excited states.

Some workers have included excited states in their calculations. For example, reference 25 lists reactions involving a single vibrational level each for N_2 and NO and reference 52 includes a crude model for coupling the dissociation rate of diatomic molecules to the calculated state of vibrational excitation. Consideration of excited states is common in chemical shock tube studies such as those reviewed in references 20, 21 and 110. Generally these were made at very much lower temperatures than were achieved in the free piston shock tunnels, and used gases other than the "atmospheric" constituents considered here. The techniques were used in the determination of the carbon dioxide reaction system described later in this section.

Reference 139 gives an experimentally determined reaction rate for the "dissociative-recombination" reaction:

$$NO^+ + e^- \rightleftharpoons N + O$$

As can be seen from figure 2 (where *9 corresponds to reference 139), the nozzle reservoir conditions used in this determination are different from the conditions in the free piston shock tunnels. They are, however, the closest used in a recombination rate determination and indicate the extrapolation required in this study for all reaction rate data.

The reaction rate constants for air, determined from the review papers above, were also used for the kinetics of the pure gases, oxygen and nitrogen, where applicable. The dominant ionization reactions occurring in oxygen and nitrogen were found to be:

$$O + M \rightleftharpoons O^+ + e^- + M$$

$$N + M \rightleftharpoons N^+ + e^- + M$$

respectively. The estimated error in the rate constants for these reactions is ± 20%.

Reactions in all "air-type" gases (nitrogen and oxygen mixtures with an inert diluent) can be described using the reaction rates for air above, but reactions in the other major component of "atmospheric" gases, carbon dioxide, are not well understood at present. A number of workers have measured dissociation rates of CO_2 (refs. 29,30,33,34,35) but the estimated errors are large (typically 2 orders of magnitude). Estimates of reaction rates for the dissociation of CO_2 to C and O via CO also have been made from collision theory (refs. 31,32) and found to lie within the limits determined experimentally.

A reasonable system for carbon dioxide dissociation includes:

$$CO_2 + M \rightleftharpoons CO + O + M$$

$$CO + M \rightleftharpoons C + O + M$$

$$CO_2 + O \rightleftharpoons CO + O_2$$

$$CO_2 + C \rightleftharpoons 2CO$$

$$CO + O \rightleftharpoons O_2 + C$$

Of these, reaction (a) is the fastest by up to a factor of 100.

In a recent paper (ref. 35), the presence of the Swann bands of the diatomic carbon molecule, C_2, during CO dissociation gave rise to a suggested reaction system involving C_2 reactions, which behaved in a similar fashion to the NO "shuffle" reactions in air (reactions 4 and 5 above) in that the intermediate product (C_2 in carbon monoxide, NO in air) concentration was low, but its reactions were rapid producers of other species. The proposed system was:

$$CO + M \rightleftharpoons C + O + M$$

$$C + CO \rightleftharpoons C_2 + O$$

$$O + CO \rightleftharpoons O_2 + C$$

$$C_2 + M \rightleftharpoons 2C + M$$

$$O_2 + M \rightleftharpoons 2O + M$$

If correct, this mechanism would be included implicitly in the earlier rate determinations. It should be noted that C_2 is a very strong radiator so that it could be observed, but be in too small a concentration to affect the kinetics of the gas.

Because of the complexities of the reaction kinetics in a real gas, the "Freeman" ideal dissociating gas (ref. 38) is often used to obtain an insight into the influence of a reaction on a flow system. It uses a single idealised reaction and an idealised specification of the thermodynamic properties of species (ref. 37). Its main advantage is that solutions to flow problems are often obtainable in an analytical or semi-analytical (requiring very little numerical computation) form. It is mentioned here because it was used as a first approximation in the initial stages of this study.

2.2 Flow Calculations

Figure 4 is a time-distance diagram showing the waves used to generate the nozzle reservoir in a free piston shock tunnel (note the discontinuity in the distance scale). For the purposes of this study, the free piston driver technique was regarded as merely a means of producing hot, high pressure helium to drive an otherwise conventional reflected shock tunnel. (The free piston technique is an adaptation of the gun tunnel (ref. 119) and the motions of the piston and driver gas are sufficiently complicated to require study in their own right. For the purposes of this study, the piston compression ratio was kept low and the piston velocity subsonic to avoid most such complications.) Then the flow was divided into three distinct regions for the purposes of numerical calculations: the processes forming the nozzle reservoir, the nozzle exapnsion and the flow over models. In all three regions the effects of chemical nonequilibrium upon the gas were considered.

The nozzle reservoir was formed by reflection from the end wall of the shock tube of the normal, incident shock wave generated in the shock tube by the rupture of the diaphragm by high pressure driver gas (refs. 110,114). Gas processed by the incident and reflected shock waves had high values of temperature and pressure and was stationary in the laboratory frame of reference.

As the incident shock wave propagated into the undisturbed gas in the shock tube, the interface between the test gas and the driver gas (called the contact surface) followed it. When the shock wave was reflected, it moved into the gas processed by the incident shock wave and eventually met the contact surface. Depending on the impedance mis-match at the interface, either a shock wave or a rarefaction wave was reflected from the interface into the test gas, and a shock wave was transmitted into the driver gas (100,113,116,117). When the reflected wave from the contact surface reached the end wall, the steady nozzle reservoir conditions were disrupted and the useful "reflected shock" test time ended.

At one (sometimes no) set of initial shock tube conditions for a given set of driver conditions, the driver and test gases were matched across the interface and no wave was reflected from the interaction of the reflected shock wave with the contact surface. This is referred to as "tailored interface" operation (refs. 113,115,118) and it increased the useful test time until a decay in the driver gas pressure reached the shock tube end wall. The decay originated from the propagation of an expansion wave into the driver gas when the diaphragm ruptured.

It has been found elsewhere that, although the wave reflected from the contact surface upset the flow, its influence, and that of the subsequent diminishing reflections from the end wall and the interface, died out, and that the resulting steady reservoir could be used until the influences of driver pressure decay were felt (refs. 44,115). This is called "equilibrium interface" operation. It was shown that the processes after the initial shock reflection were weak, especially if a rarefaction wave was reflected from the interface. If chemical nonequilibrium was negligible and the gas could be considered either as non-reacting or in chemical equilibrium, (at the high nozzle reservoir temperatures and pressures found in most shock tunnels and, as will be shown later, at the conditions in this study, the gas was very close to equilibrium) the weakness of the interactions allowed them to be approximated by an isentropic expansion or compression. This approximation required that one of the steady state reservoir properties (after the effects of the contact surface interactions died out and before the driver decay influences were felt) be known experimentally to set a final state for the expansion or compression. Usually the pressure is measured.

Hence, to calculate properties in the nozzle reservoir, two shock compressions and an isentropic expansion or compression of the test gas were calculated.

To make estimates and to set upper and lower limits, a computer program was written to make the nozzle reservoir calculations assuming either a non-reacting (perfect) gas or a gas in chemical equilibrium (ref. 39). Programs performing a similar range of calculations were available (refs. 40,41) but they use methods of specifying the chemical properties of the gas which are not as readily adapted to unusual gas mixtures (particularly those proposed as planetary atmospheres).

Historically, calculation of flow across a normal shock wave with chemical nonequilibrium was one of the first problems considered in the field of reacting gas flows. A number of references survey the techniques and their results (e.g., refs. 43,52). The method used in this study (refs. 52,53) was selected because it gave a wide choice in the specification of the thermodynamic and kinetic models used to describe the test gas. It used a modified fourth order Runge-Kutta integration scheme (ref. 45), which ~~the~~ its author claimed would give convergence and a numerical solution in a relatively small number of steps (see section 3.4.5 for comments on this aspect of the program). Calculations were made of the effects of chemical nonequilibrium behind the incident shock wave. The program was modified to make similar calculations for the reflected shock wave. A commonly used alternative to calculating chemical nonequilibrium effects across both shock waves is to assume that the gas is non-reactive across the initial shock wave and that it reacts in the nozzle reservoir region after the passage of the reflected shock wave (refs. 42,43). As is shown in section 3.3.3, the assumption of a non-reacting gas behind the incident shock wave is invalid at the conditions of this study.

Flow in a hypersonic nozzle is also a well studied problem (e.g. refs. 44,46 to 50). The computer program (ref. 44) used in this study was chosen because of the flexibility in its specifications of nozzle shape and test gas properties (once again with the aim of using gas mixtures similar to planetary atmospheres). It calculated a quasi-one-dimensional expansion of a reacting gas through an area distribution. The area distribution could be specified by up to seven polynomials. For simple conical nozzles exhausting at medium Reynolds numbers into an evacuated dump tank, as in this study, the one-dimensional assumption is a reasonable approximation. To by-pass the saddle point singularity about the nozzle throat, the program assumed chemical equilibrium at the throat and began the nonequilibrium solution as a linear perturbation. The nonequilibrium solution could be started upstream or downstream of the nozzle throat by this method. The numerical integration was performed by a modified Runge-Kutta technique (ref. 45).

Calculations of flow over bodies moving at supersonic speeds are basic to hypersonics and a wide range of techniques have been developed for a variety of shapes. Because a great deal of information on the chemistry and physics of hypersonic flow can be derived by testing simple models such as wedges, cones and hemispheres (see chapter 4), only techniques for calculating such flows are discussed here.

As first approximations and to give limiting conditions, non-reacting (perfect gas) and equilibrium conditions were assumed. For flow over a wedge under either of these conditions, the shock wave is straight, providing that the angle it presents to the flow is less than the detachment angle (as the angle of a wedge increases, it appears to the flow to be more like a blunt body, until, at the detachment angle, the shock wave separates from the body nose). Properties of wedge flows were calculated by modifying the normal shock wave equations in the computer program of ref. 39 to include momentum conservation normal and transverse to the shock. This provided an extra equation to accommodate the extra variable of shock angle.

Flow over a cone also gives a straight shock wave and permits of readily determined flow field properties (refs. 62,63). A computer program (ref. 62) was used to calculate directional derivatives to give a first approximation to a cone at a small angle of attack, as well as axisymmetric flow properties. Also, it could be used in combination with a method of characteristics program (ref. 54).

The cone flow program was one of three programs (cone, blunt body and method of characteristics) developed at the NASA Ames Laboratories for non-reacting (perfect gas) and chemical equilibrium calculations of flow

/17

over vehicles with complex after-bodies. Flow near the body nose could be calculated using the blunt body or cone program, depending whether the nose was blunt or sharp, and continued downstream using the method of characteristics program. Equilibrium thermodynamic properties of 13 gas mixtures for use with these programs were stored as tables of spline-fitted polynomials, which were derived originally using the method of reference 52. Modifications to allow more general specifications could be made simply, but were unnecessary for this study as properties of all of the mixtures used were included in the tables.

The Ames blunt body program (refs. 54,55) used the inverse method to solve for the body shape, given the shock shape. It allowed specification of the shock and body shapes by polynomials and had an iterative scheme which modified the shock shape coefficients until the calculated body shape accurately matched the specified shape.

The method of characteristics program allowed calculation of embedded shock waves (compression corner or flare), expansion waves and coalesced shock waves. It was found to be inaccurate when flare and bow shock waves intersected but otherwise adequate for all the shapes used in this study.

Model flows with chemical nonequilibrium have been studied by many workers, but, because of the difficulties of coupling a multi-component, multi-reaction chemical system to an already complicated set of flow equations, and the very long times required on a high speed computer to solve the equations, few calculations have been made. It is under these conditions that the "Freeman" gas mentioned in section 2.1.2 becomes such a valuable method of approximation.

Nonequilibrium blunt body calculations have been made by a number of methods (refs. 52,56 to 59). The main method used in this study (ref. 52) is an inverse one with the "Cornell" method of specifying the chemical properties of the gas (see section 2.1.1).

Such flow fields have been carefully studied and several approximate "scaling" techniques have evolved (refs. 60,61,77,79). One of these was incorporated into a computer program (ref. 60) and was available for use in this study. It relied on a property common to the relaxation zones along a streamline and behind a normal shock: the enthalpy remains nearly constant. An analogy was established by transforming and mapping the normal shock solution onto the blunt body streamlines. An accuracy of 2% in the shock stand-off distance compared with a full nonequilibrium calculation is claimed by its authors.

Nonequilibrium relaxation along a stream tube could be calculated from specifications of the conditions at a point in the flow and the area or pressure distribution along the stream tube using a version of the nozzle flow computer program (ref. 44). The area or pressure distribution could be obtained experimentally, or from equilibrium or perfect gas calculations using the methods described above.

Nonequilibrium flow over cones, wedges, and other sharp-nosed bodies have also been studied extensively (refs. 64 to 69). The difficulties in programming any of these techniques prevented their inclusion in this work and the method of stream line relaxation was used.

The computer programs listed above are described in detail (techniques, input and output formats and sample input decks and output listings) in reference 72. Detailed results from the programs for the shock tunnels T.1 and T.2 are presented in graphical form in references 84 and 83, respectively.

3. SHOCK TUNNEL CALIBRATIONS

As described in chapter 1, calibration of the free piston shock tunnels is an essential preliminary to testing vehicle models. A summary of the shock tunnels and a review of previous work precedes descriptions of the calibrations conducted in this study. A description of the experimental techniques is given in appendix B.

3.1 The A.N.U. Free Piston Shock Tunnels

Three free piston shock tunnels were used in this study. Their physical dimensions and typical operating conditions are given in tables 1 and 2. The tunnels T.1 and T.2 were operable before this study commenced, but T.3 was first available for use early in 1970.

The distinguishing feature of the free piston shock tunnel is that it uses the momentum of an unconstrained piston to generate high temperature, high pressure driver gas (refs. 119, 120), rather than the more direct and conventional methods of electrical or chemical heating (ref. 114). Briefly, it achieves this as follows. The driver end of the tunnel (upstream of the high pressure diaphragm) consists of a reservoir and a compression tube separated by a free-sliding piston, which is initially held on a launcher at the upstream end of the compression tube. The compression tube is evacuated and then filled with helium driver gas (pressure = 16 psia, typically). The reservoir is filled with high pressure air (700 psi, typically). The piston is then released and it is accelerated down the compression tube by the difference in the pressures on its two exposed faces. At the point where the pressures on both sides of the piston are the same, the piston has quite a high velocity (300 ft/sec, typically) and it continues down the compression tube until its momentum has been lost in further compression of the helium. The pressure at this stage (7000 psi, typically) is just sufficient to burst the diaphragm and cushion the piston to a gentle halt at the end of the compression tube, while the compression-heated helium acts as driver gas for the shock tube.

Each tunnel was equipped with pressure gauges attached to the reservoir and the compression tubes, which were used to set the firing conditions for a given diaphragm material and thickness. Pressures could be set with an accuracy of 1%. This was for shot-to-shot reproducibility, the value of the aboslute pressure being unimportant once correct firing conditions had been established. Static bursting pressures were tested with an hydraulic pump for a random sample of diaphragms. They were reproducible within 5% when different batches of material were involved and 1% for material from the same batch.

The shock tube was evacuated using a rotary pump to less than 0.05 torr and then filled with test gas using a mercury column as a pressure gauge. Accuracy was typically 0.02 in Hg in 1 to 10 in Hg, or better than 2%. The leak rate was such that no observable change in pressure occurred in 15 minutes, (the longest checked in this study), which compared favourably with the 3 minutes or thereabouts required to fire the tube after isolating the shock tube.

The initial shock speed was measured by recording the time, or times, between the arrival of the shock wave pressure rise at two or more piezoelectric pressure transducers separated by known distances. The transducers were made from 0.125 in diameter, PZT-5A ceramic cylinders and were mounted flush with the shock tube side wall. Each tube had at least three positions at which the transducers could be mounted. The time was recorded directly on an oscilloscope (calibrated with a Tektronix Type 181 Time-Mark Generator), on a Marconi Counter/Frequency Meter Type TF1417A, or after pulse shaping, on a Racal Microsecond Chronometer Type 5A45.

Experiments showed that the shot-to-shot reproducibility of the initial shock speed was better than 2%.

Pressure behind the reflected shock wave was measured with a SLM Type HPZ-14 transducer on T.1 and T.2 and a Kistler Type 6201 transducer on T.3. The device was mounted flush with the side wall of the shock tube, approximately 0.75 in from the nozzle throat in T.1 and T.2 and 1.5 in from the throat in T.3. For accurate and absolute measurements of the pressure in this region, the transducer was connected to a SLM PV 16 No. 16050 electrometer and the result recorded on an oscilloscope. Accuracy in determining a value from the oscilloscope traces was about 5%. For monitoring purposes only, the transducer was shunted by a condenser (0.1 μF).

The nozzles listed in table 1 had conical profiles and, with the exception of the nozzle used on T.1, used throat inserts constructed from commercially available, tungsten-carbide wire dies. The nozzle throat insert on T.1 was made of stainless steel. A nozzle with a parabolic profile was also available for use on T.1. The nozzle exit-to-throat area ratios used in this study were 560 on T.1; 155 or 560 or 1300 or 5000 on T.2; and 720 on T.3.

The test sections of the tunnels T.1 and T.2 were equipped with high quality Schlieren windows and vacuum-tight electrical connections and could be used with either the shock tube or with one of the nozzles.

The test section and dump tank of each tube (for shock tunnel work this region extended to the nozzle throat where a thin "Mylar" diaphragm separated it from the shock tube) were evacuated with a rotary type pump to a pressure of the order of 0.1 torr. In addition, T.2 and T.3 had oil diffusion pumps installed, which evacuated the test sections to a pressure of approximately 0.001 torr.

The test gases, with the exception of air, which was obtained direct from the Canberra atmosphere, were supplied by Commonwealth Industrial Gases Ltd., who specified 99.99% purity for helium and argon, 99.995% for nitrogen, 99.5% for oxygen and "better than 99.0%" for carbon dioxide.

No special care beyond an occasional washing out with hexane was taken to keep the tunnels clean.

3.2 Previous Work on the A.N.U. Shock Tunnels

When this study commenced, the following tests had been carried out in the shock tunnels T.1 and T.2.

The free piston driver technique had been carefully examined. Measured shock speeds were compared with results from an approximate theory with good agreement (refs. 119, 120), the effects of the driver compression ratio on the nozzle reservoir pressure were evaluated (ref. 120) and performance levels with and without an area change at the diaphragm position were plotted (refs. 120, 130). These measurements were repeated for T.3 as soon as that tube was commissioned (ref. 147).

In the free stream of the tunnels, a variety of properties had been evaluated. The pitot pressure was measured on the nozzle axis (refs. 120, 135, 136) and axial and radial surveys of the pitot pressure were made. Stagnation point heat transfer rates were measured with a platinum calorimeter heat transfer gauge on a model with a hemispherical nose, and reasonable agreement was obtained with theory (refs. 120, 136). These results, while being of limited accuracy and too slow to show many of the transient features of the flow, do indicate that the stagnation enthalpies calculated from shock tube measurements are realised in the test section and that the flow is aerodynamically useful.

In T.1, some measurements had been made of the free stream velocity using a spark tracer technique (ref. 136) (See Appendix B). These results were confined to a narrow period of time, just after the completion of the nozzle starting processes (see section 3.4.3), and gave no information on the effects of contamination of the flow by helium driver gas.

Measurements had been made in T.2 of the effect of the initial pressure in the dump tank, test section and nozzle on the nozzle starting processes (ref. 134). A slit was set up parallel to the nozzle axis and the luminosity of the flow emerging from the nozzle was recorded on an image converter camera operated in the streak mode. A starting shock wave and other phenomena observed in conventional tunnels (refs. 102, 103) were observed and their behaviour with variations of the initial pressure correlated with theory with reasonable agreement. Under normal operating conditions, such processes were observed to be of approximately 30 microsec duration.

The level of contamination of the test flow by helium driver gas had been monitored in T.2 using an ingenious but fairly insensitive technique with a relatively long response time (ref. 120).

Considerable work had been done on optical spectra (in the range 2000 to 10000 Angstroms) of gas emerging from the nozzle exit in T.2 (ref. 137). Time resolution was achieved using a rotating slit device or an image converter camera. The main result from these experiments was that the spectrum of the flow was dominated by radiation from iron atoms. This was a result of the high radiant efficiency of iron, and did not imply high iron concentrations. Estimates gave iron concentrations of less than 0.01%.

The possible effects of iron contamination on flow properties at the nozzle exit were extremely difficult to estimate. Thermodynamic properties of iron and of oxides of iron are given in reference 9, but no information could be found by the author on possible reactions between such species, particularly at the very high temperatures used in this study. The very low concentrations and medium formation enthalpies (99 kcal/mole for Fe gas and 60 kcal/mole for FeO gas) indicated that the iron species would follow the temperature and density changes of the test gas and would have only a very small effect on the enthalpy and velocity of the gas at the nozzle exit. Confirmation that the iron had a negligible effect on the aerodynamic properties of the flow was obtained from the agreement between experimental values and values calculated assuming that iron was absent described in the subsequent chapters of this thesis.

During the early stages of this study, a parallel project was proceeding to develop a Quadrupole Mass Spectrometer with a sufficiently short response time for measurement of species concentrations at the nozzle exit (ref. 138). It was used mainly to detect the level of contamination by helium driver gas, but some measurements were made of the concentrations of other species. The results are compared with results from this study in section 4.2.

Also, two parallel studies were in progress to determine radiation and ionisation properties of argon in T.2. In one a time-resolved channelled-spectrum technique was used to determine species concentrations behind the incident shock wave (ref. 131). Incident shock Mach numbers up to 25 in 10 torr initial shock tube pressure were used. In the other a Mach Zehnder interferometer and thin film resistance heat transfer gauges on a flat plate were used in an attempt to determine properties at the nozzle exit (ref. 142). The results of this study indicate that the contact surface is unstable when argon is used in the free piston shock tunnels (see section 3.4.6). It is possible that the studies mentioned above will provide additional evidence of the mechanism involved.

3.3 Formation of the Nozzle Reservoir

The processes forming the nozzle reservoir in a free piston shock tunnel are outlined in section 2.2 and illustrated in the wave diagram in figure 4, which is to scale. The purpose of this section is to compare the experimental values of gas properties in the reservoir with results calculated using the computer programs and gas properties described in chapter 2.

Incident shock wave velocities were determined in the three shock tunnels for a wide range of conditions. Figures 5, 6 and 7 summarise the results for T.1, T.2 and T.3 respectively.

Three processes may complicate the linear one-dimensional equations used to calculate properties behind the shock waves. These are (ref. 110): radiative energy transfer out of the shock heated gas, the formation of viscous boundary layers on the tube walls, and chemical nonequilibrium. The influence of each of these phenomena is described separately in the following sections.

3.3.1 Radiative Energy Dissipation

The problem of determining the radiation from a reacting mixture of molecules, atoms, ions and electrons is beyond the scope of this study and has yet to be solved fully (refs. 85 to 92 consitute a useful summary). As a first step towards more complicated systems, numerous investigations have been made of radiation from shock-heated samples of the noble gases, with particular emphasis on argon. A computer program (ref. 87) for calculating properties behind a normal shock wave in argon was available for use in this study. It was used to set limits on the radiative losses from the complicated air and carbon dioxide - nitrogen systems.

This computer program allowed for the effects of ionisation and three-body recombination, collisional excitation and de-excitation, photo-ionisation and radiative recombination, spontaneous emission and stimulated emission and absorption. The plasma was considered optically thin to continuum radiation, but could be optically thick to radiation from some energy level transitions.

Results from two calculations of flow of argon through a normal shock wave at conditions typical of T.2 are given in figure 8. These show that chemical equilibrium is reached rapidly behind the shock front, but that radiation causes a serious decrease in the ionisation and temperature and an increase in the density. The small increases in temperature, density and ionisation ahead of the shock front which can be seen in figure 8 are caused by radiation from the shock heated gas heating the undisturbed gas (particularly exciting electrons) ahead of the shock wave. This phenomenon has been observed experimentally in luminosity photographs such as those in figure 56. Preliminary results from experiments at these conditions by others (ref. 131) give electron concentrations less than those of figure 8. They indicate some neglected phenomena and perhaps even greater energy losses.

The losses are expected to be more important in the hotter (although more optically dense) gas behind the reflected shock and to seriously affect the stagnation enthalpy.

/26

To set upper limits for the radiation losses from other than argon gases, the initial shock tube pressure and initial shock wave Mach number inputs to the program were varied until the equilibrium density and temperature behind the argon shock wave agreed with the equilibrium conditions in the other gas, which were calculated as described in chapter 2. For any gas in thermodynamic equilibrium, the radiation losses depend on the radiation constants (energy level structure, Einstein coefficients, etc. (see refs. 1, 2 and 4)) of the gas and the density and temperature only. Hence, the comparison above could be applied to conditions behind the reflected shock wave and elsewhere.

Figure 9 shows results from two calculations which give conditions similar to those behind reflected shock waves in T.2. The region ahead of the shock wave is, of course, irrelevant in this application. Up to 10 cm behind the shock front, the temperature loss can be seen to be less than 0.5%. As air radiates less than argon at the same temperature and density, this may be taken as evidence that radiation losses from air may be neglected in the shock tunnels. As stagnation temperatures in gas mixtures of carbon dioxide and nitrogen are less than in air at the same initial shock tube pressure, such mixtures may also be assumed to have negligible radiation losses.

3.3.2 Viscous Effects

The effects of viscosity on the formation of the nozzle reservoir may be considered in two parts: the formation of a boundary layer behind the incident shock wave and the subsequent interaction of the boundary layer with the reflected shock wave. Both problems have been studied by many workers because of their fundamental interest and their importance in limiting the duration of useful test flow. Figure 10 shows the effects in T.2 (the diagram is approximately to scale). References 93 to 100 constitute a useful summary of work in this field.

The formation of a boundary layer behind the incident shock wave is a fundamental aspect of any shock tube or tunnel. Its effects are removal of gas and kinetic energy from the slug of shock-heated gas (ref. 110).

The quantity of gas lost from the slug of test gas behind the incident shock wave was estimated by photographing the luminosity of the gas behind the shock wave (see appendix B.). At a typical condition in T.2, the shock heated slug length was 10 cm at the end of the shock tube. One-dimensional mass conservation calculations showed that, if no gas was lost to the boundary layer, the length would have been 30 cm. This loss would have the effect of decreasing the useful test time by 66% if all other effects (such as reflected shock-boundary layer interaction, contact surface instability and driver pressure decay) were negligible.

To estimate the kinetic energy lost from the gas, the attenuation of the velocity of the incident shock wave as it moved along the shock tube was measured. At typical conditions, the incident shock velocity decreased by approximately 7% over 3 ft in T.1, 5% over 4 ft in T.2 and 17% over 12 ft in T.3. As the energy in the system is proportional to the square of the incident shock wave velocity, these were equivalent to energy losses of 5, 2.5 and 2.7% per foot, respectively. This effect was incorporated into the calculations only by extrapolating to obtain the incident shock wave velocity at the end of the shock tube.

Calculations using the method of reference 95 with Sutherland's law for the viscosity of the gas gave a boundary layer thickness of approximately 0.03 cm at a distance of 10 cm behind the shock front, at typical conditions. It was impossible to check such a small thickness experimentally.

When the incident shock wave reflects from the end wall of a shock tube, the reflected wave presents an increase in pressure to the boundary layer formed behind the incident shock wave. This causes the boundary layer to separate from the shock tube wall and a bifurcated foot to form at the extremities of the reflected shock wave (see figure 10).

/28

References 97 and 99 consider the reflected shock-boundary layer interaction in low enthalpy shock tubes. Using their results, a height of approximately 1 cm was estimated for the bifurcated foot when the reflected shock wave was 1 cm from the shock tube end wall, at typical conditions in the free piston shock tunnels. This was expected to have a significant effect on the flow duration in T.1 and T.2, where the shock tube diameters are small, but negligible effect in T.3. Results discussed in section 3.4.6 indicate the existence of large scale turbulence and driver-test gas mixing at the contact surface, which could be due, in part, to this phenomenon.

3.3.3 Chemical Nonequilibrium

Reaction profiles behind the incident shock waves were calculated for air and nitrogen as described in section 2.2. Figure 11 shows a typical result for air.

From the results in figure 11, it can be seen that air was very close to equilibrium at distances greater than 0.01 cm behind the shock front. This distance was very much less than the length of the slug of shock-heated gas and the assumption of equilibrium was a good approximation for calculations of the gas properties.

The fastest reaction was the bimolecular exchange reaction.

$$O_2 + N \rightleftharpoons NO + O$$

which was followed by $N_2 + O \rightleftharpoons NO + N$

That these reactions dominate the dissociation of air has been observed by other workers (e.g., refs. 23 to 27). It is of interest that the higher temperatures and corresponding lower NO concentrations obtained in this study do not alter the dominance of these nitric oxide shuffle reactions.

A similar calculation behind the reflected shock wave, showed that the distance for equilibrium to be reached was 0.001 cm. The slug of test gas processed by the reflected shock was over 1 cm in length, making the assumption of equilibrium valid here also.

Distances required to reach equilibrium in nitrogen were similar to those in air, despite the lack of oxygen excluding the bimolecular shuffle reactions, because the gas was almost 15% hotter behind the incident shock than air at the same initial shock tube conditions. This was because less energy was absorbed in dissociation. In almost all of the cases considered in this study (the exceptions were very low enthalpy shots in T.1), the total flow enthalpy was sufficient to dissociate the oxygen in air fully.

Equilibrium lengths in carbon dioxide, estimated from experimental and theoretical results of others (refs. 31, 32), appeared to be similar to those found in air.

Hence, the assumption of chemical equilibrium in the processes forming the nozzle reservoir was valid.

3.3.4 Results

Two techniques were used to investigate properties of the gas in the nozzle reservoir: pressure measurement near the end of the shock tube (see section 3.1) and streak photography of the luminosity of the initial and reflected shock waves.

The interesting feature of the measurements of pressure in the nozzle reservoir was that the value relaxed (after the reflected shock-contact surface interactions described in section 2.2) to a constant value for given driver conditions, which was unaffected by either the type or initial shock tube pressure of the test gas. Figure 12 shows calculated results behind the reflected shock and experimental values after relaxation in T.2. Less than 2% deviation was obtained for the experimental points in over 800 shots. Features of the variation of reservoir pressure with driver conditions have been discussed elsewhere (ref. 120). The response times of the piezoelectric transducers were insufficient to record the passage of the incident and reflected shock waves and only noted the disturbances before an equilibrium interface was established (see section 2.2) as lasting less than 100 microsec in T.1 and T.2 and 200 microsec in T.3. Decay of the reservoir pressure occurred after approximately 300 microsec in T.2 and 600 microsec in T.3.

Figure 56 shows a typical streak photograph of luminosity from the incident and reflected shock waves. The most important result from this photograph is that the reflected shock is straight for a distance of approximately 1 cm from the end wall. If this indicates the extent of uniform test gas, (until the contact surface is reached) it should be compared with approximately 3 cm, which is predicted from one-dimensional mass conservation across the shock waves. That is, over 60% of the gas is lost to boundary layers or other sinks (e.g. diffusion of test gas through the contact surface). Similarly, if the length of the slug of gas behind the initial shock at the end of the shock tube is given by the length of the uniform luminosity, approximately 50% of the gas is lost after only the initial shock wave. These figures agree with current theory (refs. 95, 96) within the large experimental errors.

Comparison of the slope of the reflected shock wave on figure 56 with the calculated velocity gives agreement within the 20% experimental errors.

Figure 13 shows calculated values of temperature in the nozzle reservoir. Figures 14 to 17 show species concentrations in air, 50% N_2 - 50% CO_2, carbon dioxide and argon, respectively.

3.4 Nozzle Flow

The nozzle is the most important part of any flow simulation facility. It determines the free stream conditions and the accuracy of the simulation. As stated in chapter 1, it is essential to calibrate the flow from the nozzle as accurately as possible. This is difficult in a very high enthalpy shock tunnel as there are few techniques which measure properties of direct interest such as gas composition, density and velocity (see chapter 1), and the deduction of such properties from readily measured properties involves assumptions which may be difficult to justify.

For example, pitot pressure is relatively easy to measure; velocity is somewhat more difficult; and density is extremely difficult to determine accurately. However, if the flow is hypersonic, the assertion that

$$\text{pitot pressure} = \rho u^2$$

is approximately true, so that the density may be derived from the two simpler measurements. This depends on the Mach number being greater than 5. Mach number is extremely hard to measure, so that this assumption is difficult to justify. Indeed, calculations for the 0.125 in throat, 7.5° half-angle nozzle on T.2 at 2 in Hg initial shock tube pressure of air, showed tha the free stream Mach number varied between 10.12, if no reactions occurred in the nozzle flow, 5.85, if finite reaction rates were assumed, and 4.76, if the flow was in chemical equilibrium. That is, the assumption may or may not be true depending on the extent of reactions in the gas.

As a result of the difficulties of direct experimental calibration, considerable reliance has been placed by workers in the field on computer calculations such as those discussed in section 2.2, backed up by investigations of model flows. Similarly, in this study, the effects of chemical nonequilibrium and viscosity in the nozzle flows were determined theoretically and confirmed by a limited number of experiments. Simple model flows were also considered as part of the calibrations (see chapter 4).

3.4.1 Chemical Nonequilibrium

As the test gas expands in the nozzles on the free piston shock tunnels, ionised and dissociated species recombine at rates which are limited, in the main, by the rates of collisions between reaction partners (see chapter 1). That is, the reaction rates decrease with increasing area ratio until a point is reached where all recombinations are negligible and the gas may be considered as non-reactive and as obeying the perfect gas laws. At the nozzle exit, energy, which would be released to the flow in an equilibrium expansion, is retained as formation energy of species formed at high temperatures. As a result, the velocity, pressure and temperature are less and density, ratio of specific heats and Mach number are greater in the free stream than would be the case if the reactions were infinitely fast.

Figure 18 shows species concentrations in a typical nozzle expansion in T.2, calculated as described in chapter 2. The nozzle reservoir enthalpy was considerably higher than values used elsewhere (see chapter 1). Oxygen, which was almost completely dissociated in the reservoir, remained dissociated and nitrogen remained significantly dissociated at the nozzle exit. One cause of this was that the high enthalpy caused low concentrations of nitric oxide (a factor of 10 less than the example in reference 44) and hence a lessening of the effectiveness of the shuffle reactions. At area ratios greater than 10, the atom transfer (shuffle) reaction

$$N + NO \rightleftharpoons N_2 + O$$

was the fastest reaction, followed by

$$N + O + M \rightleftharpoons NO + M$$

and $$3N \rightleftharpoons N_2 + N$$

In some cases examined here and elsewhere (ref. 76), reactions were found to overshoot equilibrium and to reverse direction. For example, in the expansion shown in figure 18, the reactions

$$NO + NO \rightleftharpoons N_2 + O_2$$

and $$N^+ + O \rightleftharpoons N + O^+$$

/33

change direction at area ratios of 5 and 6 respectively. "Overshoot equilibrium" does not convey fully the mechanism of this phenomenon, which results from the efficiency of some reactions in depleting concentrations of one or more species preferentially, and the subsequent decrease in temperature in the expansion making conditions favourable for an increase in those species.

Figure 19 shows species concentrations in a typical nozzle expansion in nitrogen. The fastest reaction was found to be:

$$3N \rightleftharpoons N_2 + N$$

followed by: $2N + N_2 \rightleftharpoons 2N_2$

Recombination of ionised species occurred through the reactions:

$$N^+ + N_2 \rightleftharpoons N_2^+ + N$$

$$N_2^+ + \bar{e} \rightleftharpoons 2N$$

or through the single step:

$$N^+ + 2\bar{e} \rightleftharpoons N + \bar{e}$$

As would be expected from the single step atomic recombination of N to N_2, no equilibrium overshoot was observed for non-ionised species. The reactions for recombination of N^+ and N_2^+ ions listed above have the potential for such an overshoot, but none was found to occur at the conditions of this study.

The effects of chemical nonequilibrium in flow properties at the nozzle exit have been studied by many workers (e.g. refs. 44, 76 and 77).

Reference 78 describes one early attempt to correlate concentrations of non-ionised species in terms of nozzle reservoir entropy. (Entropy is a logical parameter for a correlation of nonequilibrium nozzle properties. Both frozen and equilibrium expansions are isentropic, so the entropy increase in a nozzle expansion may be considered as a measure of the magnitude of the nonequilibrium.) The value of such correlations is, in the author's opinion, strictly limited. They are useful for "rule of thumb" estimates, but give no

/34

information on fundamental mechanisms and are not sufficiently accurate or versatile to include the effects of variations in, for example, nozzle geometry. For example, the correlation of reference 78 implies that, if the reservoir temperatures and pressures are the same, species concentrations at the exits of the nozzles on T.2 and T.3 will be the same (the nozzles have the same half angle and can be given the same area ratio by increasing the exit diameter of the nozzle on T.2). In fact, calculations using the computer program of reference 44 show that the slower rate of change of area ratio with distance in the large nozzle on T.3 (see table 1 for dimensions) gives greater recombination of N to N_2. The concentration of N_2 in T.3 was found to exceed that in T.2 at 2 in Hg of air initial shock tube pressure by approximately 50%.

Also, the need for such correlations has largely been removed by the enormous advances, both in speed and availability, of modern high speed digital computers, in the years between the publication of reference 78 and the publication of this thesis. The techniques described in section 2.2 are, thanks to the generosity of their authors, readily available; as are programs in almost all fields. The additional information and accuracy which can be achieved by obtaining and running a program for a specific application now outweigh the costs and inconvenience of such an exercise.

Reference 46 describes a "sudden freezing" model for recombination of atoms in an expansion nozzle. This model considers species to be in equilibrium up to a specified area ratio and non-reactive for area ratios greater than the specified value. Although this model has been improved on by the reaction rate calculations described above, the concept is of practical use in specifying a point in the nozzle expansion, beyond which the gas may be considered to obey the perfect gas laws. At the conditions of this study, subsequent changes in species concentrations were less than 1 part in 10^6 for area ratios greater than 150 in air and 70 in nitrogen.

/35

The effect of nonequilibrium among the vibrational states of molecular species formed in the nozzle expansion must be considered here.

Reference 114 gives estimates of the fraction of the enthalpy of equilibrium air contained in specified energy modes up to temperatures of 8000°K. The fraction contained in vibrational states of N_2, O_2 and NO decreased with increasing temperature and was, by extrapolation, less than 5% at nozzle reservoir conditions typical of this study. If this energy was withheld from the flow during the nozzle expansion, then, for example, the free stream velocity would be decreased by approximately 2.5%. The authors of reference 114 considered that, above stagnation temperatures of 4000°K, the total chemical energy becomes so large that chemical nonequilibrium is of far greater significance than vibrational nonequilibrium, although the coupled effects of vibrational lag on the chemical rate processes involved could be of significance.

Reference 148 gives a detailed analysis of the coupling of vibrational and dissociational nonequilibrium in a divergent nozzle and describes calculations of flow properties for oxygen at stagnation temperatures and pressures of 4000 to 5900°K and 10 to 80 atm respectively. These conditions were very much lower than those used in this study (12000°K and 240 atm are typical values). The author of reference 148 noted particularly that, even in cases where the fraction of energy in vibration was low, the coupling of vibration and dissociation could give values of, for example, the free stream Mach number, which differed by up to 20% from values calculated assuming vibrational equilibrium.

For most of the conditions of this study, the oxygen component of air is fully dissociated, so that only N_2 need be considered as contributing to vibrational nonequilibrium.

Reference 149 reports results of a study of nitrogen dissociation behind a normal shock wave at temperatures of 8000 to 15000°K. The authors indicate that vibrational relaxation is approximately 100 times as fast as dissociational relaxation, but speculate on a dissociation mechanism for N_2 through its vibrational states based on their measured reaction activation energy. The reverse of such a mechanism would be of great importance in a recombining gas. It would, however, be included implicitly in experimental reaction rate determinations.

To sum up, the results of references 148 and 149 indicate that vibrational relaxation is considerably faster than chemical recombination, so that the assumption of vibrational equilibrium is a reasonable approximation. This view is reinforced by the extrapolated results of references 114 and 148, which indicate that even if vibration was frozen, the free stream properties would differ from those calculated assuming equilibrium by amounts too small to be detected in any of the experiments described in this study. Lastly, of the techniques for specifying the thermodynamic properties of species (section 2.1.1), only the harmonic oscillator model could be used to include frozen vibration in the calculations used in this study and that model is inaccurate at temperatures above approximately 5000°K.

3.4.2 Viscous Effects

As the gas expands in the nozzle, it forms a boundary layer on the nozzle wall. This is true for nozzles on all types of facilities and the resulting effects on the flow properties at the nozzle exit have been studied by many workers (e.g., refs. 101, 121, 122).

In this study, boundary layer thicknesses were calculated using Sutherland's law for the viscosity of the gas together with the results in reference 93 to account for the effect of free stream Mach. number. Calculations for a multi-element, multi-species gas in chemical nonequilibrium with heat transfer to the nozzle wall and possible transition from laminar to turbulent flow were beyond the scope of this study and have yet to be done fully anywhere. Reference 101 contains polynomial expressions for mass and momentum boundary layer thicknesses obtained by fitting experimental results from a wide variety of facilities. The boundary layer calculations above were compared with results using the polynomials of reference 101 and agreement was within 10%. Typical values for the displacement thickness at the nozzle exit, 13.8 cm from the nozzle throat, using air in T.2 with the 7.5° half angle nozzle were 0.3 cm with the 0.125 in throat and 0.6 cm with the 0.0625 in throat.

The main effect of the boundary layer on the nozzle wall was to reduce the effective cross-sectional area of the nozzle. It was assumed that, at any point on the nozzle axis, the effective radius of the nozzle was equal to the true radius minus the boundary layer displacement thickness at the point.

As a first approximation, the boundary layer displacement thickness was assumed to be a linear function of distance from the nozzle throat. Thus the effect of the boundary layer was to reduce the cone angle of the nozzle.

Conditions at the nozzle exit were calculated by two methods: (i) the free stream conditions were taken as those calculated at an area ratio equal to the effective area ratio of the nozzle exit using the unaffected nozzle profile calculation, and (ii) a second calculation was made using a cone angle which gave the effective area ratio at the nozzle exit. Method (ii) was more accurate, but it was found that method (i) gave close agreement with method (ii), particularly because the effective area ratio was greater than 100, which was the area ratio found for freezing of reactions, and beyond which the test gas obeyed the perfect gas laws. (See section 3.4.1). Method (i) required no extra computing and was preferred in those cases where the effective area ratio was large.

Properties most affected by the nozzle boundary layer were pressure and density, followed by temperature and velocity. Neither the free stream static pressure nor density could be measured directly. Pitot pressure was the most easily determined property which could be used to detect the effects of the nozzle boundary layer.

Axial and transverse pitot pressure profiles were measured by Stalker (ref. 135) using a relatively large, slow probe. Typical results are shown in figures 22 and 23 which are for the shock tunnel T.1. Method (ii) above gave an effective nozzle cone of approximately 5.2° half angle, which can be seen from figure 22 to give good agreement with the experimental results. Similar results are claimed by Stalker for T.2. (Ref. 135).

A small probe of fast response was placed in the nozzle boundary layer in T.2 as shown in figure 69. The output of this probe in the free stream is shown in figure 67. The boundary layer displacement thickness was smaller during the nozzle starting processes and also when the flow was contaminated with cool, helium driver gas than during flow of pure test gas. Hence, during those periods, the probe measured pitot pressure values approximating the free stream values, and these were larger than values at positions within the boundary layer. Accurate pressure profiles could not be measured using this technique because the probe was almost as wide as the boundary layer.

3.4.3 Useful Test Time

The duration of useful test flow ("useful" is defined in section 2.2) is extremely important in shock tunnel experiments, in that it determines the time at which measurements must be taken, the response time required of instrumentation and the value of the tunnel for the study of time dependent phenomena, such as the aerodynamic heating of models. The following techniques were used to determine the useful test time in the free piston shock tunnel T.2.

Luminosity of Gas at the Nozzle Exit

Because of its high temperature, the test gas at the nozzle exit was luminous to the image converter camera. A 0.0625 in slit, parallel to the nozzle axis, was used for spatial resolution and the image converter camera was used in the streak mode, as described in Appendix B. A typical result is shown in figure 57.

The features on the photographs were an initial bright line due to a fast, starting shock wave (refs. 102, 103), followed by a small dark space until gas processed by the reflected shock wave emerged from the nozzle at a lower velocity than the starting shock wave. Values of the two velocities, measured from streak photographs such as figure 57, agreed with calculated values within the 20% experimental error. Steady flow then persisted until approximately 80 microsec after the start of the pulse from the reservoir pressure transducer, and was followed by gas with a slightly lower velocity and decreased luminosity, which continued until approximately 200 microsec (up to 300 microsec at 6 in Hg initial shock tube pressure), and whose velocity agreed with the value calculated from the measured nozzle reservoir pressure.

As the tube was operated for most of this study at lower shock speeds than were required to tailor the contact surface (tailoring was calculated to take place in air at 1 in Hg initial shock tube pressure, 0.658 cm/microsec incident shock velocity), the duration of the bright, reflected-shock-processed region was used to calculate the length of the reservoir region by assuming that an expansion wave travelled across it twice before it reached matched conditions, as in the "equilibrium interface" operation (see section 2.2). The length so derived, approximately 1 cm, agreed with that found from the reflected shock streak photography (see section 3.3.4).

Gas Velocity at the Nozzle Exit

Two techniques were used to determine the free stream gas velocity: a spark tracer method, in which a short duration spark was injected into the flow and its path followed with the image converter camera, and a magnetohydrodynamic method, which measured the voltage generated when the ionised and conducting test gas passed through a magnetic field (ref. 128). The M.H.D. technique was particularly suited for time resolution of the flow.

Figure 64 shows typical oscilloscope traces of the output from the magnetohydrodynamic velocity measurement experiment. The starting processes show clearly up to 60 microsec, and a plateau follows to 200 microsec. The sudden drop in the trace after the plateau was caused by contamination of the flow by helium driver gas, which was relatively cold and non-conducting. Tests with the spark tracer technique indicated that the drop was not due to a reduction in the flow velocity.

Pitot Pressure at the Nozzle Exit

Figure 67 shows oscilloscope traces of the output of the pitot pressure probe, which was positioned on the nozzle axis at the exit. Traces for the same initial shock tube conditions show that, while the starting processes varied with undetermined variables such as the initial vacuum in the test section and dump tank, the plateau pressure stayed constant. The time-dependent features of the traces corresponded with those found with the magnetohydrodynamic velocity probe. The calculated results predicted a higher pitot pressure from the reflected-shock-processed gas than from the "equilibrium interface" gas for shots with lower incident shock velocities than that required for tailored interface operation.

Figure 69 shows an oscilloscope trace with the probe close to the nozzle wall. During the starting processes, the Reynolds number was high, which made the boundary layer thin and the measured pitot pressure nearer to the free stream value. The same effect occurred when helium contaminated the flow, but in the plateau region, there was a considerable drop in the pitot pressure due to the probe being in the boundary layer.

Shock Wave Shapes on Simple Models

Some simple models (a wedge, a cone and a hemisphere) were placed in the flow (see chapter 4 for details) and the shapes of the shock waves formed on them were examined using the Image Converter Camera on the framing mode, a single pass Schlieren system, and a Mach-Zehnder interferometer. (See Appendix B).

Figure 58 shows a typical framing photograph of the luminosity of the gas flow over a 35°half angle wedge. Such photographs showed variations in the luminosity from the shock heated gas with time, which were similar to those of the free stream luminosity.

The value of the shock to wedge angle increased in an erratic fashion during the first 80 microsec following shock reflection, while the starting processes established the nozzle flow. Then followed over 100 microsec during which the shock angle was constant. Contamination of the flow after 300 microsec was observed as an increase in the shock to wedge angle, which was caused by an increase in the ratio of specific heats of the test gas. At the conditions of this study, an increase of 15% by mass of helium caused an increase in the shock angle of 1°.

The increase in the shock wave angle on a wedge caused by an increase in the ratio of specific heats of the test gas was also used as a method of driver gas detection in T.1. Schlieren photographs were taken as described in Appendix B, with the results shown in figure 34.

Useful Test Time Results

Figures 32 and 33 show the times of occurrence of important features in the flow with 0.125 and 0.0625 in nozzle throat diameters respectively in the 7.5° half angle nozzle on T.2.

Consider the time to the start of the plateau. The magnetohydrodynamic probe was sensitive to velocity. Its output had large variations during the nozzle starting processes, but was nearly constant during the contact surface interactions. Hence, its results gave the duration of the nozzle starting processes. The pitot probe output had large variations during both the nozzle starting processes and the contact surface interactions and so measured the duration of the latter. Both phenomena were visible on the luminosity photographs and the times agreed with those from the two probes. The similarity between figures 32 and 33 shows that the duration of the contact surface interactions was almost unaffected by the nozzle throat diameter. This is to be expected because the throat diameter was very much smaller than the shock tube diameter, so that the nozzle orifice had very little effect on the reflection of waves from the shock tube end wall. The nozzle starting processes lasted longer with the smaller diameter throat. This is to be expected if the function of the starting processes is considered to be "sweeping" residual gas from the nozzle. To move a fixed mass of stationary gas from the nozzle requires a related quantity of momentum from the gas flowing into the nozzle. As the flow of momentum is less from the small nozzle throat, it takes longer to supply the required momentum and to establish a steady flow.

With the magnetohydrodynamic probe output, the end of the plateau could be taken as either the start of fall-off or as the zero voltage point (see fig. 64). The former was caused by a decrease in the velocity and conductivity of the gas as helium contamination started, and the latter occurred when the conductivity had fallen to zero. These two times set limits on the mixing process causing contamination. The oscilloscope trace with the large nozzle throat shows fluctuations after the zero-voltage point, which were caused by pockets of ionization in the gas. The fluctuations and decrease in voltage to zero were much less apparent with the smaller nozzle throat. The fall-off in pitot pressure was also due to contamination by helium. (When helium contamination starts, there is no corresponding reduction in the nozzle reservoir pressure because a condition for a steady contact surface is that the pressure is constant. The helium is much colder than the test gas (3500°K, typically) so that, while its density may be very similar to that of the test gas, its enthalpy is very much lower. Hence, the velocity at the nozzle exit, and therefore the pitot pressure, are lower for the helium driver gas.) It was less sensitive than the magnetohydrodynamic probe and did not fluctuate after contamination started. Pitot pressure measurements in the nozzle boundary layer were more sensitive to helium contamination than measurements made on the nozzle axis. Helium caused the boundary layer thickness to decrease and the probe measured more of the free stream value. Thus, when contamination started, the probe output increased until the contamination level was sufficient to decrease the free stream value.

Comparison of the results in figures 32 and 33 shows that the contamination started earlier when the larger nozzle throat diameter was used. This implies that there existed a "slug" of uncontaminated test gas, which exhausted at a rate determined by the throat size, rather than a contamination-causing event which occurred at a fixed time. That is, following the pure test gas was a region of mixed test and driver gases, which was caused by large scale processes rather than by diffusion of atomic particules (hence, the pockets described above). The degree of small scale mixing increased with time as shown in the magnetohydrodynamic traces with the two throat sizes. The time before contamination occurred with the small nozzle throat was much less than four times as long as with the large throat, although the ratio of their areas was four, showing that the mixed region diffused into the pure gas slug.

3.4.4 Results

Figures 22 and 23 show the results of pitot pressure surveys in T.1. They indicate the validity of the boundary layer model outlined in section 3.4.2. Figure 24 shows pitot pressure measured on the axis, at the exit of nozzle on T.3. Accurate results for T.2 were obtained by Stalker (refs. 120, 135).

Figures 25 to 27 show measured and calculated values of the free stream gas velocity. (The diagnostic wedge technique is discussed in section 4.2).

Standard deviations were calculated for the large number of determinations of pitot pressure and velocity made in this study. It was found that the pitot pressure could be measured to an accuracy of 15% and the velocity to 10%. Assuming that the flow was hypersonic (see section 3.4), the density could then be calculated to an accuracy of 35%.

Also the diagnostic wedge technique (see section 4.2) gave concentrations of the major chemical constituents of the free stream in air and nitrogen to an accuracy of 15% (weighted calculations were made according to the concentrations) and the ratio of specific heats to an accuracy of 10%.

In all of these cases, the experimental results agreed with the calculated results within the experimental errors.

3.4.5 Flows in Carbon Dioxide and Nitrogen Mixtures

The atmospheres of Mars and Venus are thought to contain significant quantities of carbon dioxide and nitrogen. Several theoretical evaluations of the aerodynamic parameters for high speed entry into such atmospheres have been made (refs. 13 to 15, 31, 32, 80, 81), but few experimental results are available because few simulation facilities are capable of producing clean test gas at the high enthalpy levels required. One paper (ref. 81) reports stagnation point heat transfer measurements on a hemisphere and truncated cylinders in a mixture of 90% CO_2, 10% N_2 in a free piston shock tube; the shock wave moved into a 0.25mm Hg of the gas at speeds up to 9 km/sec and the shock heated gas flowed directly over the model. Chemical equilibrium was assumed for the gas, which is reasonable for the conditions studied, but does not apply over the full planetary entry corridor. The purpose of the work described in this section was to investigate nonequilibrium effects in mixtures of carbon dioxide and nitrogen, particularly in nozzle and model flows.

Attempts were made to calculate nozzle flow properties assuming chemical nonequilibrium with reaction rates obtained from review papers as described in chapter 2. The integration technique used was adequate for air and nitrogen, but was found unsuitable for the wide variation in the eigenvalues of the solution matrix for gas mixtures containing more than 50% of carbon dioxide. This problem has been noted elsewhere and the suggestion made that the implicit modified Runge-Kutta technique (ref. 45) be replaced by an explicit scheme (ref. 49). Results of such a modification using nitrogen test gas have been published (ref. 50). Preliminary results using the explicit scheme with single precision on an IBM 360/50 computer indicated that the wide spread of reaction rates in the carbon dioxide system allowed the numerical errors to swamp the eigen-values (ref. 51). Also, reactions in carbon dioxide are not well understood, as explained in section 2.1.2.

Figure 20 shows species concentrations in typical nozzle expansions of 50% Nitrogen, 50% Carbon Dioxide.

Figure 28 shows measured values of the free stream velocity (see Appendix B) at the exit of a conical nozzle (0.125 in throat diameter, 7.5° half angle) on T.2. Also shown on the graph are values calculated assuming that all the stagnation enthalpy is converted to gas velocity and values for nitrogen calculated assuming nonequilibrium. The agreement between the experimental and nonequilibrium results with nitrogen is within the experimental errors.

The differences between the experimental points and the curves of theoretical maximum velocity are indicative of the energy required to form species in the high temperature nozzle reservoir, and which was not recovered by recombination in the nozzle expansion. The fraction of the stagnation enthalpy which had been frozen is similar in the pure gases and in the mixture, suggesting that, while there may have been an extremely fast reaction in carbon dioxide which affected the "stiffness" of the numerical solution, it had little effect on the release of energy. Calculations with mixtures containing up to 50% of carbon dioxide indicated that the fast reaction was:

$$CO + O \overset{M}{\rightleftharpoons} CO_2$$

$$(\text{actually: } CO + O \rightleftharpoons CO_2^*$$

$$CO_2^* + M \rightleftharpoons CO_2 + M, \text{ where } M = N_2,\ CO_2)$$

This is apparent in the curves in figure 20. (The concentration of carbon dioxide is increasing rapidly when all other species concentrations are decreasing or constant.)

/46

The nozzle flow program (ref. 44) was not designed to include recombinations to different energy levels within a species and the reaction rate was taken to be an average value, as described in section 2.1.2.

It was noted that this recombination was limited by the rate at which CO was formed from C and O.

Figure 40 shows angles formed on wedges of 25 and 35° placed at the nozzle exit. Also shown are values calculated for nitrogen assuming that the gas did not react behind the shock wave. Figure 41 shows experimental angles on a 35° wedge using a nozzle throat of 0.0625 in diameter, as well as 0.125 in as used for the rest of these experiments. (Model flows are discussed in chapter 4.)

Four factors affect the shock angle: the free stream Mach number, the free stream ratio of specific heats, the boundary layer on the wedge surface and reactions taking place behind the shock wave on the wedge.

It is shown in chapter 4 that nitrogen does not react behind the oblique shock wave at the conditions of figure 40. The difference between the calculated and experimental points for nitrogen shown in figure 40 was due to the wedge boundary layer, which decreased in thickness with increasing initial shock tube pressure and increased with decreasing nozzle throat size. As the Mach number was almost constant (6.0 with the 0.125 in throat, 8.0 with the 0.0625 in throat), the decrease in the shock angle for an increase in initial shock tube pressure was caused, in the main, by a decrease in the ratio of specific heats, . The decrease in the free stream was related to the decrease in nozzle reservoir dissociation through the nozzle expansion.

Carbon dioxide can be expected to behave like nitrogen in that the of specific heats and boundary layer thickness decrease with increasing shock tube pressure. Calculations with 50% N_2, 50% CO_2 showed that the Mach number remained almost constant (approximately 5.0 with the 0.125 in throat, 6.0 with the 0.0625 in throat). Chemical nonequilibrium was expected to cause a decrease in the shock angle as CO_2, some of which was formed by recombination during the nozzle expansion, re-dissociation behind the shock waves. Other reactions were found to be too slow to react significantly. (See sections 4.1 and 5.2)

Consider figure 40. Reactions were more probable in the hotter, higher density gas behind the shock wave on the large angle wedge. With the 25° wedge, the shock angles for carbon dioxide were greater than, and followed the trend of, the nitrogen results up to 4 in Hg initial shock tube pressure. At higher initial pressures, the shock angles for carbon dioxide were significantly less than for nitrogen. With the 35° wedge, the decrease in shock angle for carbon dioxide occurred at a lower initial shock tube pressure.

For an increase in the initial shock tube pressure, the temperature behind the oblique shock wave decreases and the density increases. It was found that, at the conditions of this study, the increase in reaction rates caused by the increase in density was greater than the decrease caused by the decrease in temperature (see chapter 1). That is, the rate of reaction was found to increase with increasing initial shock tube pressure. (See also section 5.2)

Consider figure 41. The small nozzle throat led to higher free stream Mach numbers and smaller shock angles. For carbon dioxide, the reactions with the large throat were sufficient to decrease the angle below that with the small throat. The angles with carbon dioxide with the small throat showed no decrease, which may have been because the gas did not react behind the shock wave at the lower density levels.

Figure 44 shows the shock wave stand-off distance on a hemisphere-cylinder. The curve for carbon dioxide decreases with increasing initial shock tube pressure until 4 in Hg. For pressures greater than this, it remains almost constant. As the temperature and density behind the detached bow shock on this model were greater than on a wedge, it is thought that this phenomenon was due to equilibrium of one or more reactions being reached at initial shock tube pressures greater than 4 in Hg.

In calculations with mixtures containing up to 50% of carbon dioxide, it was noticed that interactions between elements were limited to reactions between nitrogen and oxygen or carbon and oxygen. The carbon-oxygen reactions were independent of the nitrogen-oxygen reactions as relatively little oxygen was lost to nitric oxide and there was always a large concentration of atomic oxygen. The concentration of CN was low at all times and reactions involving CN made a negligible contribution to the flow kinetics. The CN molecule was included as it is believed to radiate very strongly and so to be detectable, even though its concentration was low. Thus, flows in carbon dioxide-nitrogen mixtures were of limited interest in a study of chemical kinetics as they could be related to flows in nitrogen-oxygen and carbon-oxygen mixtures, which are easier to investigate.

3.4.6 Flows in Argon

As a first approximation and to find limiting values, it was assumed that radiation losses in argon could be neglected (see section 3.3.1). Nozzle reservoir conditions were calculated using the method described in section 2.2 and nozzle expansions were calculated with the assumption that the gas was in thermodynamic equilibrium. A typical plot of species concentrations in a nozzle is given in figure 21.

Flows in argon differ from flows in the other atmospheric gases (oxygen, nitrogen and carbon dioxide) in two aspects. Firstly, being monatomic, argon loses no energy to dissociation and is generally much hotter (figure 13) and has higher levels of ionization than the other gases. For example, in the nozzle reservoir, the calculations indicate that a significant quantiy of energy is absorbed by second ionization of the argon atom (figure 17). Secondly, the very rapid recombination reactions (approximated here by the assumption of equilibrium) maintain the high temperatures and ionization levels in the nozzle expansion by releasing the formation energy of the ions. This process is limited by the number of ions in the reservoir, and when recombination is complete, the temperature drops rapidly as the expansion continues with the argon behaving as a monatomic perfect gas.

Experimental tests with argon test gas indicated that his simple description is inadequate.

The magnetohydrodynamic velocity measurement technique output (figure 64) gave a positive (or negative, depending on the magnetic field direction) voltage during the first 70 microsec after shock reflection only, and then dropped to zero in a manner exactly similar to that of air after the onset of helium driver gas contamination. The first 80 microsec is shown in section 3.4.3 to be approximately the duration of the contact surface interactions. In this case, the 70 microsec may be considered as the time for the reflected shock to reach the contact surface and for an expansion wave to return to the end wall.

The spark tracer technique showed high velocities to 250 microsec, which indicated that the decrease in the magnetohydrodynamic probe output was not due to a decrease in velocity, but to a decrease in the conductivity of the gas.

The pitot probe gave results similar to the MHD probe, except that the duration of the period before the decrease was shorter (50 microsec, typically). Also the output increased after 150 microsec and then decreased slowly. The level after 150 microsec was comparable to that of pure driver gas flow.

Schlieren photography of the shock wave on a two-dimensional wedge of 35° half angle (see sections 4.1.1 and 4.2 for techniques) gave shock-to-wedge angles which varied in an apparently random fashion during the first 200 microsec.

Radiation losses as described in section 3.3.1 are not sufficient to explain these phenomena. A possible explanation is that the contact surface is unstable, particularly when interacting with the reflected shock wave. A model for contact surface instability of the Rayleigh type is given in reference 98, and flows in argon in the shock tunnels at the conditions

/50

in this study fitted the conditions required for the instability to be present.

The effect of the instability is that the contact surface becomes a zone of mixed pockets of helium and argon, which become mixed into all the test gas following the passage of the reflected shock wave through the zone. To detect such non-uniformity requires instruments with very short response times, such as the magnetohydrodynamic and pitot pressure probes. Previous experiments using the stagnation pressure transducer, a stagnation point heat transfer model and a pitot pressure probe (ref. 120) involved response times sufficient only to record average values for the gas, which were reasonably close to values expected from pure gas. With the pitot probe, low values due to helium contamination could be accounted for by ignoring the nozzle boundary layer correction.

The magnetohydrodynamic velocity probe output for argon, measured between 60 and 80 microsec after shock reflection, was compared with similar results for air measured on the plateau (150 microsec) (see figure 64). Calculations predicted velocities for argon between 10 and 20% greater than for air. The results showed velocities in argon approximately equal to those in air. This indicated a significant energy loss, which may have been due to radiation, as explained in section 3.3.1. At the conditions of this study, a reduction of 10% in the test section velocity in argon is equivalent to a reduction of 12% in the nozzle reservoir temperature, which is not incompatible with radiation losses.

4. SIMPLE MODEL FLOWS

In chapter 3, various techniques designed to calibrate the flow emerging from the nozzle are described. As a final calibration, flows over simple models, for which the free stream conditions may be related to the experimental results, were examined.

The simplest model would appear at first sight to be a two-dimensional wedge of sufficiently small angle for the shock wave it forms in the flow to be attached to the body nose. For such a flow, if the gas is non-reacting or in chemical equilibrium, the shock wave is straight, conditions behind the shock are spatially uniform and the conservation equations may be made quasi-one-dimensional. Two effects destroy this simplicity. Firstly, the gas forms a viscous boundary layer on the wedge surface of a thickness approximately proportional to the square root of distance from the body nose. This appears to the free stream gas as a curved surface and curvature of the shock wave may result. Secondly, the nozzle flow is axisymmetric and the wedge is two-dimensional. The effects of nozzle flow divergence have been shown elsewhere (ref. 70) to include curvature of the shock wave both parallel and transverse to the flow. (However, reference 70 showed that curvature of the shock wave transverse to the flow was a second order effect. It was calculated to be negligible at conditions typical of this study, which implied that Schlieren photography would give an accurate picture of the location of the shock wave.)

The second of these problems can be avoided by using a conical model. A cone at zero angle of attack has a conical shock wave if its angle is less than the detachment angle, if the gas is non-reacting or in equilibrium and if the viscous boundary layer thickness is negligible. At the conditions in this study, the last of these conditions did not hold.

A model on which the boundary layer displacement thickness is negligible at the conditions of this study is a blunt body, which has the shock wave standing off from the body nose and a gas velocity of zero at the stagnation point. The separated shock wave gives rise to a region of subsonic flow about the body nose and supersonic flow elsewhere. Such flows are difficult to calculate and consequently free stream conditions are hard to derive from experimental results. A sphere is the simplest axisymmetric blunt body, but because flow upstream of the sonic line (the locus of transition from subsonic to supersonic flow) is unaffected by flow downstream, a hemisphere - cylinder model was used for the tests reported here.

In all of these model flows, the effects of vibrational and chemical nonequilibrium must be established. The latter will be dealt with in subsequent sections. The former posed problems similar to those encountered in the nozzle flow (see section 3.4.1). Particularly, the programs used for calculating flow over wedges, cones and hemispheres (see section 2.2) did not allow estimates of vibrational relaxation. (See section 2.2.1 for a summary of the techniques used for specifying the thermodynamic properties of the test gas.) Estimates of relaxation rates for N_2 and O_2 vibration (references 148 and 149) indicated that, for conditions typical of this study, there was considerable vibrational nonequilibrium and that, in none of the model flows described in the subsequent sections of this chapter, could either equilibrium or frozen vibration be assumed as an accurate approximation. However, the very high stagnation enthalpy produced in the free piston shock tunnels greatly decreased the possible effects of vibrational nonequilibrium on the flow properties. For example, across the oblique shock wave formed on a 35° wedge at typical conditions in T.2, the increase in enthalpy, assuming the gas to be non-reactive, was 1×10^{11} erg/gm. At these conditions, the enthalpy in vibration was estimated to be less than 1×10^{10} erg/gm. Hence, the effects of vibrational nonequilibrium on the model flows was neglected.

4.1 Wedge Flow

As described above and in section 2.2, if the effects of chemical nonequilibrium, viscosity and free stream divergence can be neglected, flow over a wedge may be characterised entirely by the angle of the shock wave formed on it by the flow.

Experimental determinations of the shock angle formed on wedges of angles between 15 and 50° were made using Schlieren and Mach Zehnder interferometry. Figures 71 and 72 show typical examples of these techniques in T.2. Within the accuracy of measurement from such photographs (approximately 5%), the shock waves on wedges of 35° half angle or less were straight for all cases in T.1 and T.2. Figure 71 also shows a Schlieren photograph of the shock wave on a 45° half angle wedge. The curvature of the shock suggests that it was near the point of detachment. (Because the free stream was axisymmetrically divergent, there was not a sharp transition from an attached to a detached shock wave as the wedge angle was increased. Instead, there existed a range of angles within which the shock wave curved like a detached wave, but remained attached to the body nose.) This is in agreement with perfect gas equations (ref. 74), which predict a detachment angle of 43° at these conditions. To ensure attachment, angles less than 35° were used for this study.

Figures 35 to 37 show the agreement between experimental shock angles and those calculated assuming no reaction behind the wedge shock.

The method of streamline relaxation was used to investigate the effects of chemical nonequilibrium on the wedge flow. Highest density and temperature behind the wedge shock were obtained with the 0.125 in throat with the 7.5° half angle nozzle on T.2. At these conditions, reactions behind the wedge shock were most probable. Reaction lengths were found to be of the order of 100 cm in air and 1000 cm in nitrogen at these conditions on a 35° wedge. As these lengths were very much greater than the model length of 1 cm, non-reactive flow over the wedges was a reasonable assumption

/54

(see section 5.2 for a further discussion of reactions behind a wedge shock).

Using the flow properties calculated behind the oblique shock (ref. 39), the effects of the wedge boundary layer were estimated using simple theory (ref. 93) with Sutherland's law for the viscosity of the gas. At a distance of 1 cm from the model nose, the boundary layer displacement thickness was typically 0.01 cm for a 35° wedge with the 0.125 in throat in the 7.5° half angle nozzle on T.2.

The slope of the oblique shock wave on a wedge may be defined as a function of the effective slope of the wedge, which may be obtained from the profile of the boundary layer displacement thickness on the wedge surface. Because flow behind an oblique shock wave is supersonic, the shock wave shape at any point is influenced only by that part of the flow which is upstream of a Mach line from the wedge surface through the point. That is, the effective wedge slope is approximately equal to an average slope of the boundary layer displacement thickness up to the origin of the Mach line described above. A less subtle approximation to the effective wedge slope is the slope of a straight line through the wedge tip and the boundary layer displacement thickness at the required distance up the wedge. At the conditions of this study, it was found that these approximations gave approximately the same value for the effective wedge slope.

Then, assuming that the boundary layer displacement thickness could be considered simply as causing a small increase in the wedge angle (of between 0.5 and 2°), the calculated curves in figures 35 to 37 were corrected. The resulting curves show improved agreement with the experimental values.

A second effect of viscosity occurred at the nose of the body where the shock layer and boundary layer were of comparable thickness. The interaction of shock waves and boundary layers has been studied by many workers (e.g. refs. 94, 99, 104, 109 and 114). Interactions on a body nose

/55

are generally characterised by the viscous interaction parameter $\bar{\chi}$, where:

$$\bar{\chi} = M^3 \sqrt{\frac{C*}{Re}}$$

$\bar{\chi}$ can be considered as a measure of the size of the strong interaction region compared with the body length. At conditions typical of this study ($\frac{1}{8}$ in throat, 7.5° half angle nozzle), the Reynolds number behind the shock wave on a 35° wedge was approximately 1×10^4/cm. For a leading edge thickness of 0.001 cm (the wedge was manufactured by grinding tool steel), this gave a leading edge Reynolds number of 10. The value of $\bar{\chi}$ 1 cm up the wedge was approximately 1.8. The results of reference 114 indicate that, at these conditions, the interaction is weak. The results of reference 109 confirm that, for this value of $\frac{\bar{\chi}}{M^2} = 0.05$, the interaction is not strong.

The effect of the conical nozzle flow divergence on the two-dimensional wedge shock wave was estimated using the theory of reference 70. At conditions typical of this study, the distance of the shock wave from the wedge was decreased by less than 5% at the rear of the wedge face.

Several determinations of pitot pressure behind the oblique shock wave on a wedge were made using the probe described in appendix B. A typical result is shown in figure 68. Agreement between the experimental values and values calculated assuming no reactions and no nozzle flow divergence was within the errors in reading from the oscilloscope traces. The probe was damaged before a full study could be made of the effects of varying wedge angles and free stream conditions.

4.2 Cone Flow

Flows over cones at zero angle of attack were examined in much the same way as were the two-dimensional wedges. Figure 71 shows a Schlieren photograph of flow over a cone and figure 42 compares calculated and experimental shock angles. The effects of the boundary layer are apparent although the thickness was less than on the wedges. Both the shock layer and boundary layer are thinner on a cone than on a wedge because the cross sectional area of the cone stream tubes increases with increasing distance from the body nose. For the same reason, a cone has a larger shock wave detachment angle than a wedge at the same free stream conditions.

Flow over a cone at an angle of attack to the free stream has been studied by many workers (e.g. ref. 63) because of its application to real flight of sharp-nosed bodies and because it is a relatively simple model on which to study the generation of vorticies by bodies at yaw. Figure 71 shows a Schlieren photograph of a 30° half angle cone at 10° yaw. Measurements showed that the shock wave followed the cone rather than the free stream at these conditions (that is, the angle the shock wave made with the upper and lower parts of the cone remained almost constant). This agrees with the predictions of the perturbed cone flow computer program. As the gas was not reacting on the cone, it was thought that increasing the angle of attack out of the range of accuracy of the perturbation calculation would achieve little to advance this study and no further work was done with cones.

4.3 Hemisphere-Cylinder Flow

Flows over simple blunt bodies have been studied by many workers because of their direct applicability to shapes used in flight (e.g. refs. 79, 82, 144). The property most commonly used to characterise such flows is the shock stand-off distance; that is, the distance between the shock and the body along a line normal to the body and passing through the stagnation point. (This definition is adequate and unambiguous for the axisymmetric blunt bodies at zero incidence used in this study.)

Shock wave shapes on a hemisphere-cylinder were determined using Schlieren and Mach Zehnder interferometry. Figure 72 shows a typical interferometer photograph. The shock stand-off distance was measured as a fraction of the body radius directly from the photographs with an error of less than 5%. Figure 43 shows shock stand-off distances in T.2. The agreement is excellent and is a good indication of the accuracy of the complex, numerical calculations used to obtain the theoretical points. In particular, it is an indication either that the assumption of vibrational equilibrium in the calculations was valid or that the effects of vibrational nonequilibrium on the shock shape (see also section 5.1 for the full shock shape) were negligible (see sections 3.4.1 and 4.1).

4.4 The Diagnostic Wedge

In the model flow calculations discussed in the preceding sections of this chapter, the starting point has been the free stream conditions as calculated and confirmed, where possible, by experiment. The results of the calculations have been compared with experimentally determined shock wave shapes and the agreement or otherwise used to deduce the accuracy of the assumed free stream conditions. During the development of the wedge flow program (ref. 39) it was noticed that deductions could be made in the opposite direction for this simple model.

The equations for the conservation of mass, momentum and energy across the oblique shock wave may be written:

$$p_2 = p_1 + \rho_1 \; (u_1 \sin \theta)^2 \quad (1 - \frac{\rho_1}{\rho_2}) \qquad (1)$$

$$h_2 = h_1 + \tfrac{1}{2} \; (u_1 \sin \theta)^2 \quad (1 - (\frac{\rho_1}{\rho_2})^2) \qquad (2)$$

$$\rho_1 \tan \theta = \rho_2 \tan (\theta - \phi) \qquad (3)$$

If the gas does not react across the shock wave, it may be considered perfect and:

$$h = \frac{\gamma}{\gamma - 1} \; p/\rho \; + h_f \qquad (4)$$

Substituting in (2), for h using (4) and p using (1), gives:

$$\frac{\rho_1}{\rho_2} = \frac{\gamma - 1}{\gamma + 1} \left[1 + \frac{h_1 - h_f}{\frac{1}{2}(u_1 \sin \theta)^2} \right]$$

$$= \frac{\tan (\theta - \phi)}{\tan \theta} \qquad \text{from } (3)$$

that is,

$$\frac{\gamma + 1}{\gamma - 1} = \frac{\tan \theta}{\tan (\theta - \phi)} \left[1 + \frac{h_1 - h_f}{\frac{1}{2} (u_1 \sin \theta)^2} \right]$$

$$\gamma = \frac{\sin (2\theta - \phi)}{\sin (\theta)} + \delta \qquad (5)$$

where $\delta = \left(1 - \frac{\sin (2\theta - \phi)}{\sin \theta}\right) / \left(1 + \frac{\frac{1}{2} u_1^2 \sin \theta \sin \phi}{(h_1 - h_f) \cos (\theta - \phi)}\right)$

Assuming that the flow is hypersonic implies:

$$h_1 - h_f \ll \tfrac{1}{2}(u_1 \sin \theta)^2$$

and $\delta = 0$

Then the shock angle on the wedge gives a direct measure of the ratio of specific heats of the test gas.

At conditions typical of this study ($^1/_{16}$ in throat, 7.5° half angle nozzle on T.2), the error introduced in γ by assuming $\delta = 0$ was approximately -5%.

Also $\gamma = \dfrac{\sum x_i c_{pi}}{\sum x_i c_{vi}}$ (6)

where c_p and c_v are assumed to be constants for each species.

For nitrogen, the species considered are N_2 and N and coupling the conservation of elements with equation (6) allows solution for the mass fractions X_{N_2} and X_N. Similarly for oxygen. For air, the molecular species N_2 and O_2 are lumped together as are the atomic species N and O. The concentration of NO is considered sufficiently small for that species to be disregarded. This has been shown to be reasonable at the very high enthalpy levels obtained in the free piston shock tunnels in section 3.4.1. It is unlikely to be accurate in lower enthalpy machines. Then, if it is assumed that all O_2 dissociates before any N is formed, conservation equations may be set up and solved for X_{N_2}, O_{O_2}, X_N and X_O. The difference between the dissociation energies of N_2 and O_2, 9.76 eV and 5.12 eV respectively makes this assumption plausible. Air, containing only N_2 and O, has $\gamma = 1.465$.

Using the species concentrations derived above, the enthalpy frozen into the flow equals the enthalpy required to form the species.

That is, $h_f = \sum X_i h_{fi}$

Then, if the stagnation enthalpy is known, the free stream velocity may be evaluated from:

$$u = \sqrt{2 (h_s - h_f)}$$

Consider the results for a 35° half angle wedge in T.1 shown in figure 35. As discussed in section 3.4.3, a period of approximately 70 microsec after shock reflection is required for the nozzle starting processes to decay and for steady flow to be established. After 100 to 300 microsec of uniform flow, during which the shock angle remains constant, driver gas (helium) begins to contaminate the flow and, being a monatomic gas, it increases the ratio of specific heats of the gas and, therefore, the shock angle. For typical conditions in figure 35, a 15% increase by mass of helium increases the shock wave angle by approximately 1°. Hence, the first use of this technique is as a detector of contamination by driver gas.

Figures 25, 26 and 27 show values of the free stream velocity derived using this technique from the shock angle shown in figures 35, 38 and 39. Figures 29 to 31 show values of species concentrations. In all cases, the results agree with calculated results within the experimental errors. Figures 30 and 31 also show results obtained with a Quadrupole Mass Spectrometer (ref. 138). The voltage outputs from the Spectrometer were related to species concentrations through ionization cross-sections obtained from reference 36. (These differ from the cross-sections used in reference 138, especially since no experimental values were quoted there for atomic species.) The agreement with the calculated results is within the experimental errors.

There are a number of limitations to the diagnostic wedge technique. The flow enthalpy and density must be within certain limits so that the assumptions of no reactions in the flow and the presence of certain species only are valid. The flow enthalpy must be very high so that there is a large variation in the fraction of molecules dissociated and a corresponding large variation in γ. If this is not so, then the accuracy with which the shock angle must be measured becomes excessive. Also, the boundary layer thickness must either be measurable or readily estimated, and the flow must be hypersonic. The low hypersonic Mach number with the $\frac{1}{8}$ in throat, 7.5° half angle nozzle on T.2 prevented the use of the technique with that nozzle.

All these limitations may be removed by suitable correction factors in the equations above. However, the assessment of the correction factors requires prior knowledge of the flow properties, and this causes the technique to degenerate from an independent determination to one which depends on, for example, the nozzle flow calculations to verify the nozzle flow calculations.

In its present form, it provides a means (albeit rather rudimentary) of completing the calibration of the free stream properties (see section 3.4.4); particularly until such devices as the Mass Spectrometer of reference 138 are fully developed.

5. MODEL FLOWS WITH CHEMICAL NONEQUILIBRIUM

The close agreement between experiment and perfect gas calculations reported in chapter 4, the results of the diagnostic wedge technique (section 4.4), and estimates of relaxation lengths using nonequilibrium model flow programs, all show that only non-reacting gas flows were produced for flight simulation in the shock tunnels T.1 and T.2. If this is the case for all the tunnels, then the free piston technique loses a lot of its appeal and becomes a simple extension of existing techniques. Because of the considerable importance of nonequilibrium model flows, the following technique was evolved from the diagnostic wedge as a means of detecting the presence of chemical reactions.

5.1 The Flared Hemisphere-Cylinder

Calculations showed that flow over a blunt body in T.2 with the $\frac{1}{8}$ in throat, 7.5° half angle nozzle was closest to exhibiting nonequilibrium effects on the shock wave shape. (This nozzle has the smallest area ratio and the highest free stream density, and a blunt body gives the strongest possible shock wave.) It was proposed that any change in the ratio of specific heats of the gas caused by reactions in the stagnation region of such a body (the temperature, density and, therefore, reaction rates are greatest at the stagnation point) could be observed by the change in the shock angle on a wedge placed downstream in the model flow. Hopefully, the gas would react in the stagnation region, freeze again as it flowed around the body through the sonic line and give perfect gas flow over a diagnostic wedge. To preserve the symmetry of the flow, the wedge was, in fact, a flare placed downstream of the nose of a hemisphere-cylinder.

Perfect gas calculations were performed for the final model (several models were tried in an effort to give maximum density gradients for the Schlieren system while retaining the features above and remaining in the core of the nozzle flow) using the inverse blunt body method followed by the method of characteristics (see section 2.2). To calculate the effects of chemical reactions, a nonequilibrium bow-shock calculation was made to a line past the sonic line, the average ratio of specific heats was taken across the line, small changes were made to the Mach number to compensate for the changes in the ratio of specific heats required to give the constant average value, and the calculation was continued with the perfect gas method of characteristics program. The flare shock shape obtained by this method could then be compared with experiment.

The compensating changes in Mach number across the output line were made so as to keep the ratio of static to total pressure constant.

That is, $p/p_s = \left(1 + \frac{\gamma - 1}{2} M^2\right)^{(-\gamma/\gamma-1)}$ = constant

For example, if the average value of across the output line was 1.40, then a point with γ= 1.41 and M = 1.2 would have γ changed to 1.40 and M changed to 1.198.

The calculated results could not be compared with experimental results because boundary layer separation was induced by the pressure rise across the shock wave on the flare. A Schlieren photograph of such a flow is shown in figure 52 and an interpretive diagram is shown in figure 53.

To eliminate the separation, a bleed was introduced at the base of the flare which vented the boundary layer to the wake. A drawing of the model is given in figure 54. With a 1/64 inch gap between the lip of the flare and the cylinder, it was found that separation was completely removed.

Figure 55 shows a Schlieren photograph with points, calculated with the assumption of no reactions behind the model shock wave, superimposed. The agreement is within 2%, which indicates that the effects of reactions in the stagnation region are negligible.

These results are also reported in reference 145.

5.2 Model Flows in T.3

Early in 1970, the Free Piston Shock Tunnel T.3 was at a stage where useful experiments could be done at reasonably high performance levels. Calculations showed that, with the high densities available and

/63

a factor of 8 increase in model dimensions, chemically reacting model flows were possible. There was just sufficient overlap between the completion of T.3 and of this project for some elementary tests to be made.

To this time, there appear to have been no results reported in the literature at sufficiently high temperatures and densities for nitrogen to react as it passes over models, a phenomenon which occurs on missiles re-entering the Earth's atmosphere after space voyages. (Compare figures 1 and 3.)

Properties selected for comparison with the nonequilibrium theory were shock wave shapes on a 5 cm diameter hemisphere and on a wedge consisting of a flat plate inclined at 25° to the nozzle axis. Measurements of the shock wave shapes were made with a Mach Zehnder Interferometer and a single pass Schlieren system (see Appendix B). The flow consisted of approximately 0.4 msec of nozzle starting processes followed by 0.5 msec of steady flow before contamination by helium driver gas. The photographs were taken between 0.5 and 0.7 msec.

Blunt Body Results

Figures 45 and 46 show the variation of species concentrations calculated along the stagnation streamline on a blunt body for air and nitrogen respectively. An important feature is the shorter relaxation length in air caused by the well-studied nitric oxide shuffle reactions. For both of these results, it is apparent that the relaxation length is comparable to the shock stand-off distance, which is the only condition for which the approximate method (ref. 60) is valid. At conditions near equilibrium or for non-reacting gas behaviour, the method showed marked disagreement with results from the full inverse methods (refs. 52,54). (For this reason and because the free stream conditions differed (see section 3.4.1), these results should not be related to wedge flows in T.1 or T.2.)

Figure 47 shows experimental and calculated stand-off distances on a hemisphere in air. From the agreement between the experimental points, and the nonequilibrium calculations, it is apparent that the gas is reacting as it passes over the model, but that it is not rapid enough to reach equilibrium.

Since the free stream Mach number is almost constant, the variation of stand-off distance in figure 47 is due to the variation of free stream dissociation (only for the perfect gas calculations) and the reaction rates on the model.

Wedge Results

A first approximation to relaxation behind the oblique shock wave on the wedge was calculated assuming a constant pressure along each stream-tube. Figure 48 shows the change in cross-sectional area of the stream-tubes so calculated.

The results and the theoretical shock angles in figure 50 show that the nitrogen test gas was recombining rather than dissociating as it passed over the wedge, thus adding energy to the flow. This was caused by the species "freezing" in the nozzle at a higher temperature than was reached behind the oblique shock wave. The function of the shock wave was therefore to increase the density sufficiently to allow reactions to proceed. Although these results are in accord with exothermic nitrogen relaxation, the reaction length was too large for any effects to be detectable in this study. The experimental results in figure 50 agree with this prediction as the trend of the experimental angles follows that of the frozen shock angle calculations closely. The constant difference between these two curves is probably due to inaccuracies in the boundary layer estimates.

The results in figure 48 show that air was reacting significantly in 10 cm. The magnitude of the change in stream-tube area shown in figure 45 is a function of the difference between the frozen and equilibrium shock wave angles and is considerably in error because of the assumption of constant pressure along the stream tubes. The point at which the rate of change of area ratio with distance begins to decrease (points of inflection in the curves of figure 48) is relatively independent of this assumption and is a reasonable measure of relaxation length.

Using this criterion for the reaction length, only the flow with 4 in Hg initial shock tube pressure should give an observable relaxation effect (the difference between the frozen and equilibrium angles is too small at 8 in Hg) and this is confirmed by the experimental data in figure 49.

Figure 51 shows a Schlieren photograph of the shock wave at 4 in Hg. initial shock tube pressure. There appears to be some curvature of the shock as predicted elsewhere (refs. 64,65).

Flared-Hemisphere-Cylinder

The next step in this tunnel was to use the flared-hemisphere-cylinder in the method outlined in section 5.1. Calculations indicated that a body with a nose radius of 1.0 in would give a reasonable nonequilibrium effect in the stagnation region and that the gas would freeze before it reached the sonic line and remain frozen across the flare shock. The absence of Schlieren quality windows for this tunnel prevented experimental verification of these calculations. (The wedge flow photographs described above were taken through discs of commercial plate glass. The striations in the glass were aligned perpendicular to the expected line of the wedge shock and the Schlieren slits (see appendix B) were aligned perpendicular to the striations. Thus the slits were approximately parallel to the wedge shock wave, which gave maximum sensitivity. Even with these precautions, striations and perpendicular "rolling" marks were visible in the originals of photographs such as the one shown in figure 51. The shock wave formed on an axisymmetric body such as the flare gives a very much smaller path length for the Schlieren system than a two dimensional wedge. Both in Schlieren and interferometry the flare shock could be seen, but it was sufficiently blurred and distorted by the windows to be useless for accurate measurements.)

Summary

The results described above for simple model flows in the shock tunnel T.3, particularly the experimental results from the blunt body model, indicate that chemical nonequilibrium is affecting the shock wave shapes. This has been confirmed since the conclusion of this study by a series of experiments which measured fringe shifts on a Mach Zehnder interferometer (ref. 150).

CONCLUSIONS

The work described in this thesis contributes to current knowledge in the field of laboratory simulation of hypersonic flow in the following ways:

The existence of uniform test gas flow in a free piston shock tunnel with a stagnation enthalpy up to 6 x 10^{11} erg/gm and its suitability for hypersonic testing have been demonstrated. Experiments with air and nitrogen test gases have been performed in the very high enthalpy gas flow and good agreement with results of calculations using currently available techniques and chemical data was found.

The same techniques and data have been shown to be inadequate for a description of carbon dioxide at these conditions.

Flows with argon as the test gas have been shown to have short test times, compatible with the formation of a driver-test gas contact surface instability.

A technique referred to as the "Diagnostic Wedge" has been developed, which, for the conditions peculiar to this study, derived the ratio of specific heats, the atomic and molecular species concentrations, the frozen enthalpy and the velocity of the test gas from measurements of one property - the angle formed by the oblique shock wave on a wedge.

The existence of model flows with cehmical nonequilibrium has been demonstrated and measurements of the shock wave shapes agreed approximately with computed values.

In more general terms, several observations may be made from this study.. Firstly, the free piston shock tunnel has been shown to be a useful extension to the range of devices for laboratory simulation of very high speed flight. Secondly, the facility has been shown to produce clean gas at very high temperature and density levels, suitable for studies of fundamental thermodynamic, kinetic and radiation properties. Thirdly, the comparison of experiment and theory (both here and elsewhere) has shown that many of the problems which plagued shock tunnel development a decade ago are now understood and, in most cases, have been overcome. Finally, it is the author's opinion that, for many problems in high enthalpy gas flows, modern computer techniques provide a powerful and general method of solution which has yet to be exploited fully.

ACKNOWLEDGEMENTS

The author wishes to thank Dr. H.G. Hornung for his stimulating advice, Dr. R.J. Stalker for provision of the shock tunnel facilities, Dr. M.R. Osborne and the staff of the A.N.U. Computer Centre for their assistance, the Cornell Aeronautical Laboratories and the NASA Ames Laboratories for the use of their computer programs, and Mr. R. French for his assistance in the operation of the shock tunnel.

APPENDIX A List of Publications

The publications listed below were written from the work described in this thesis. The papers described as "yet to be published" are being held until publication of papers containing essential preliminary information is completed, and must not be considered as final.

1. McIntosh, M.K. "A Fast Miniature Pitot Pressure Transducer" J. Sci. Instruments Vol. 4, No. 2, p.145, February, 1971.
2. McIntosh, M.K. "A Computer Program for the Numerical Calculation of Equilibrium and Perfect Gas Conditions in Shock Tunnels" W.R.E. Tech. Note CPD-169, July, 1970.
3. McIntosh, M.K. "Computer Programs for Supersonic Real Gas Dynamics" W.R.E. Tech. Note CPD-180, December, 1970.
4. McIntosh, M.K. "Results of a Digital Computer Simulation of a High Enthalpy Shock Tunnel" W.R.E. Tech Memo 93 (WR&D), May, 1971.
5. McIntosh, M.K. "A Digital Computer Simulation of Some Experiments in a Free Piston Shock Tunnel" W.R.E. Tech Memo 428 (WR&D) July, 1971.
6. McIntosh, M.K. "Useful Test Time in a Very High Enthalpy Shock Tunnel" Yet to be published. Prepared for A.I.A.A. J. as a paper.
7. McIntosh, M.K. "Free Stream Velocity Measurements in a High Enthalpy Shock Tunnel". Physics of Fluids, Vol. 14, No. 6, p.1100, July, 1971.
8. McIntosh, M.K. "Flow Diagnostics with a Wedge in a High Enthalpy Shock Tunnel". Submitted to Physics of Fluids, July, 1971.
9. McIntosh, M.K. and Slade, J.C. "Some Estimates of Free Stream Species Concentrations in a Very High Enthalpy Shock Tunnel". Yet to be published. Prepared for A.I.A.A. J. as a Tech. Note.
10. McIntosh, M.K. and Hornung, H.G. "Prevention of Flare-Induced Separation by Boundary Layer Bleed". A.I.A.A. J., Vol. 8, No. 6, pp.1156, June 1970.
11. McIntosh, M.K. "Some Chemically Reacting Model Flows in a High Enthalpy Shock Tunnel". Submitted to Physics of Fluids, August, 1971.

12. Stalker, R.J. and McIntosh, M.K. "Experiments in a Small, High Enthalpy Shock Tunnel" Yet to be published. Prepared for Aust.J.Phys. as a paper.

13. McIntosh, M.K. "Some Experiments with Carbon Dioxide in a High Enthalpy Shock Tunnel" Yet to be published. Prepared for A.I.A.A.J. as a paper.

14. McIntosh, M.K. "Some Evidence of Contact Surface Instability in Argon in a High Enthalpy Shock Tunnel" Accepted by A.I.A.A.J. as a Tech note, August, 1971.

APPENDIX B Experimental Techniques

From an experimental point of view, two properties of the flow combined to limit the techniques which could be used in the free piston shock tunnel: the short times during which measurements had to be made, and the high flow enthalpy. The latter had two main effects - it caused the gas to be highly luminous (making Schlieren and interferometry difficult) and it gave rise to considerable ionization of the gas flow (making interpretation of electrical measuring techniques such as piezoelectric pressure transducers, hot wire aenemometers, Langmuir probes and thin film resistance heat transfer gauges, difficult). The techniques used in this study are described below. They concentrated on resolving problems associated with chemical nonequilibrium rather than aerodynamics, as described in chapter 1.

Image Converter Photography of Gas Luminosity

A STL Model 1D Image Converter Camera was used to time resolve the luminosity from the incident and reflected shock waves by "streaking" the light from a 1/16 in slit cut parallel to the tube axis. Figure 56 shows typical photographs.

The camera was used with a 'Fast Sweep' Plug-In-Unit, which gave sweep times from 20 to 200 microsec. Calibration with respect to the time axis was made by photographing the output of a Tektronix Type 181 Time-Mark Generator as it appeared on an oscilloscope screen.

The same technique was used to observe the luminous gas emerging from the nozzle exit. A $\frac{1}{8}$ in slit was taped to the test section window and the camera aperture set to a minimum for spatial resolution. A typical photograph is shown in figure 57.

A series of photographs of the luminosity from the shock wave on a model were taken using a high speed framing unit. This allowed three exposures to be made at present times relative to a triggering pulse (usually from the stagnation pressure transducer) and at preset exposures (usually 5 microsec). Figure 58 shows a typical result using a wedge model.

/73

Spark Tracer Velocity Measurement

Free stream flow velocity is a particularly important parameter as explained in chapter 1. There have been very few techniques which measure velocity directly; that is, without making assumptions about other flow properties, which may not be true in the high enthalpy, free piston, shock tunnels. References 126 and 127 record measurements at velocities approximately half those found in this study. The spark tracer and magnetohydrodynamic (described next) techniques used in this study are also described in reference 128.

A short duration spark (approximately 0.1 microsec half width) was injected into the test section flow, 0.25 in from the nozzle exit, by two fine tungsten wire electrodes approximately 1 cm apart. The 12nF condenser bank supplying the power for the spark was charged to 15kV typically (20kV maximum) and was triggerable through an auxiliary gap with a tickler electrode. It was noted that most of the available power went into this gap rather than into the spark.

The Image Converter Camera in the streak mode was aligned to look along the spark and thus used to track the resultant point of luminosity as it was swept downstream by the test flow, at what has been assumed to be the velocity of the gas.

Figure 59 shows a schematic diagram of the configuration and figure 60 shows examples of the image converter photographs. It was assumed that the spark expanded cylindrically as it was swept downstream by the flow and that its luminosity decreased as it expanded. The bow shock on the thin electrodes was thought to have a negligible effect on the flow.

Magnetohydrodynamic Velocity Measurement

This technique measured the voltage generated by a plasma moving through a magnetic field. Figure 61 shows a schematic diagram of the configuration. The properties of the magnetic field used with the probes are shown in figure 62 and a photograph of the gas flow over the electrodes is given in figure 63.

The assumptions and equations used in the analysis of the probe output are as follows:

(i) The gas velocity u, the magnetic field B, and the axis of the voltage probes are mutually at right angles.

(ii) The inter-probe distance is sufficiently small compared with the nozzle exit diameter that the nozzle boundary layer may be neglected.

(iii) The magnetic field is uniform over the width of the probe faces, but need not be over the inter-probe distance.

(vi) The gas flow between the electrodes may be divided into discrete regions of free stream, oblique shock wave and boundary layer, and further, only the velocity component parallel to the nozzle axis need be considered in each (see figure 63). The origin of this flow structure is explained later.

(v) Currents flowing in the plasma as a result of the generated voltage are sufficiently small as not to alter the properties of the flow significantly; that is, $\underline{j} \times \underline{B}$ forces and Ohmic heating may be neglected.

(vi) Current loops which close within the gas due to field inhomogeneities or other causes may be neglected.

Then, for a charged particle in the magnetic field

$\underline{F} = q(\underline{E} + \underline{u} \times \underline{B})$ (in vector form)

But $\underline{F} = 0$ from assumption (v), and thus, from assumption (i)

$E = u * B$ (now in scalar form)

Then for a small element of gas between the probes, the voltage drop is given by

$$dV = u(x) * dx$$

which gives the total voltage drop across the inter-probe space as

$$V = \int_{-d}^{d} u(x) * B(x) * dx$$

$$= 2 * \int_{0}^{d} u(x) * B(x) * dx \quad \text{from symmetry}$$

where d = half the inter-probe spacing

If the magnetic field can be represented by a power series in x

$$B(x) = \sum_{i = o}^{n} c_i x^i$$

and the velocity in each region of assumption (v) is given by

$$v(x) = u_1 \text{ in the free stream } o < x < (d - s)$$

$$= u_2 \text{ behind the shock wave } (d - s) < x < (d - \delta)$$

$$= u(x) \text{ in the boundary layer } (d - \delta) < x < d$$

where s = distance from shock to probe face

δ = boundary layer thickness

and if the boundary layer velocity profile may also be represented as a power series in x,

$$u(x) = \sum_{j = o}^{m} a_j s^j$$

with the conditions $u(x) = o$ at $x = d$

$= u_2$ at $x = d - \delta$

then the total voltage can be separated into three integrals over the three velocity regions. Each integral is the integral of a sum of powers of x, which can be made a sum of integrals of powers of x. These integrals are readily evaluated. The final result is

$$\frac{V}{2} = u_1 * \sum_{i = o}^{n} \frac{c_i (d - s)^{n + 1}}{(n + 1)}$$

$$+ u_2 * \sum_{i = o}^{n} \frac{c_i * (d - s)^{n + 1} - (d - \delta)^{n + 1}}{(n + 1)}$$

$$+ \sum_{j = o}^{m} \sum_{i = o}^{n} c_i * a_j * \frac{d^{m + n + 1} - (d - \delta)^{m + n + 1}}{(m + n + 1)}$$

Similarly, if the current is assumed to be carried by a cylinder whose cross-sectional area is the same as that of the probe faces, then the plasma resistance, R_{plasma}, may be calculated in terms of the gas conductivity.

Assumption (v) will be satisfied if R_{plasma} is much smaller than the load resistance, R_{load}, which includes the oscilloscope input impedance.

By using two values of the load resistance, the plasma resistance may be deduced from

$$\text{Measured Voltage} = \frac{V * R_{load}}{(R_{load} + R_{plasma})}$$

It was found that the plasma resistance was much less than the 2 megOhm input resistance of the oscilloscope used and that load resistances of 10 K Ohms or less had to be used to reduce the signal appreciably.

Then, if two values of the probe separation are used, the effects of the oblique shock and the boundary layer should cancel out to a first approximation, and the free stream velocity can be obtained directly.

In some cases, the predicted test section conditions were used to calculate the MHD voltage, which was then compared to the experimental value. For this comparison, the oblique shock wave was calculated by assuming the probe faces were acting as flat plates inclined at the local flow divergence angle to a parallel free stream. Agreement was obtained to within 15% with the angles (neglecting shock curvature) obtained from photographs like that in figure 63. The boundary layer velocity profile was assumed to be parabolic and its calculated thickness was compared with the luminosity photographs (figure 63).

For typical conditions (2 in Hg of air in T.2 with the 7.5° half angle nozzle with the $\frac{1}{8}$ in diameter throat), comparison with the voltage expected for a uniform magnetic field and free stream flow only showed a 6% loss due to the pressure of the oblique shock and the boundary layer, and a further loss of less than 0.5% due to the magnetic field inhomogeneity (2 cm probe separation.

Output traces from the technique are shown in figure 64.

Pitot Pressure Measurements

The object of this device was not merely to measure pitot pressures in the shock tube & tunnel, but to make the probe as small as possible so that pressures could be measured behind wedge and blunt body shocks and, hopefully, in boundary layers. Reference 123 describes the principle used for the probe and reference 124 gives an independent record of the use of a MOS FET. This probe is also described in reference 125.

Consequently the cylindrical piezoelectric element used was small (0.75mm in diameter and 1.0mm in length) and was built into a bar gauge as shown in figure 65. Initially the bars were to be of zinc as this material gave best matching of acoustical impedance with the PZT-5A ceramic, but a prototype built with copper bars performed so successfully that this was abandoned.

To avoid the integrating and differentiating problems associated with the resistance-capacitance time constant of the probe, the output of the crystal was fed directly into a MOS Field Effect transistor which gave an effective input resistance of 10^{12} Ohms and an output resistance of 10 K Ohms, which was suitable for direct display on an oscilloscope. The circuit is shown in figure 66. Analysis of the transistor's characteristics showed that an applied drain-source voltage of -15 volts would have given a more linear response.

Traces of the free stream pitot pressure are given in figure 67. Figure 68 shows pitot pressure behind the oblique shock wave on a wedge and figure 69 shows the probe in the nozzle boundary layer.

The sensitivity of the pitot probe was calculated using the PZT-5A characteristics supplied by the manufacturers (Brush Clevite Co., U.K.), the probe dimensions and the MOS FE transistor characteristics (Fairchild, U.S.A.). A value of 58 p.s.i./volt was obtained. Estimates were made for the capacitance of the crystal, the probe assembly and the connections to the MOSFET circuit. The final sensitivity was directly proportional to the crystal capacitance, and errors of 30% may have occurred in this estimate. Serious deterioration of the MOSFET occurred before accurate calibration measurements could be made. The damage was caused by overheating which resulted from the lack of convective cooling in the evacuated test section.

Schlieren Photography

The Schlieren system built for this study was designed, after study on a prototype, to allow for either single or double pass operation, as shown in Figure 70. A general outline of Schlieren systems is given in reference 129.

The main mirrors used were purchased from Optical Works Ltd. of the U.K., but have since been re-aluminised at the Mount Stromlo workshops of the A.N.U. Astronomy Department. Their surfaces are accurate to 0.1 of a wavelength at the mercury green line. The small beam-folding mirrors were constructed at Mount Stromlo to a similar standard.

To time-resolve within the period of the flow, a variety of short duration light sources were used. These included an Optical Works Argon Jet Source of 0.2 microsec duration, a Hadland Microflash Unit of 20 microsec half width and an exploding wire unit (400 microF condenser charged to 6 kV maximum and discharged through $\frac{1}{2}$ in of 30 gauge copper wire) of 20 to 100 microsec duration, depending on the external inductance. Each was triggerable to emit its flash at any desired time relative to the start of the stagnation pressure transducer output.

In all cases, difficulty was experienced in getting sufficient light from the source to swamp the natural luminosity present in most shock tube and tunnel flows. To overcome this problem, a variety of filters were introduced into the system - Wratten Types 47 and 35 proving most generally effective in the shock tunnel - and a masking slit was placed at the second knife edge position to utilise the focussing of the Schlieren light over the non-focussing of the flow luminosity.

A Fiber optic light guide with a round-to-slit end configuration was purchased from the American Optical Company, U.S.A., for use in the double pass system. Light from the source was focussed on the round end and transmitted from the slit end, which served as the source slit for the system. The narrow width of this end allowed close coincidence of source and image slits. Alternative methods used a mirror or a prism to turn the source or image rays into a new path.

A dispersive but non-deviating (for the mercury green line) composite prism was purchased from John Unertl Optics of the U.S.A. and was used to construct a colour Schlieren system in which optical path gradients were shown as colour variations rather than the usual light density variations.

A long focal length camera was designed and built for the system. Some photographs of model flows are given in figure 71.

B.6 Mach-Zehnder Interferometry

A Carl Zeiss Interferometer (No. 2388) was used extensively on T.2 to augment the Schlieren photography. Using the light sources previously described, finite and infinite fringe interferograms were made of a variety of model flows, some of which are shown in figure 72. Shock shapes only were derived from these photographs.

REFERENCES

Equilibrium Thermodynamic Properties

1. Herzberg G. "Atomic Spectra and Atomic Structure". Dover Publications, 1937.

2. Herzberg G. "Molecular Spectra and Molecular Structure Part I: Spectra of Diatomic Molecules" D. Van Nostrand Co. Ltd.

3. Moore C.E. "Atomic Energy Levels. Volume I" National Bureau of Standards Circular 467, June, 1949.

4. Eisberg R.M. "Fundamentals of Modern Physics" John Wiley and Sons Inc., 1961.

5. Rushbrooke "Introduction to Statistical Mechanics", Oxford University Press, 1949.

6. Gilmore, F.R. "Equilibrium Composition and Thermodynamic Properties of Air to 24000°K". Rand Report RM-1543, August, 1955.

7. Gilmore F.R. "Additional Values for the Equilibrium Composition and Thermodynamic Properties of Air". Rand Report RM-2328, December, 1959.

8. Raymond, J.L. "Thermodynamic Properties of Carbon Dioxide to 24000°K - with possible Application to the Atmosphere of Venus" Rand Report RM-2292, November, 1958.

9. "JANAF Thermochemical Tables" Dow Chemical Co. August, 1965. Addendum I, August, 1966. Addendum II, August, 1967.

10. McBride B.J., Heimel S., Ehlers J.G. and Gordon S. "Thermodynamic Properties to 6000°K for 210 Substances Involving the First 18 Elements" NASA Report SP-3001, 1963.

11. Logan J.G. and Treanor C.E. "Tables of Thermodynamic Properties of Air from 3000°K to 10000°K at Intervals of 100°K" CAL Report BE-1007-A-3, January, 1957.

12. "Thermodynamic Properties of High Temperature Air" Vought Research Centre Report RE-1R-14.

13. Bailey H.E. "Equilibrium Thermodynamic Properties of Carbon Dioxide" NASA SP-3014, 1965.

14. Bailey H.E. "Equilibrium Thermodynamic Properties of Three Engineering Models of the Martian Atmosphere" NASA SP-3021, 1965.

15. Bosworth F, Cook C, Gilbert L. and Scala S. "Normal Shock Parameters for the Martian Atmosphere" General Electric Report R63SD12, 1963.

16. Brahinsky H.S. and Neel C.A. "Tables of Equilibrium Thermodynamic Properties of Argon" Arnold Engineering Development Centre Report AEDC-TR-69-19, March, 1969.

Chemical Kinetics

17. Benson S.W. "The Foundations of Chemical Kinetics" McGraw Hill Book Co., 1960.

18. Clarke J.F. and McChesney M. "The Dynamics of Real Gases" Butterworths, 1964.

19. Norrish, R.G.W. "The Kinetics and Analysis of Very Fast Chemical Reactions" Chemistry in Britain, July, 1965.

20. Penner S.S. "Introduction to the Study of Chemical Reactions in Flow Systems" AGARDograph No. 7, 1955.

21. Greene E.F., and Toennies, P.J. "Chemical Reactions in Shock Waves" Edward Arnold Publisher, 1964.

22. Huff, V.N., Gordon S. and Morrell V.E. "General Method and Thermodynamic Tables for Computation of Equilibrium Composition and Temperature of Chemical Reactions" NACA Report 1037, 1951.

23. Wray K.L. " Chemical Kinetics of High Temperature Air" Progress in Astronautics and Rocketry, Vol. 7, Academic Press, 1962.

24. Bortner M.H. "Chemical Kinetics in a Re-Entry Flow Field" General Electric Missile and Space Division Report R63SD63, August, 1963.

25. Heicklen J. "Gas Phase Chemistry of Re-Entry" A.I.A.A. J. Vol. 5, No. 1, p.4, January, 1967.

26. Mavroyannis, C. and Winkler, C.A. "Chemical Reactions in the Lower and Upper Atmosphere". Interscience, N.Y., 1961.

27. Sutton A.E. "The Chemistry of Electrons in Pure Air Hypersonic Wakes" A.I.A.A. Paper No. 68-200, January, 1968.

28. Bortner, M.H. "A Review of Rate Constants of Selected Reactions of Interest in Re-Entry Flow Fields in the Atmosphere" N.B.S. Tech Note 484, May, 1969.

29. Baulch D.L., Drysdale D.D., Horne D.G. and Lloyd A.C. "Critical Evaluation of Rate Data for Homogeneous, Gas Phase Reactions of Interest in High-Temperature Systems" No. I, May, 1968, No. 2, Nov. 1968. No. 3, April, 1969, No. 4, December, 1969, Department of Physical Chemistry, the University, Leeds, U.K.

30. Carnicom M.L. "Reaction Rates for High Temperature Air with Carbon and Sodium Impurities" Sandia Labs Report SC-R-68-1799, May, 1968

31. Howe, J.T. and Sheaffer Y.S. "Chemical Relaxation behind Strong Normal Shock Waves in Carbon Dioxide Including Interdependent Dissociation and Ionisation Processes" NASA TN-D-2131, February, 1964.

32. McKenzie R.L. "An Estimate of the Chemical Kinetics behind Normal Shock Waves in Mixtures of Carbon Dioxide and Nitrogen for Conditions Typical of Mars Entry" NASA TN-D-3287, February, 1966.

33. Davies W.O., "Carbon Dioxide Dissociation at 3500 to 6000°K" J. Chem. Phys. Vol. 41, No. 6, p.1846, Setpember, 1964.

34. Weihs D. and Mannheimer - Timnat Y. "Carbon Dioxide Relaxation Times, Measured in a Shock Tube" A.I.A.A. J., Vol. 7, No. 4, p.764, April, 1969.

35. Fairbairn A.R. "The Dissociation of Carbon Monoxide" Proc. Roy. Soc. A., 312, 207-227, 1969.

36. Kieffer L.J. and Dunn G.H. "Electron Impact Ionization Cross-Section Data for Atoms, Atomic Ions and Diatomic Molecules: I. Experimental Data" Reviews of Modern Physics, Vol. 38, No. 1, p.1, January, 1966.

37. Lighthill M.J. "Dynamics of a Dissociating Gas. Part I: Equilibrium Flow" J. Fluid Mech. Vol. 2, p.1, 1957.

38. Freeman N.C. "Nonequilibrium Flow of an Ideal Dissociating Gas" J. Fluid Mech. Vol. 4, p.407, 1958.

Theoretical Techniques

39. McIntosh M.K. "A Computer Program for the Numerical Calculation of Equilibrium and Perfect Gas Conditions in Shock Tunnels" W.R.E. Tech Note CPD-169, April, 1970.

40. Horton T.E. "The JPL Thermochemistry and Normal Shock Computer Program" JPL Technical Report No. 32-660, November, 1964. Jet Propulsion Laboratory California Institute of Technology.

41. Greene S.A. and Vale H.J. "The Aerospace Corporation Computer Programs for the Solution of Multielement Chemical Equilibria" Aerospace Corporation Report No. TDR-69 (2240-51) TR-2 June, 1962.

42. Emanuel G. and Vale H.J. "A Generalised Major-Product Solution Method for Nonequilibrium Thermochemical Problems" Private Communication from Aerospace Corporation, November, 1967.

43. Vale H.J. "A Generalised Method for the Solution of Nonequilibrium Thermo-Chemical Problems. I: Analysis of a Shock Tube System" Private Communication from Control Data Australia Pty., Ltd., November, 1967.

44. Lordi J.A., Mates R.E. and Moselle J.R. "Computer Program for the Numerical Solution of Nonequilibrium Expansions of Reacting Gas Mixtures" CAL Report AD-1689-A-6, October, 1965.

45. Treanor C.E. "A Method for the Numerical Integration of Coupled First Order Differential Equations with Greatly Different Time Constants" CAL Report No. AG-1729-A-4, January, 1964.

46. Bray K.N.C. "Atomic Recombination in a Hypersonic Wind-Tunnel Nozzle" J. Fluid Mech. Vol. 6, p.1, 1959.

47. Ransom V.H., Thompson H.D. and Hoffman J.D. "Three-Dimensional Supersonic Nozzle Flowfield Calculations". J. Spacecraft. Vol.7, No.4, p.458, April 1970.

48. Prozan R.J. and Kooker D.E. "The Error Minimisation Technique with Application to a Transonic Nozzle Solution" J. Fluid Mech. Vol. 43, Part, 2, p.269, 1970.

49. Bailey H.E. "Numerical Integration of the Equations Governing the One-Dimensional Flow of a Chemically Reactive Gas" Phys. Fluids, Vol. 12, No. 11, p.2292, November, 1969.

50. Bowen S.W. and Park C. "Computer Study of Nonequilibrium Excitation in Recombining Nitrogen Plasma Nozzle Flows" A.I.A.A. J. Vol. 9, No. 3, p.493, March, 1971.

51. Hornung H.G. Private Communication, A.N.U., May, 1971.

52. Marrone P.V. "Inviscid Nonequilibrium Flow Behind Bow and Normal Shock Waves. Parts I and II" CAL Report QM-1626-A-12, May, 1963.

53. Garr L.J., Marrone P.V., Joss W.W. and Williams M.J. "Inviscid Nonequilibrium Flow behind Bow and Normal Shock Waves. Part III: The Revised Normal Shock Program" CAL Report No. QM-1626-A-12 (III), October, 1966.

54. Inouye M., Rakich J.V. and Lomax H. "A Description of Numerical Methods and Computer Programs for Two-Dimensional and Axisymmetric Supersonic Flow over Blunt-Nosed and Flared Bodies" NASA TN-D-2970, August, 1965.

55. Lomax H. and Inouye M. "Numerical Analysis of Flow Properties about Blunt Bodies Moving at Supersonic Speed in an Equilibrium Gas" NASA TR-R-204, July, 1964.

56. Bohachevsky I.O. and Rubin E.L. "A Direct Method for Computation of Nonequilibrium Flows with Detached Shock Waves" A.I.A.A. J. Vol. 4, No. 4, p.600, April, 1966.

57. Lick W. "Inviscid Flow of a Reacting Mixture of Gases around a Blunt-Body" Journal of Fluid Mechanics, Vol. 7, Part 1, January, 1960.

58. Conti R.J. "A Theoretical Study of Nonequilibrium Blunt Body Flows" J. Fluid Mech. Vol. 24, part 1, p.65, 1966.

59. Kuby W., Foster R.M. and Byron S.R. "Symmetrical, Equilibrium Flow Past a Blunt Body at Superorbital Re-Entry Speeds" A.I.A.A. J. Vol. 5, No. 4, p.610, April, 1967.

60. Gibson W.E. and Marrone P.V. "A Correspondence between Normal Shock and Blunt-Body Flows" CAL Report QM-1626-A-7, June, 1962.

61. Gibson W.E. "Dissociation Scaling for Nonequilibrium Blunt-Nose Flows" ARS Journal, Vol. 32, No. 2, p.285, February, 1962.

62. Rakich J.V. "Numerical Calculation of Supersonic Flows of a Perfect Gas over Bodies of Revolution at Small Angles of Yaw" NASA TN-D-2390, July, 1964.

63. Rakich J.V. "Calculations of Hypersonic Flow Over Bodies of Revolution at Small Angles of Attack" A.I.A.A. J., Vol. 3, No. 3, p.458, March, 1965.

64. Herman R. "One and Two Strip Method of Integral Relations for Nonequilibriu Flow over Sharp Nosed Bodies" Private Communication, Physics Department A.N.U., February, 1970

65. Capiaux R. and Washington M. "Nonequilibrium Flow Past a Wedge" A.I.A.A. J. Vol. 1, No. 2, p.650, March, 1963.

66. Thoenes J. "Nonequilibrium Flow Past a Circular Cone Including Free-stream Dissociation". A.I.A.A. J., Vol. 4, No. 8, p.1447, August, 1966.

67. Spurk J.H., Gerber N. and Sedney R. "Characteristic Calculation of Flow fields with Chemical Reactions" A.I.A.A. J., Vol. 4, No.1, p.30, January, 1966.

68. South J.C. "Application of the Method of Integral Relations to Supersonic Nonequilibrium Flow Past Wedges and Cones" NASA TR-R-205, August, 1964.

69. Lee R.H.C. and Baker R.L. "Binary Scaling of Air Ionisation on Slender Cones at Small Yaw" A.I.A.A. J., Vol, 7, No. 2, p.355, February, 1969.

70. Hall J.G. "Effects of Ambient Nonuniformities in Flow over Hypersonic Test Bodies" CAL Report No. 128, August, 1963.

71. Hornung H.G. "The Use of NASA Computer Programs for Supersonic Flow" ARL Tech. Memo. 235, August, 1967.

72. McIntosh M.K. "Computer Programs for Supersonic Real Gas Dynamics" WRE Tech. Note CPD-180, December, 1970.

73. Crane R.I. "Numerical Solutions of Hypersonic Near-Wake Flow by the Particle-in-Cell Method" Min. Tech Current Papers. No. 1083, 1970

74. Ames Research Staff "Equations, Tables and Charts for Compressible Flow" NACA Report 1135, 1953.

75. Presley L.L. and Hanson R.K. "Numerical Solutions of Reflected Shock-Wave Flowfields with Nonequilibrium Chemical Reactions" A.I.A.A. J. Vol. 7, No. 12, p.2267, December, 1969.

Theoretical Results

76. Hall J.G., Eschenroeder A.Q. and Marrone P.V. "Inviscid Hypersonic Air flows with Coupled Nonequilibrium Processes" CAL Report AF-1413-A-2, May, 1962.

77. Harris C.J. "Correlation of Inviscid Air Nonequilibrium Shock Layer Properties" A.I.A.A. J. Vol. 9, No. 2, p.334, February, 1971.

78. Harris C.J. and Warren W.R. "Correlation of Nonequilibrium Chemical Properties of Expanding Air Flows" General Electric Report R64SD92, December, 1964.

79. Ericsson L.E. "Universal Scaling Laws for Nose Bluntness Effects on Hypersonic Unsteady Aerodynamics" A.I.A.A. J. Vol. 7, No.12, p.2222, December, 1969.

80. Allison D.O. and Bobbit P.J. "Real Gas Effects on the Drag and Trajectories of a Non-lifting 140° Conical Aeroshell During Mars Entry" NASA TN D-6270, 1971.

81. Livingston F.R. and Williard J.W. "Planetary Entry Body Heating Rate Measurements in Air and Venus Atmospheric Gas up to $T = 15{,}000^{\circ}K$" A.I.A.A. J., Vol. 9, No. 3, p.485, March, 1971.

/88

82. Galloway A.J. and Sichel M. "Hypersonic Blunt Body Flow of H_2-O_2 Mixtures" Astronautica Acta. Vol. 15, No. 2, p.89, 1969.

83. McIntosh M.K. "Results of a Digital Computer Simulation of a High Enthalpy Shock Tunnel" W.R.E. Tech Memo 93 (WR&D), May, 1971.

84. McIntosh M.K. "A Digital Computer Simulation of Some Experiments in a Free Piston Shock Tunnel" W.R.E. Tech Memo 428 (WR&D), July, 1971.

Radiating Gases

85. Anderson J.D. "An Engineering Survey of Radiating Shock Layers" A.I.A.A. J. Vol. 7, No. 9, p.1665, September, 1969.

86. Hammerling P., Tears J.C. and Kivel B. "Theory of Radiation from Luminous Shock Waves in Nitrogen" Physics of Fluids Vol. 2, No. 4, p.422, August 1959.

87. Horn K.P., Wong H. and Bershader D. "Radiative Behaviour of a Shock Heated Argon Plasma Flow" J. Plasma Physics, Vol. 1, Part 2, p.157, 5967.

88. Kuiper R.A. and Bershader D. "An Interferometric Study of the Shock Reflection Process in Ionising Argon" A.I.A.A. J., Vol. 7, No. 4, p.777, April, 1969.

89. Oettinger P.E. and Bershader D. "A Unified Treatment of the Relaxation Phenomenon in Radiating Argon Plasma Flows" A.I.A.A. Paper 66-476, June, 1966.

90. Griffith W.C. and Wood A.D. "Radiation Gas Dynamics in a Shock Tube" Physics of Fluids, Supplement I, p.30, 1969.

91. Chien K., Crompton D.L. "Radiative Cooling of Shock-Heated Air in Cylindrical Shock Tubes" A.I.A.A. J. Vol.8, No.10, p.1896, October, 1970.

92. Carlson L.A. "Radiative - Gasdynamic Coupling and Nonequilibrium Effects Behind Reflected Shock Waves" A.I.A.A. J., Vol. 9, No. 5, p.858, May, 1971.

Boundary Layers and Starting Processes

93. Hornung H.G. "A Survey of Compressible Flow Boundary Layers - Theory and Experiment" Australian Aeronautical Research Committee, Report ACA 67, February, 1966.

94. Chang P.K. "Separation of Flow" Pergammon Press, 1970.

95. Mirels, H. "Test Time in Low-Pressure Shock Tubes" The Physics of Fluids, Vol. 7, No. 9, p.1201, September, 1963.

96. Mirels H. "Shock Tube Test Time Limitations due to Turbulent Wall Boundary Layer" A.I.A.A. J., Vol. 2, No. 1, p.84, January, 1964.

97. Davies L. and Wilson J.L. "Influence of Reflected Shock and Boundary Layer Interaction on Shock Tube Flows" Physics of Fluids, Supplement I, p.37, 1969.

98. Levine M.A. "Turbulent Mixing at the Contact Surface in a Driven Shock Wave" Physics of Fluids, Vol. 13, No. 5, p.1166, May, 1970.

99. Bull D.C. and Edwards D.H. "An Investigation of the Reflected Shock Interaction Process in a Shock Tube" A.I.A.A. J. Vol. 6, No. 8, p.1549, August, 1968.

100. Kuiper R.A. and Bershader D. "An Interferometric Study of the Shock-Reflection Process in Ionizing Argon" A.I.AA. J. Vol. 7, No.4, p.777, April, 1969.

101. Burke, A.F. and Bird K.D. "The Use of Conical and Contoured Expansion Nozzles in Hypervelocity Facilities" CAL Report No. 112, July, 1962.

/90

102. Smith C.E. "The Starting Process in a Hypersonic Nozzle". J. Fluid Mech. Vol. 24, Part 4, p.625, 1966.

103. Amann H.O. "Experimental Study of the Starting Process in a Reflection Nozzle" Physics of Fluids, Supplement I, p.150, 1969.

104. Korkegi R.H. "Survey of Viscous Interactions Associated with High Mach Number Flight" A.I.A.A. J. Vol. 9, No. 5, p.771, May, 1971.

105. Softley E.J., Graber B.C. and Zempel R.E. "Experimental Observation of Transition of the Hypersonic Boundary Layer." A.I.A.A. J. Vol. 7, No. 2, p.257, February, 1969.

106. Smith A.M.O. and Jaffe N.A. "General Method for Solving the Laminar Nonequilibrium Boundary Layer Equations of a Dissociating Gas" A.I.A.A. J. Vol. 4, No. 4, p.611, April, 1966.

107. Wang K. "Electron and Ion Distributions in Chemical Nonequilibrium Boundary Layer Flows" A.I.A.A. J. Vol. 7, No. 4, p.616, April, 1969.

108. Dellinger T.C. "Computation of Nonequilibrium Merged Stagnation Shock Layers by Successive Accelerated Displacement" A.I.A.A. J. Vol. 9, No. 2, p.262, February, 1971.

109. Cheng H.K., Chen S.Y., Mobly R. and Huber C. "On the Hypersonic Leading-Edge Problem in the Merged-Layer Regime" Rarefied Gas Dynamics, Sixth International Symposium, Vol. 1, p.451, July, 1968.

Shock Tubes and Tunnels

110. Gaydon A.G. and Hurle J.R. "The Shock Tube in High-Temperature Chemical Physics" Chapman and Hall, 1963.

111. Liepmann H.W. and Roshko A. "Elements of Gas Dynamics" John Wiley and Sons Inc., 1957.

/91

112. Wright J.K. "Shock Tubes" Methuen Monograph 1959.

113. Ford C.A. and Glass I.I. "An Experimental Study of One-Dimensional Shock Wave Refraction" J. Aero. Sci., Vol. 23, No. 2, February, 1956.

114. Hertzberg A., Wittliff C.E. and Hall J.G. "Summary of Shock Tunnel Development and Application to Hypersonic Research" CAL Report No. AD-1052-A-12, July, 1961.

115. Hertzberg A., Smith W.E., Click H.S. and Squire W. "Modifications of the Shock Tube for the Generation of Hypersonic Flow" CAL Report No. AD-789-A- March, 1955.

116. Wittliff C.E., Wilson M.R. and Hertzberg A. "The Tailored-Interface Hypersonic Shock Tunnel" CAL Report No. AD-1052-A-8, March, 1958.

117. Pennelegion L. and Gough, P.J. "The Change in Shock-Tunnel Tailoring Mach Number due to Driver Gas Mixtures of Helium and Nitrogen". A.R.C., R and M. 3398, 1963.

118. Holder D.W. and Schultz D.L. "The Duration and Properties of the Flow in a Hypersonic Shock Tunnel" A.R.S. International Hypersonics Conference, August, 1961.

119. Stalker R.J. "The Free-Piston Shock Tube" Aeronaut. Quart. Vol. 17, p.351, November, 1966.

120. Stalker R.J. "A Study of the Free Piston Shock Tunnel" A.I.A.A. J. Vol. 5, No. 12, p.2160, December, 1967.

121. Dunn M.G. "Experimental Study of High-Enthalpy Shock Tunnel Flow. Part I: Shock Tube Flow and Nozzle Starting Time" A.I.A.A. J., Vol. 7, No. 8, p.1553, August, 1969.

/92

122. Dunn M.G. "Experimental Study of High-Enthalpy Shock Tunnel Flow. Part II: Nozzle Flow Characteristics" A.I.A.A. J., Vol. 7, No. 9, p.1717, Setpember, 1969.

Experimental Techniques

123. Edwards D.H., Davies L. and Lawrence T.R. "The Application of a Piezoelectric Bar Gauge to Shock Tube Studies" J. Sci. Instrum. Vol. 41, p.609, 1964.

124. Hofland R. and Glick H.S. "A Miniature Transducer for Measuring Low Transient Pressures" Rev. Sci. Instrum. Vol. 40, No. 9, p.1146, September, 1969.

125. McIntosh M.K. "A Fast Miniature Pitot Pressure Transducer" J. Sci. Instrum., Vol. 4, No. 2, p.145, February, 1971.

126. Leath P.L. and Marshall T. "Electromagnetic Probe for the Measurement of Hypersonic Flow Velocity at a Point". A.I.A.A. J. Vol. 1, No. 4, p.948, April, 1963.

127. Miller R.H. "Shock-on-Shock Simulation and Hypervelocity Flow Measurements with Spark - Discharge Blast Waves" A.I.A.A. J. Vol. 5, No. 9, p.1675, September, 1967.

128. McIntosh M.K. "Free Stream Velocity Measurements in a High Enthalpy Shock Tunnel" Phys. Fluids, Vol. 14, No. 6, p.1100, June, 1971.

129. Barnes N.F. and Bellinger S.L. "Schlieren and Shadowgraph Equipment for Air Flow Analysis" J. Opt. Soc. Amer. Vol.35, No.8, p.497, August, 1945

Experimental Results

130. Stalker R.J. "Area Change with a Free Piston Shock Tube" A.I.A.A. J. Vol. 2, No. 2, p.396, February, 1964.

/93

131. Kennett R. and Sandeman R.J. "Channelled Spectra of Argon Shock Waves" Private Communication, A.N.U., August, 1969.

132. Nerem R.M., Carlson L.A. and Hartsel J.E. "Chemical Relaxation Phenomena Behind Normal Shock Waves in a Dissociated Free Stream" A.I.A.A.J. Vol. 5, p.910, May, 1967.

133. Wood A.D. and Wilson K.H. "Thermodynamic Property Measurements in Reflected Shock Air Plasmas at 12-16,000^{O}K" NASA CR-1617, 1970.

134. Stalker, R.J. "Nozzle Starting Processes in T.2" Private Communication October, A.N.U., March 1970.

135. Stalker, R.J. "Pitot Pressure Surveys in T.1 and T.2" Private Communication. A.N.U., June, 1970.

136. Stalker, R.J. "Test Section Calibration of a Free Piston Shock Tunnel". To be Published.

137. Logan P. "Optical Spectra in T.2" Private Communication, A.N.U., December, 1969.

138. Slade J.C. "Mass Spectrometry in Shock Tunnels" M.Sc.Thesis, Australian National University, January, 1970.

139. Dunn M.G. and Lordi J.A. "Measurement of Electron Temperature and Number Density in Shock Tunnel Flows. Part II: $NO^{+} + \bar{e}$ Dissociative Recombination Rate in Air" A.I.A.A.J. Vol. 7, No. 11, p.2099, November, 1969.

140. Eschenroeder A.Q., Diaber J.W., Golian T.C. and Hertzberg A. "Shock Tunnel Studies of High-Enthalpy Ionized Air Flows" CAL Report No. AF-1500-A-1, July, 1962.

141. Spurk J.H. "Experimental and Numerical Nonequilibrium Flow Studies" A.I.A.A.J. Vol. 8, No. 6, p.1039, June, 1970.

142. Yanow G. "Heat Transfer Rate and Interferometry in Argon in a High Enthalpy Shock Tunnel" Private Communication, A.N.U., January, 1970.

143. Spurk J.H. and Bartos J.M. "Interferometric Measurement of the Non-Equilibrium Flow Field Around a Cone." Physics of Fluids, Vol. 9, No. 7, p.1278, July, 1966.

144. Wegner P.P. and Buzyna G. "Experiments on Shock Stand-off Distance in Nonequilibrium Flow" J. Fluid Mech, Vol. 37, Part 2, p.325, 1969.

145. McIntosh M.K. and Hornung H.G. "Prevention of Flare-Induced Separation by Boundary-Layer Bleed" A.I.A.A.J. Vol. 8, No. 6, p.1156, June, 1970.

146. Harris C.J. "Simple Diagnostic Techniques Used in Identifying Shock Tunnel Flow Regimes" A.I.A.A. Paper No. 68-729, June, 1968.

147. Hornung H.G. "Preliminary Experiments on the A.N.U. Free Piston Shock Tunnel, T.3" Private Communication, A.N.U., March, 1970.

<ins>Miscellaneous and Late Additions</ins>

148. Tirumalesa D. "Nozzle Flows with Coupled Vibrational and Dissociational Nonequilibrium" U.T.I.A.S. Report No. 123, August, 1967.

149. Appleton J.P., Steinberg M. and Liquornik D.J. "Shock-Tube Study of Nitrogen Dissociation Using Vacuum-Ultraviolet Light Absorption" J.Chem.Phys., Vol. 48, No. 2, p.599, January, 1968.

150. Hornung H.G. "Interferograms of Blunt Bodies in T.3" Private Communication, A.N.U., December, 1970.

TABLE 1 CHARACTERISTICS OF THE A.N.U. FREE PISTON SHOCK TUNNELS

PHYSICAL DIMENSIONS	T.1	T.2	T.3
Reservoir Capacity (cu ft)	0.077	0.78	7.85
Compression Tube Length (ft)	5.0	10.0	20.0
Compression Tube Internal Diameter (in)	2.018	3.000	11.772
Piston Mass (lb)	2.05	2.6	201.
Shock Tube Internal Diameter (in)	0.50	0.837	3.000
Shock Tube Length (ft)	5.0	6.5	20.0
Number of Timing Transducers	2	2	5
Nozzle Throat Insert Diameters (in)	1/16	1/8,1/16,1/32	1/2
Conical Nozzle Half Angle (°)	7.5	7.5,15.	7.5
Nozzle Length (in)	5.5	5.5,8.5	43.7
Nozzle Exit Diameter (in)	1.5	1.5,4.5	12.0
Dump Tank Capacity (cu. ft.)	0.78	9.5	151.0

TYPICAL OPERATING CONDITIONS	T.1	T.2	T.3
Reservoir Pressure (psi)		650.	500.
Compression Tube Helium Pressure (in Hg)		33.0	15.0
Diaphragm (Thickness (in) Material)		0.031,M.S.	0.125,M.S.
Diaphragm Bursting Pressure (psi)		6800	6700
Dump Tank Pressure (mm Hg)	0.01	0.0001	0.0001
Shock Tube Pressure Range (in Hg)		0.5-10.0	0.5-10.0
Initial Shock Speed Range (cm/usec)		0.7-0.4	0.8-0.4
Stagnation Pressure (psi)		3500	3500

TABLE 2 OPERATING CONDITIONS IN T.1

PARAMETER	I	II	III	IV
Reservoir Pressure (psi)	810	390	590	590
Compression Tube Helium Pressure (in Hg)	37	18	28	58
Diaphragm (thickness (in) Material)	0.026(M.S.)	0.035(AL)	0.024(AL)	
Diaphragm Bursting Pressure (psi)	9700	4200	2050	2050
Shock Tube Pressure Range (in Hg)	0.5-4.0	4.0	4.0	8.0-16.0
Initial Shock Speed Range (cm/μsec)	.74-.49	.41-.73	.35-.71	.29-.24
Stagnation Pressure (psi)	3300	1650	1300	1800

NOTES

(1) Shock Tunnel Materials

Reservoir.... Mild Steel (T.1)
Stainless Steel (T.2 and T.3)
Compression Tube.... Stainless Steel
Shock Tube.... Mild Steel
Nozzle.... Brass (T.1 and T.2),
Aluminium (T.1 and T.3)
Mild Steel (T.2)
Dump Tank.... Mild Steel (T.1)
Stainless Steel (T.2 and T.3)

(2) Diaphragm Materials

M.S. ... Automotive Mild Steel
Al ..... Rolled Aluminium Sheet

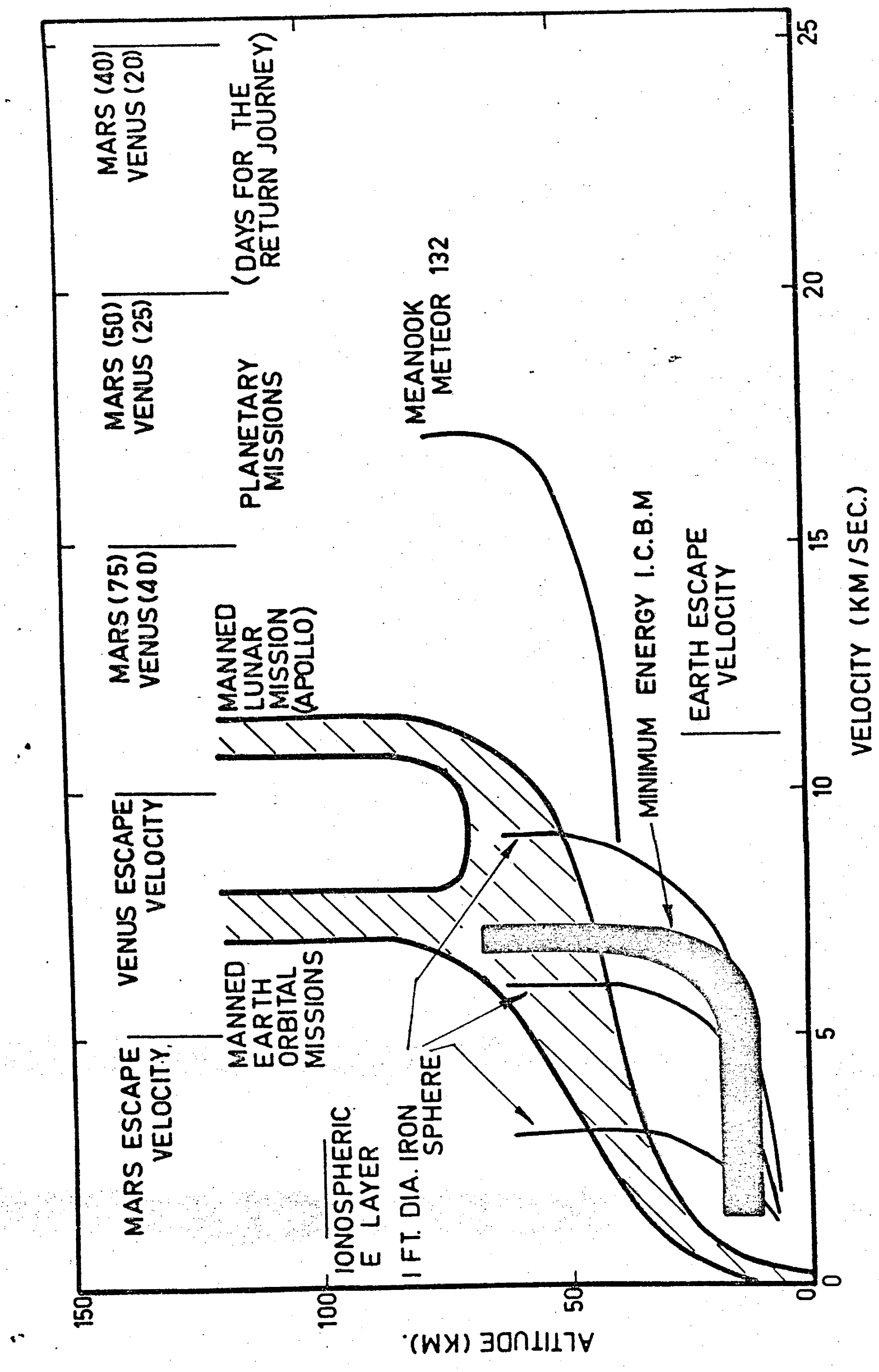

Figure 1 Direct Entry Flight Corridors

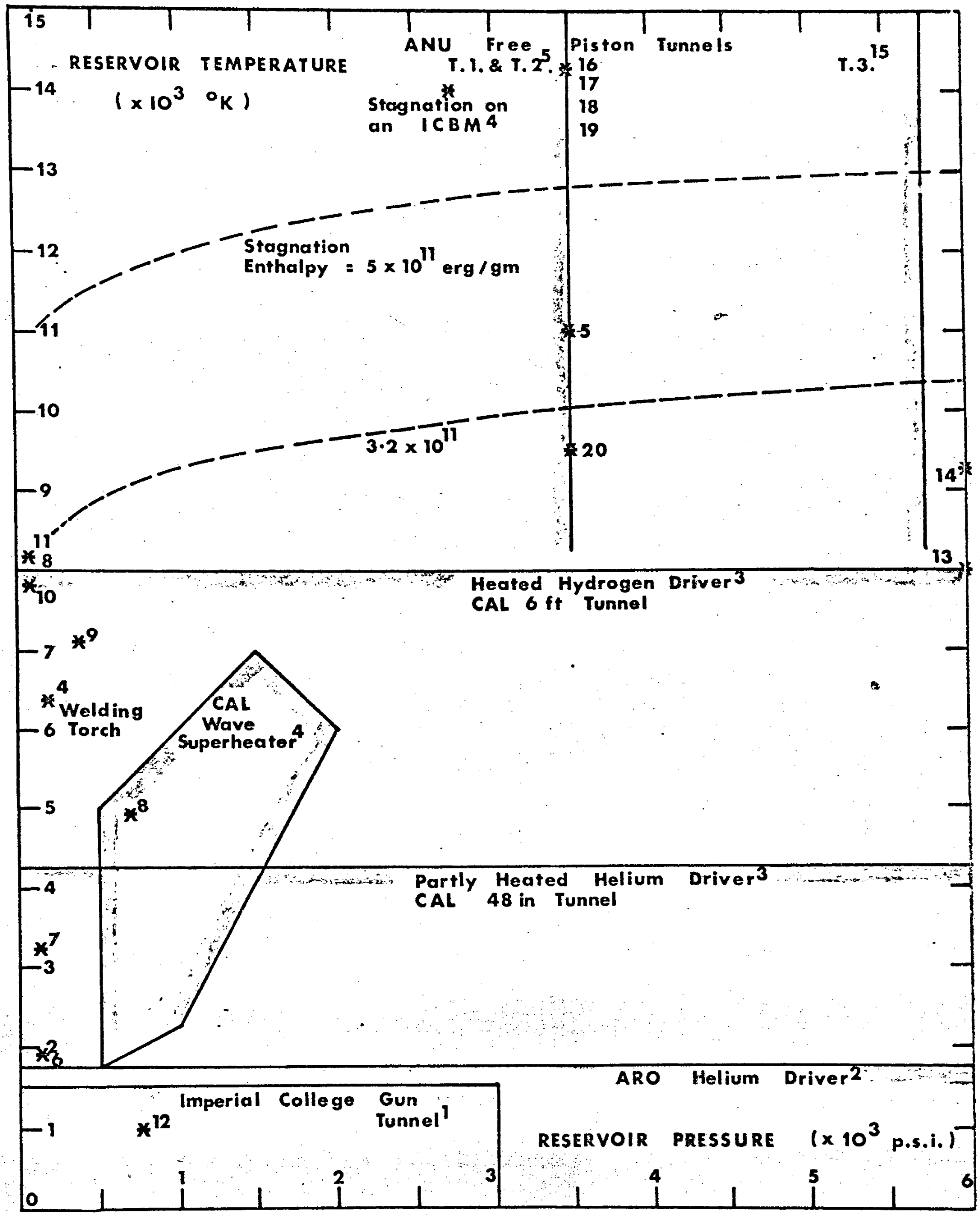

Figure 2. Hypersonic Flight Simulation Facility Summary

References for a Survey of Shock Tunnel Performance

1. Needham, D.A. "Progress Report on the Imperial College Hypersonic Gun Tunnel" Imperial College Report No. 118, August, 1963.
2. Buzyna, G. and Wegener, P.P. "Experiments on Non-Equilibrium Supersonic Flow Shock Stand-off Distance of Spheres Carried out in a New Type of Intermittent Wind Tunnel". AEDC-TR-69-81, May, 1969.
3. Hertzberg, A., Whittliff, C.E. and Hall, J.G. "Summary of Shock Tunnel Development and Application to Hypersonic Research". CAL Report AD-1052-A-12, July, 1961.
4. Colosimo, D.D. "Closer to Re-Entry Conditions" Research Trends, CAL Aeronautical Laboratory, Autumn, 1968.
5. Stalker, R.J. "A Study of the Free Piston Shock Tunnel" A.I.A.A. J. Vol. 5, No. 12, p.2160, December, 1967.
6. Amann, H.O. "Experimental Study of Starting Process in a Reflection Nozzle" Physics of Fluids, Supplement I, Shock Tube Symposium, p.150, 1969.
7. Edwards, D.H., Davies, L., and Lawrence, T.R. "The Application of a Piezoelectric Bar Gauge to Shock Tube Studies". J. Sci. Instrum. Vol. 41, No. 10, p.609, October, 1964.
8. Tirumvalesa, D. "Nozzle Flows with Coupled Vibrational and Dissociational Nonequilibrium", UTIAS Report No. 123, August, 1967.
9. Dunn, M.G., and Lordi, J.A. "Measurement of Electron Temperature and Number Density in Shock-Tunnel Flows. Part II : $NO^+ + e^-$ Dissociative Recombination Rate in Air" A.I.A.A. J. Vol. 7, No. 11, p.2099, Nov. 1969.
10. Dunn, M.G. "Experimental Study of High Enthalpy Shock Tunnel Flow, Parts I and II" A.I.A.A. J. Vol. 7, No. 8, p.1553, August, 1969, Vol. 7, No. 9, p.1717, September, 1969.
11. Spurk, J.H. and Bartos, J.M. "Interferometric Measurement of the Nonequilibrium Flowfield Around a Cone" Physics of Fluids, Vol. 9, No. 7, p.1278, July, 1966.
12. Smith, C.E. "The Starting Process in a Hypersonic Nozzle" J. Fluid Mech., Vol. 24, part 4, p.625, 1966.

13. Burke, A.F. and Bird, K.D. "The Use of Conical and Contoured Expansion Nozzles in Hypervelocity Facilities" CAL Report No. 112, July, 1962.

14. Harris, C.J. "Experimental Identification of Shock Tunnel Flow Regimes" A.I.A.A. J. Vol. 7, No. 2, p.365, February, 1969.

15. McIntosh, M.K. "Some Chemically Reacting Model Flows in a High Enthalpy Shock Tunnel" Submitted to Phys. Fluids, August, 1971.

16. McIntosh, M.K. "A Fast Miniature Pitot Pressure Transducer" J. Sci. Instrum. Vol. 4, No. 2, p.145, February, 1971.

17. McIntosh, M.K. "Free Stream Velocity Measurement in a High Enthalpy Shock Tunnel", Phys. Fluids Vol. 14, No. 6, p.1100, June, 1971.

18. McIntosh, M.K. "Useful Test Time in a Very High Enthalpy Shock Tunnel"

19. McIntosh, M.K. "Flow Diagnostics with a Wedge in a High Enthalpy Shock Tunnel" Submitted to Phys. Fluids, June, 1971.

20. McIntosh, M.K. and Hornung, H.G. "Prevention of Flare-Induced Separation by Boundary Layer Bleed". p.1156 A.I.A.A. J., Vol. 8, No. 6, June, 1970.

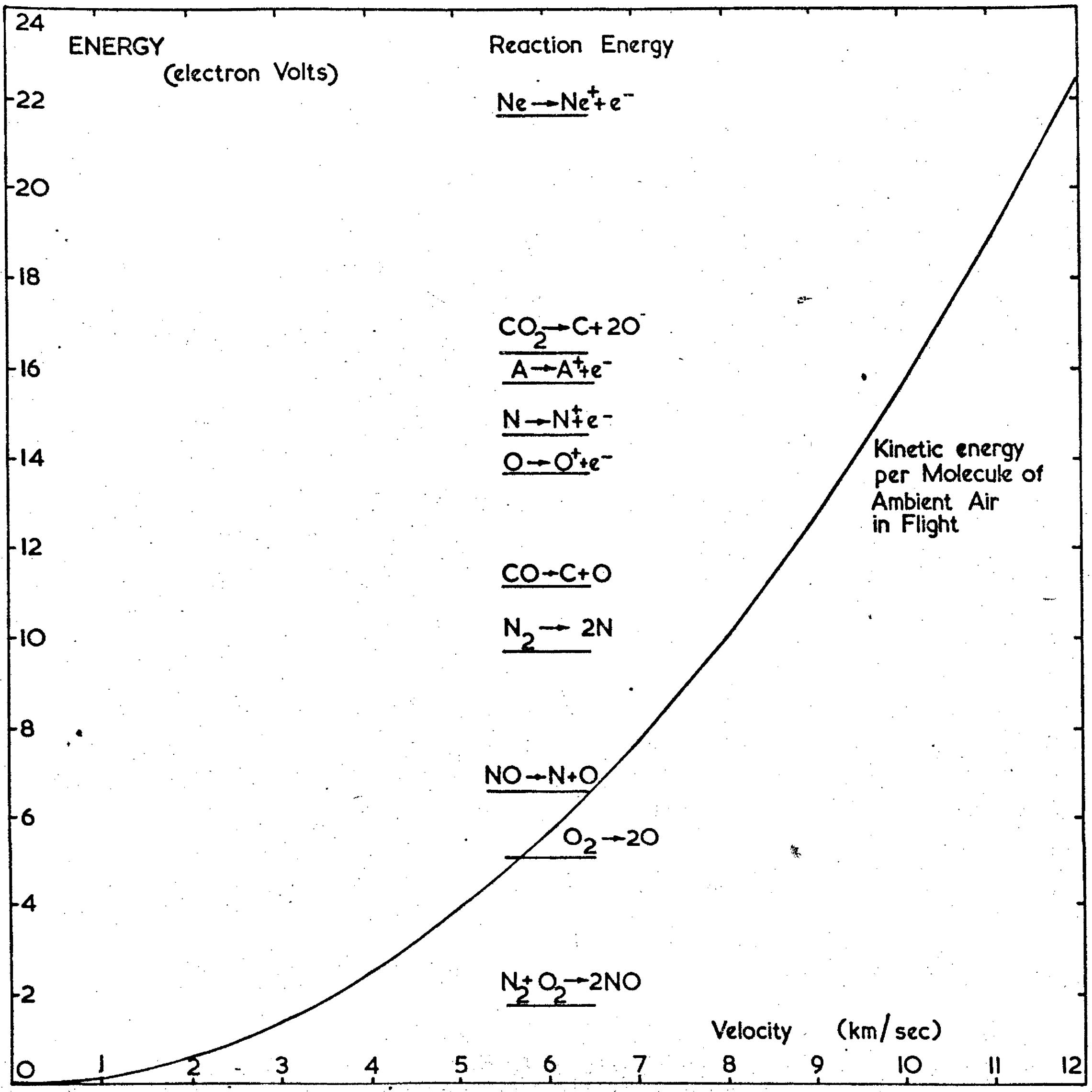

Figure No. 3 Molecular Kinetic Energy in Hypersonic Flight

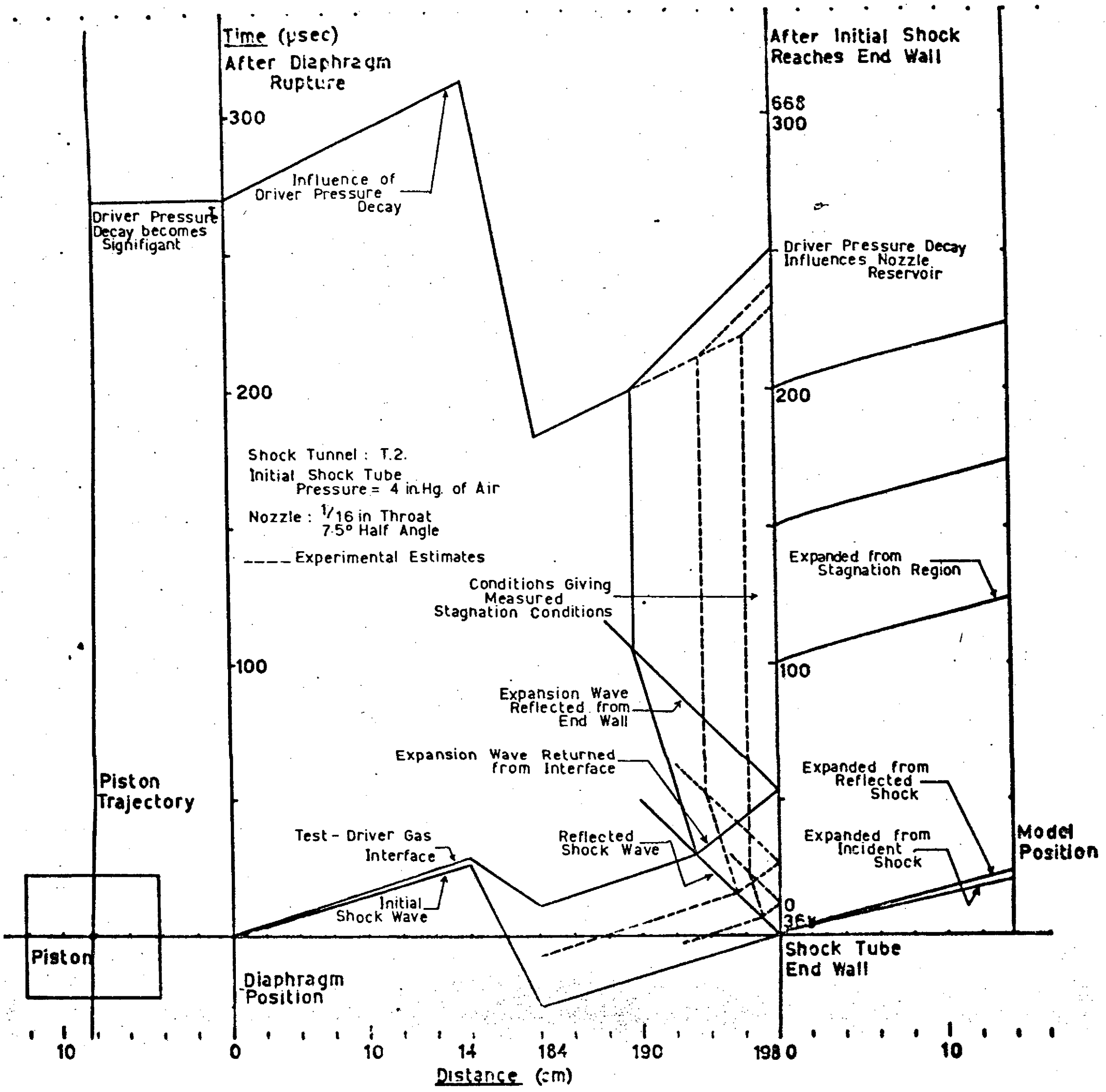

Figure No. 4 Free Piston Shock Tunnel Wave Diagram

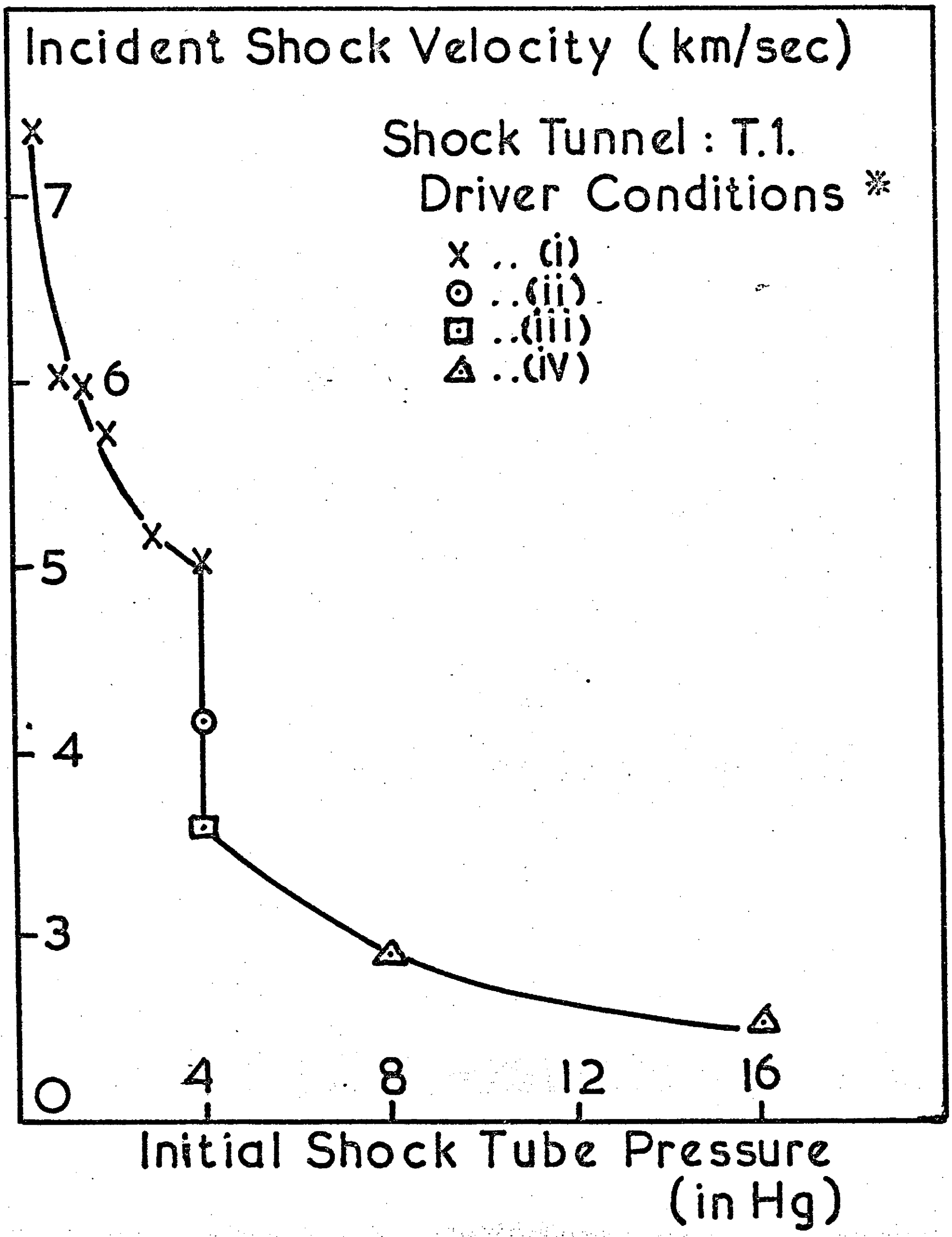

* for driver conditions, see Table 2

Figure No. 5 Initial Shock Wave Velocities in T.1

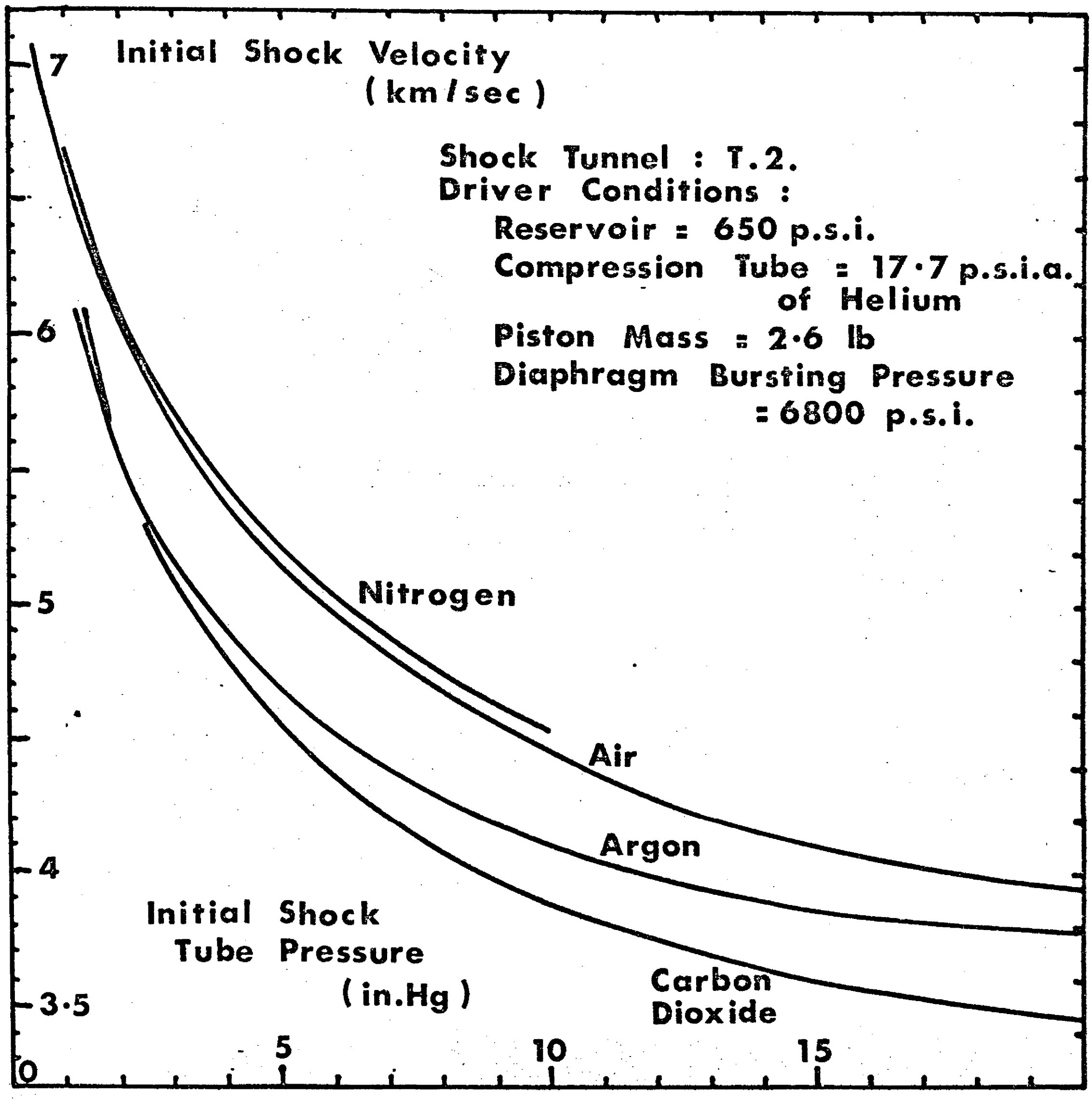

Figure No. 6 Initial Shock Wave Velocities in T.2

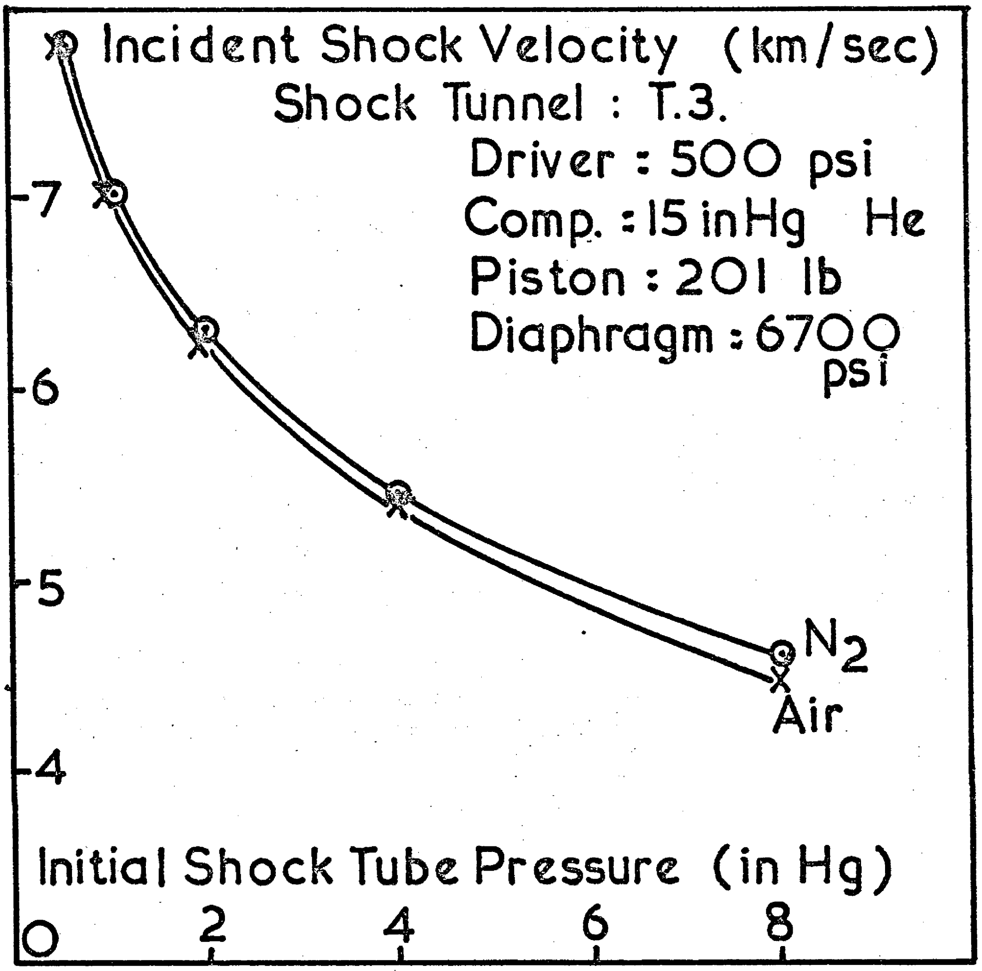

Figure No. 7 Initial Shock Wave Velocities in T.3

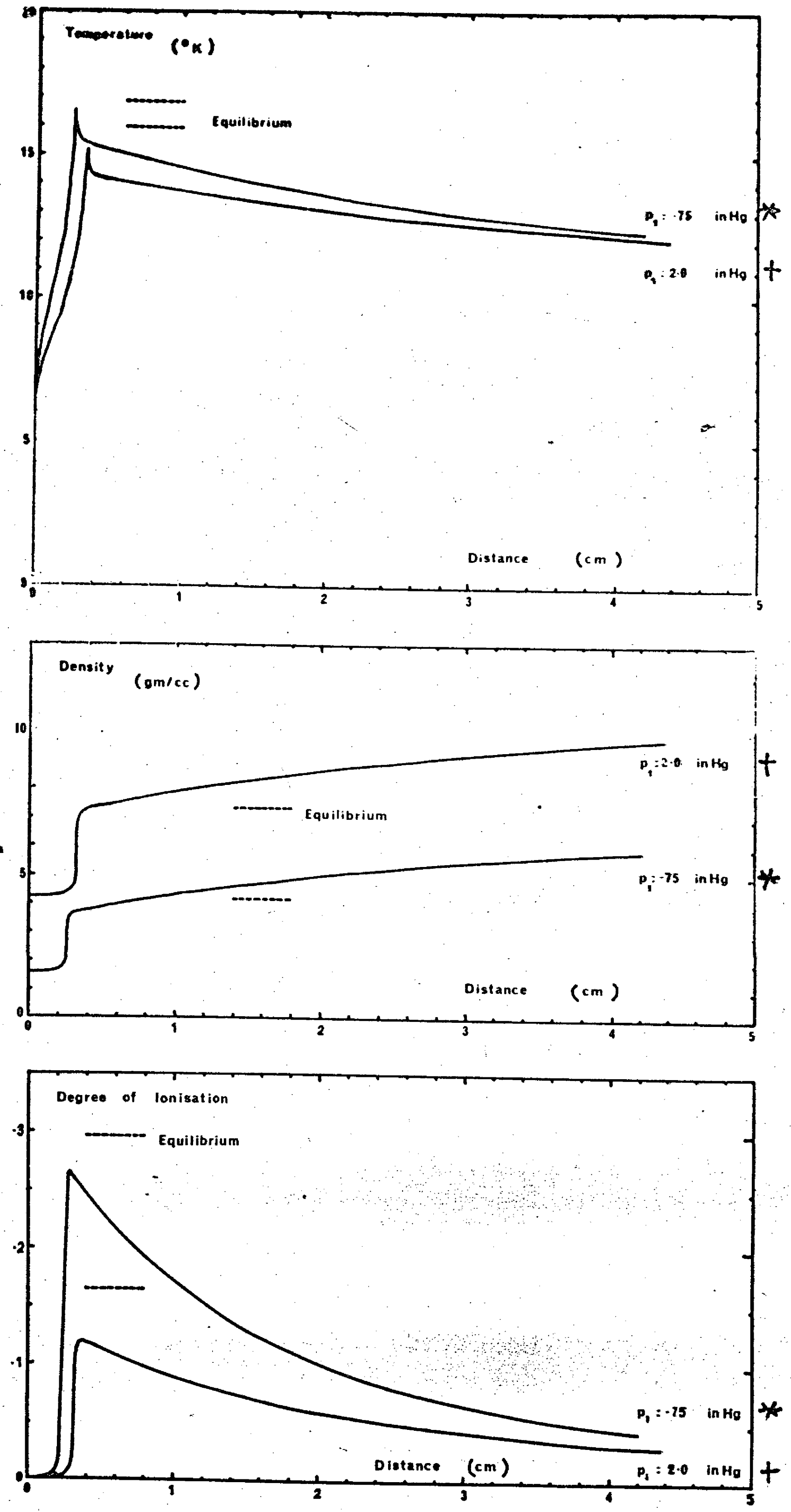

* $u_1 = 0.658$ cm/μsec
† $u_1 = 0.553$ cm/μsec

u_1 = Incident shock velocity

Figure No. 8 Radiative Relaxation in Argon in T.2

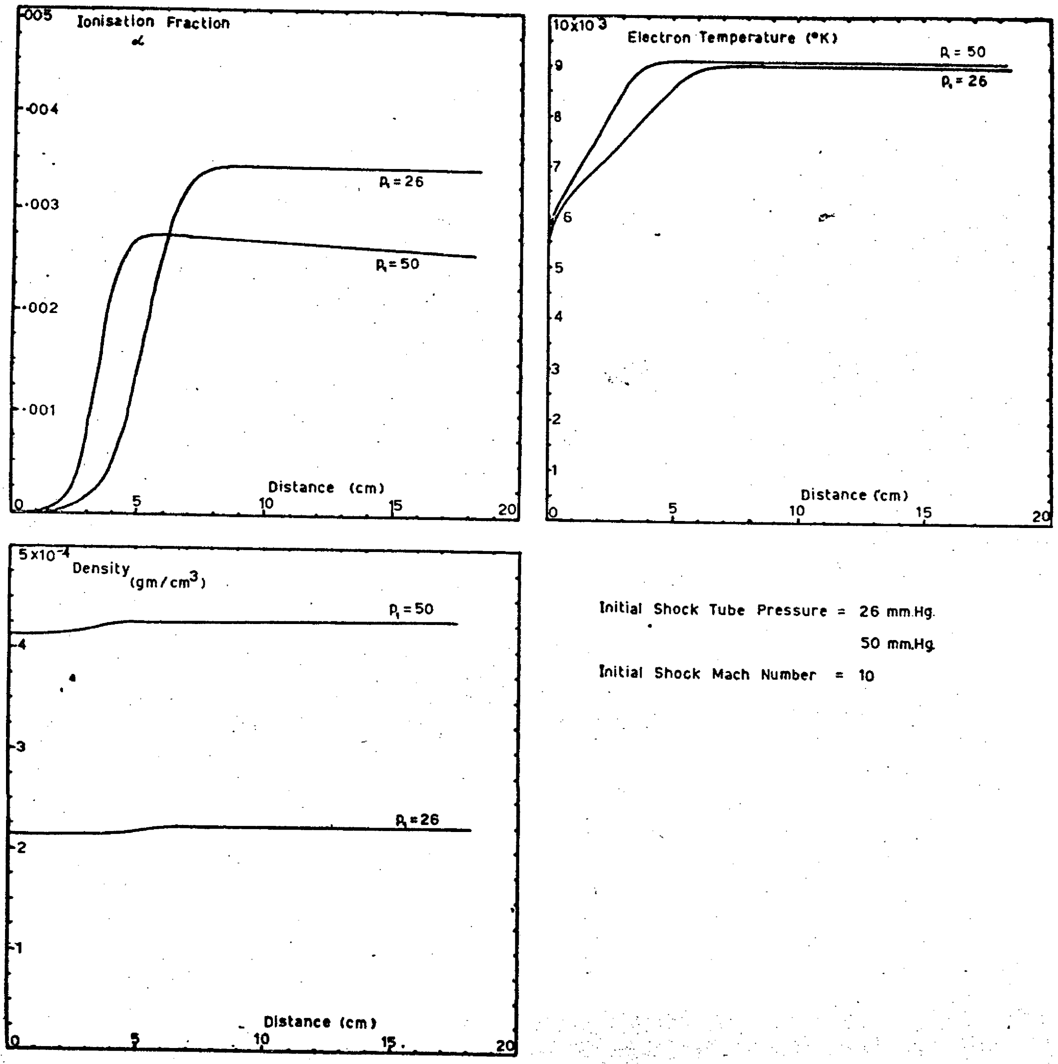

Initial Shock Tube Pressure = 26 mm Hg.
50 mm Hg.
Initial Shock Mach Number = 10

Figure No. 9 Radiative Relaxation in Argon at Conditions Comparable to Air in T.2

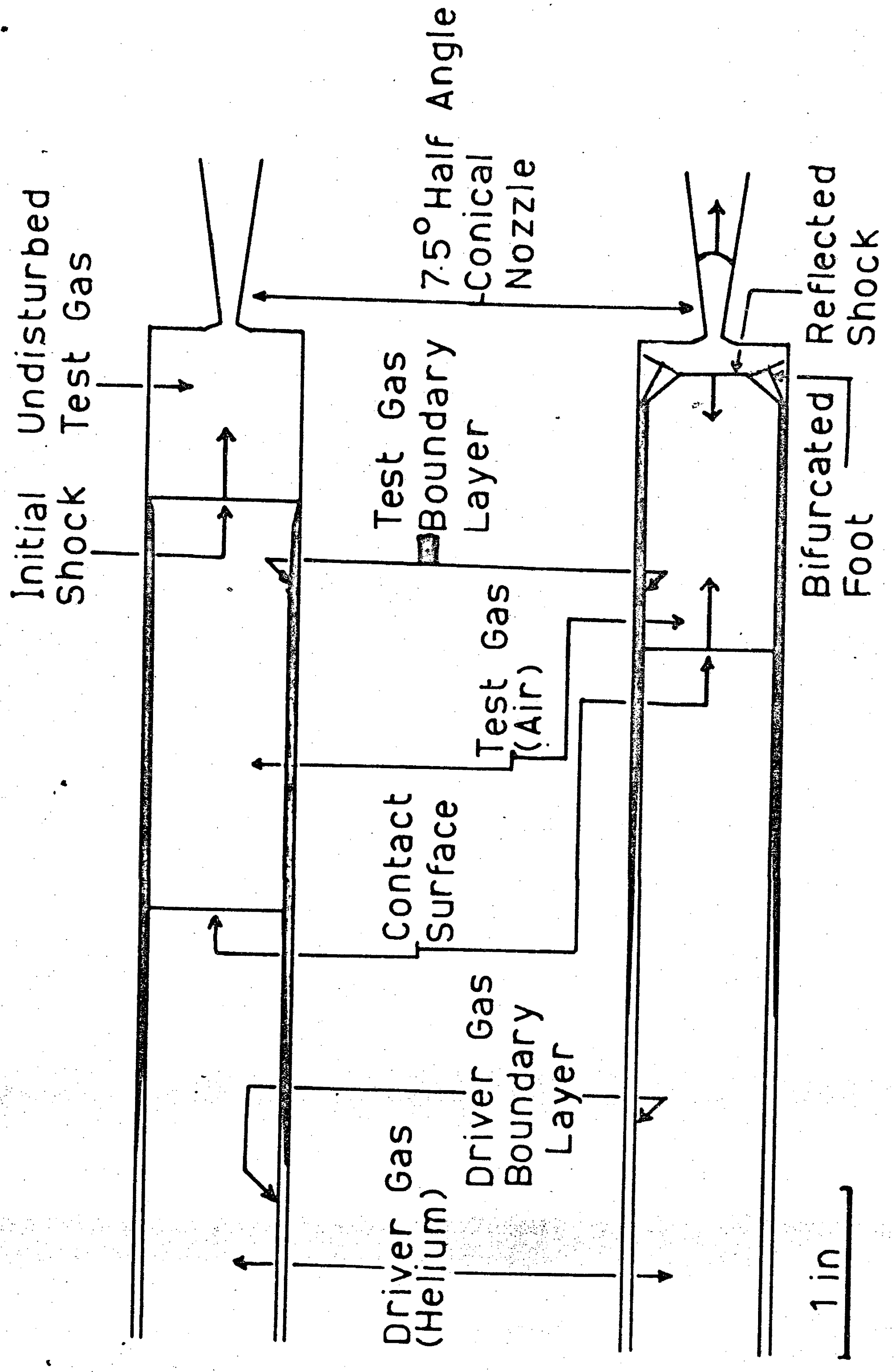

Figure No. 10. Viscous Effects in a Reflected Shock Tunnel

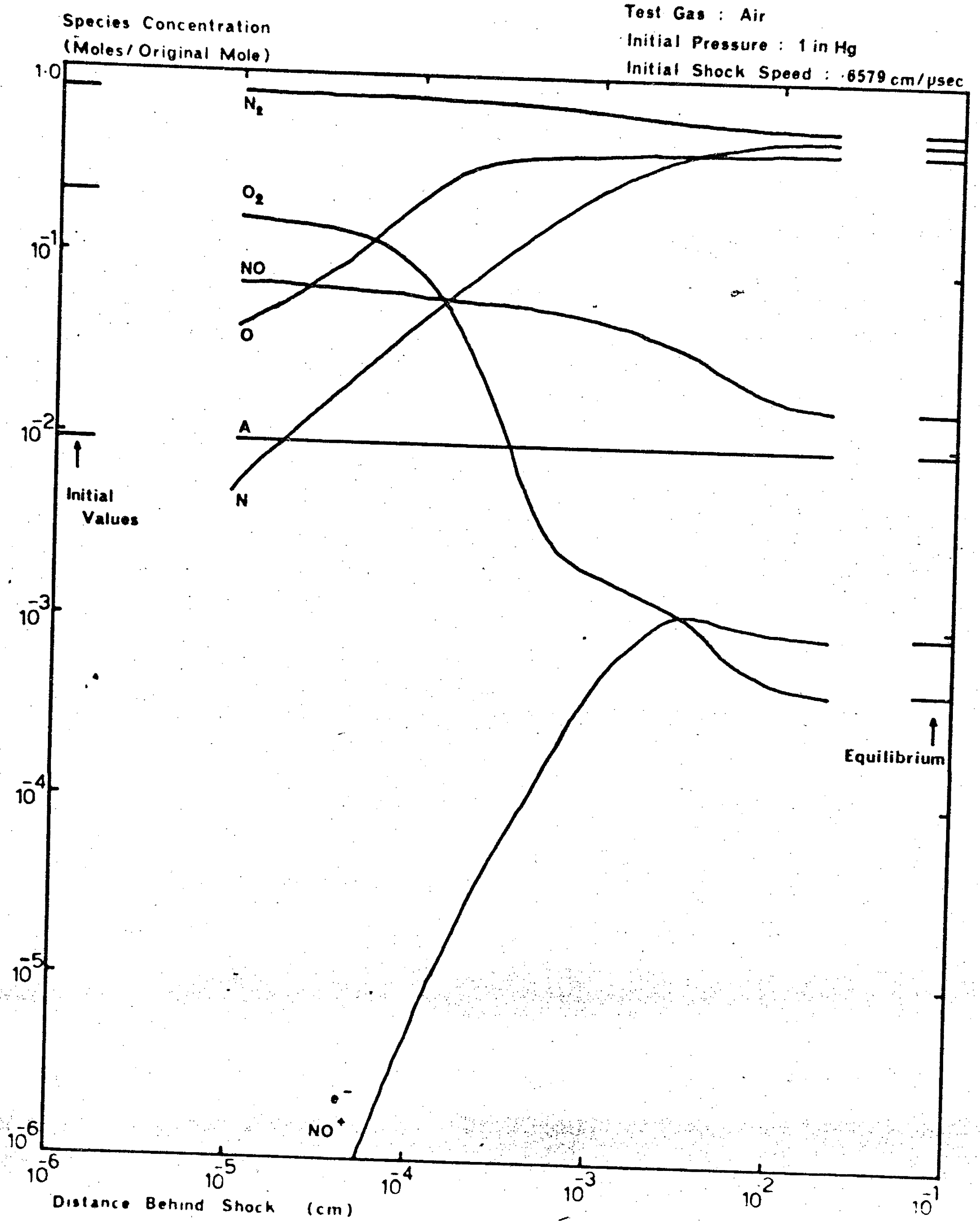

Figure No. 11. Species Concentrations behind an Incident Shock Wave in Air

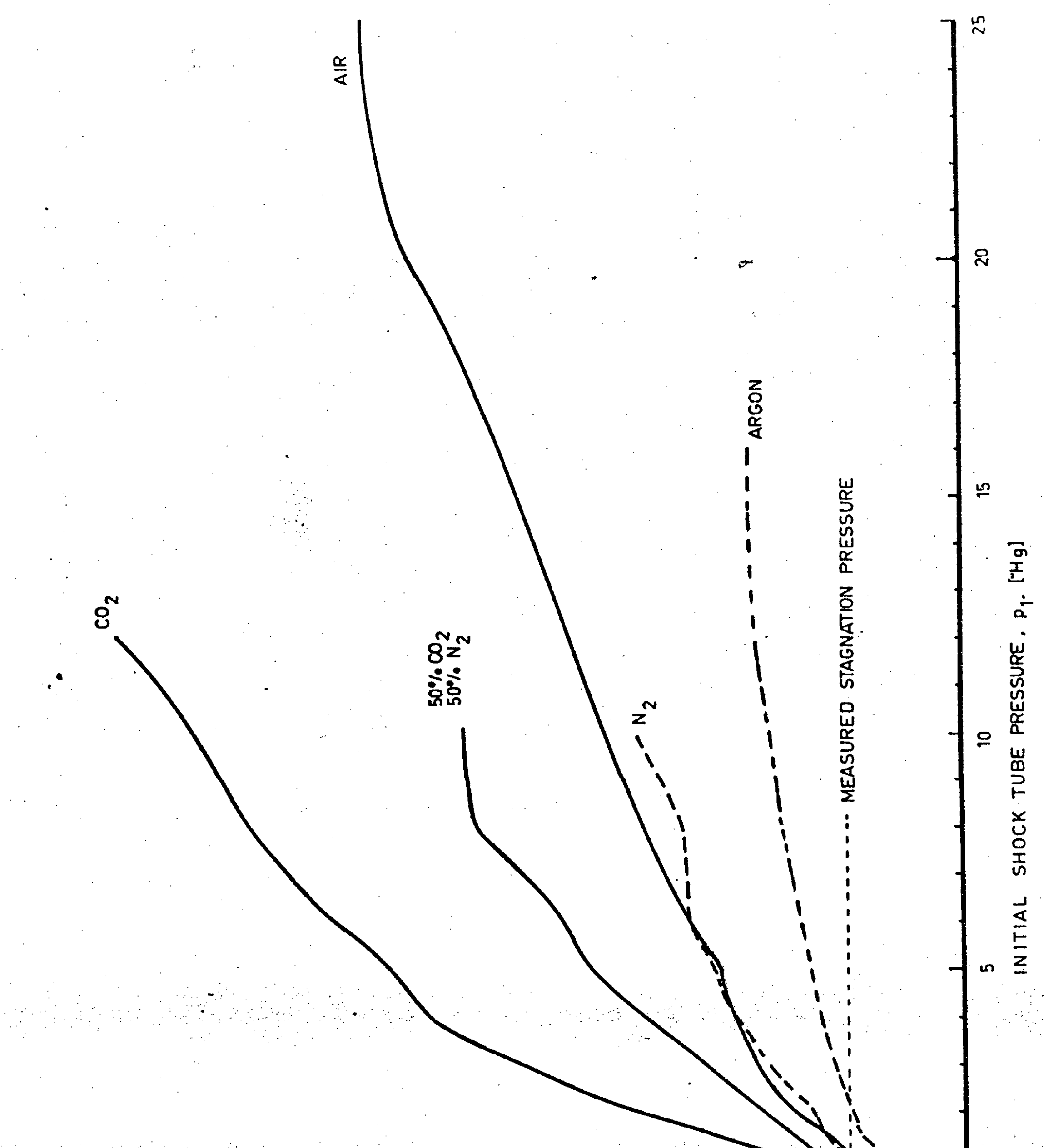

Figure No. 12. Pressure in the Nozzle Reservoir in T.2

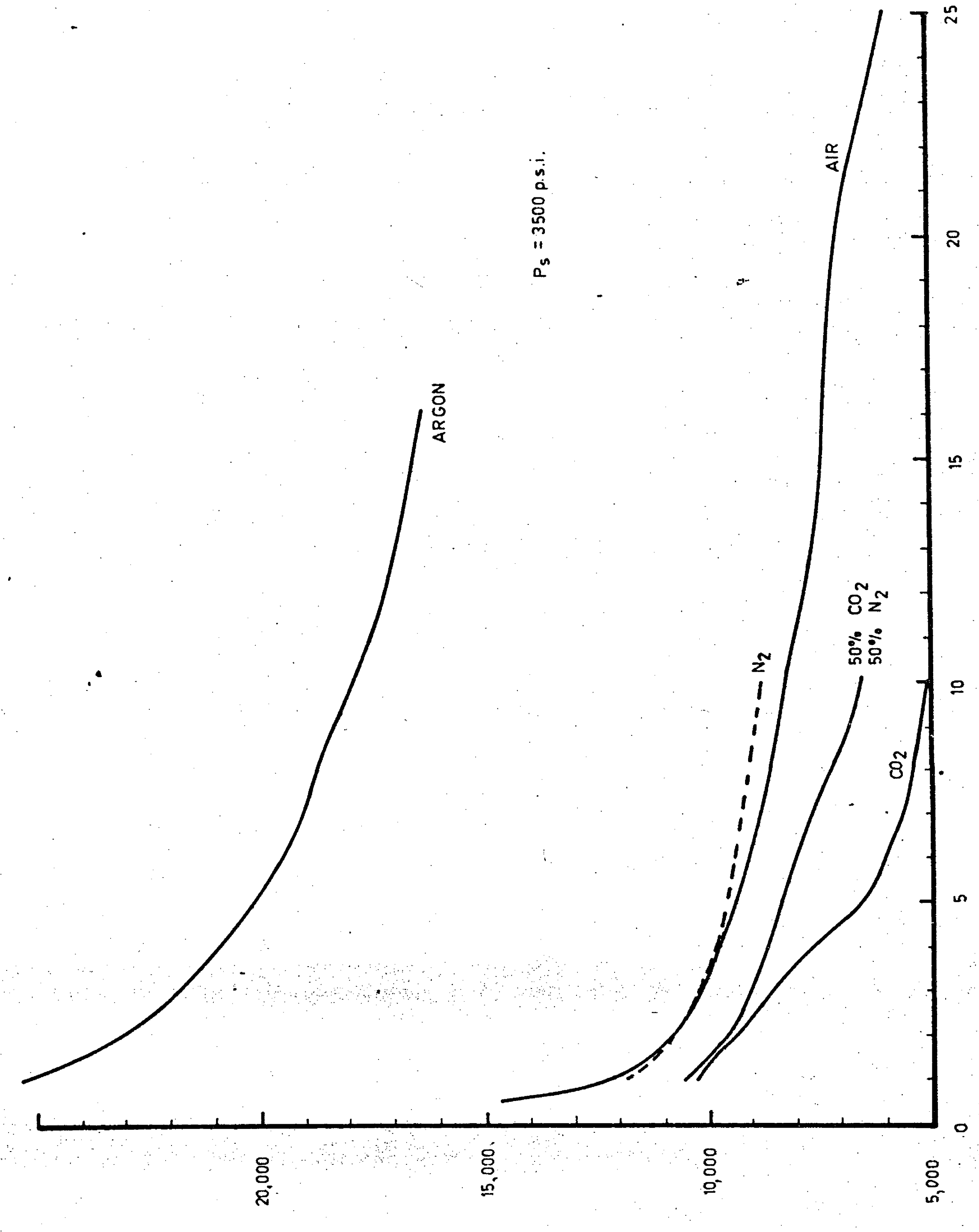

Figure No. 13 Temperature in the Nozzle Reservoir in T.2

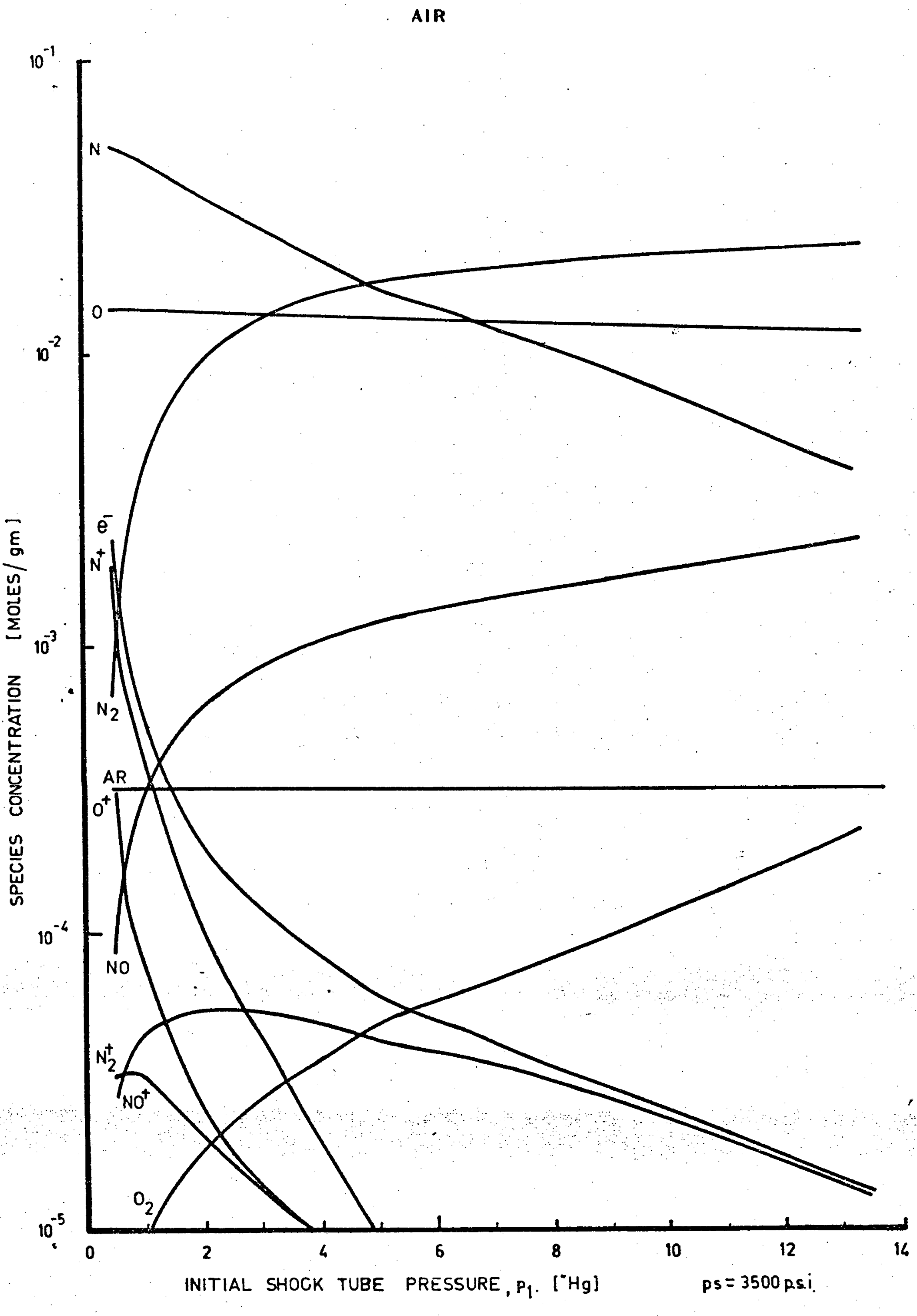

Figure No. 14 Species Concentrations in the Nozzle Reservoir in Air in T.2

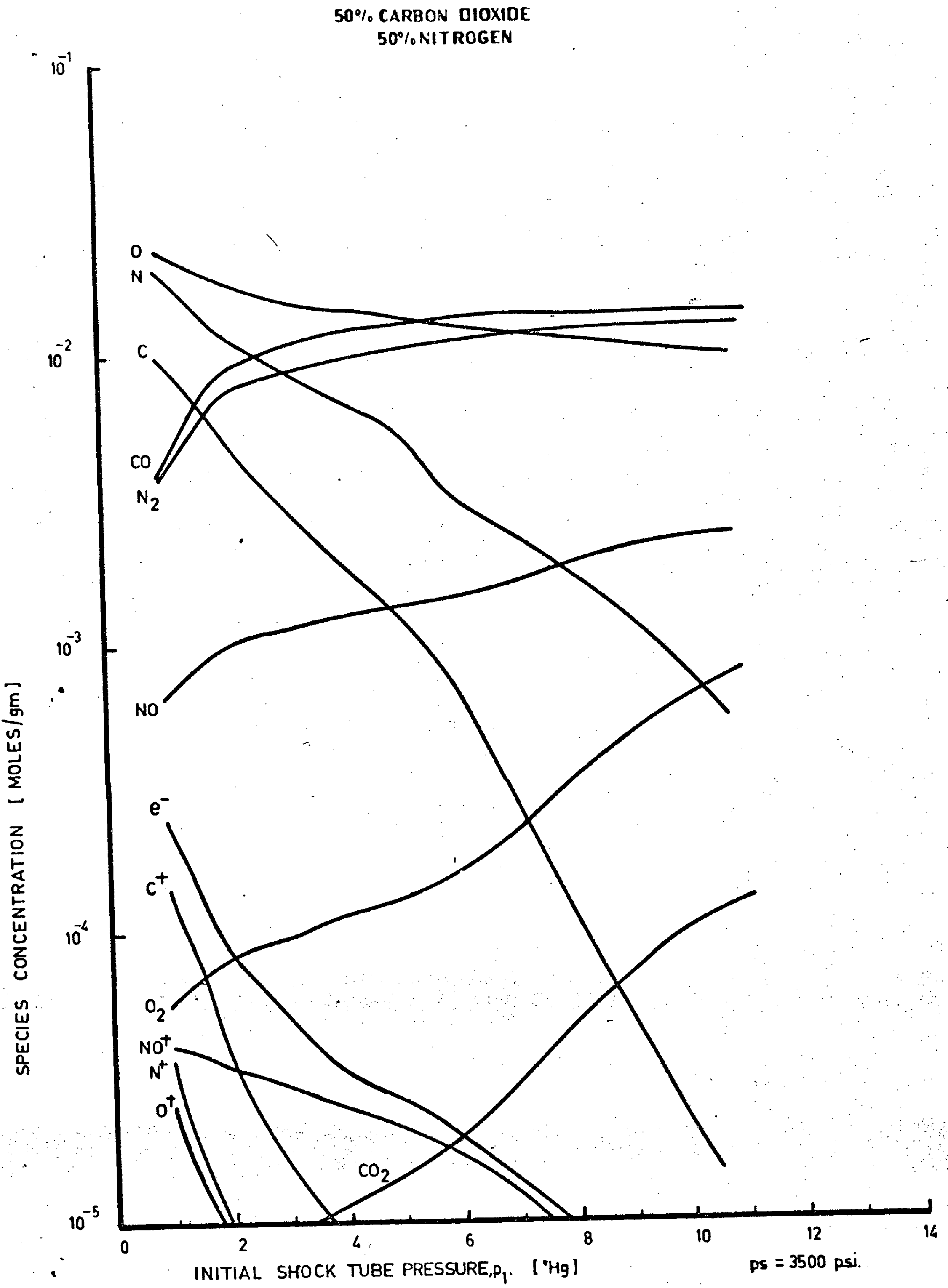

Figure 15. Species Concentrations in the Nozzle Reservoir in 50% N_2, 50% CO_2 in T.2

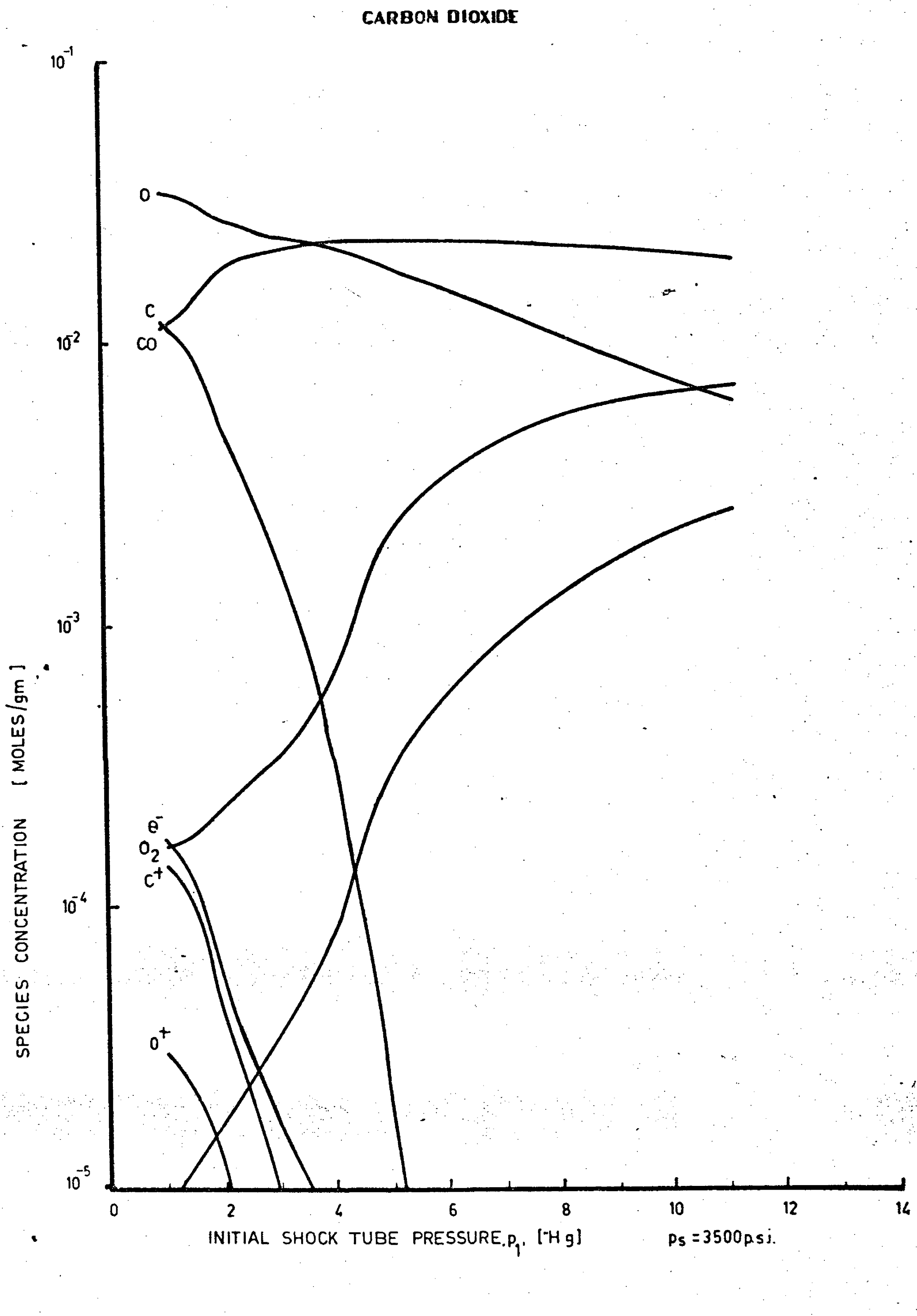

Figure No. 16 Species Concentrations in the Nozzle Reservoir in Carbon Dioxide in T.2

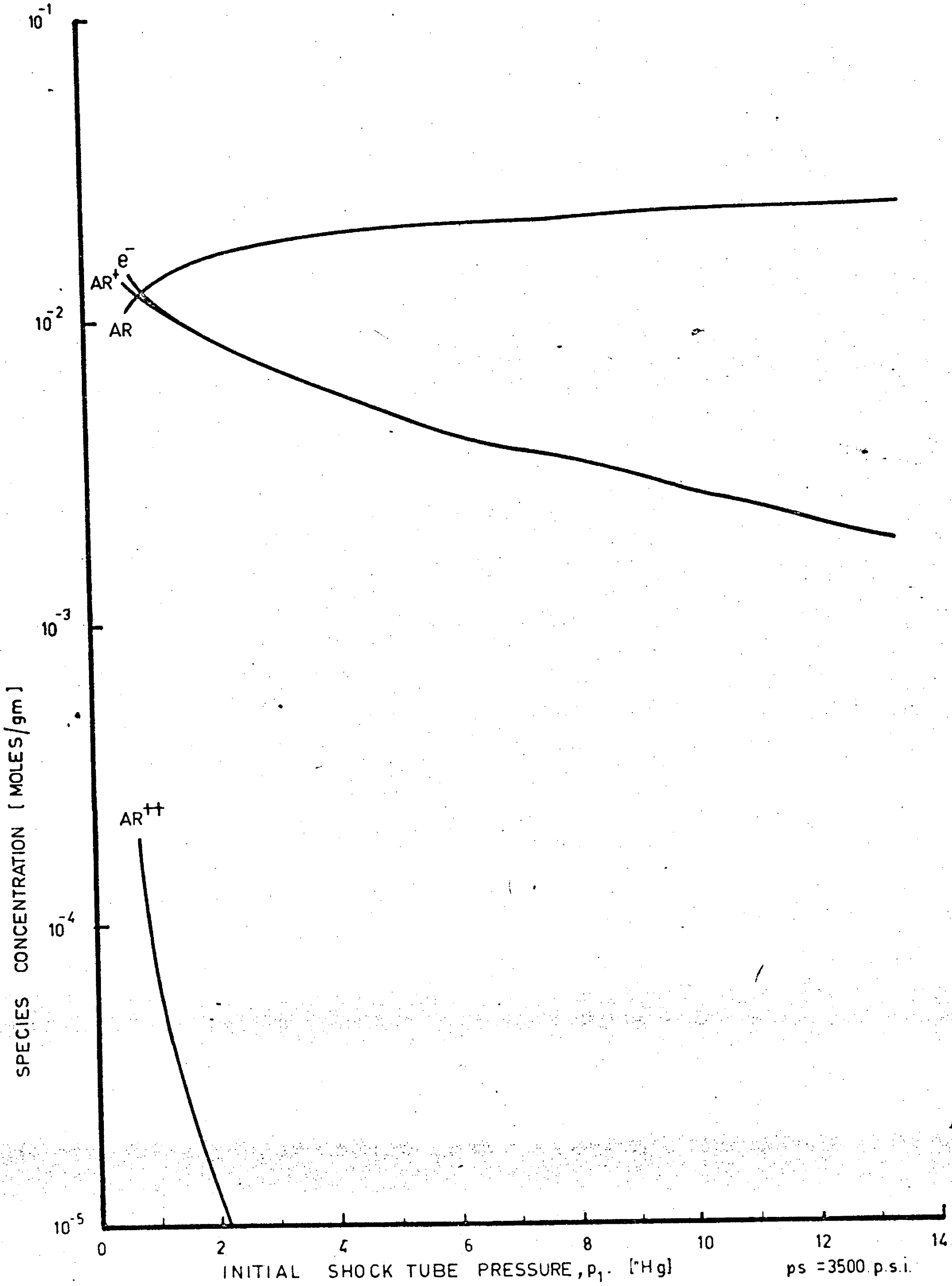

Figure No. 17. Species Concentrations in the Nozzle Reservoir in Argon in T.2

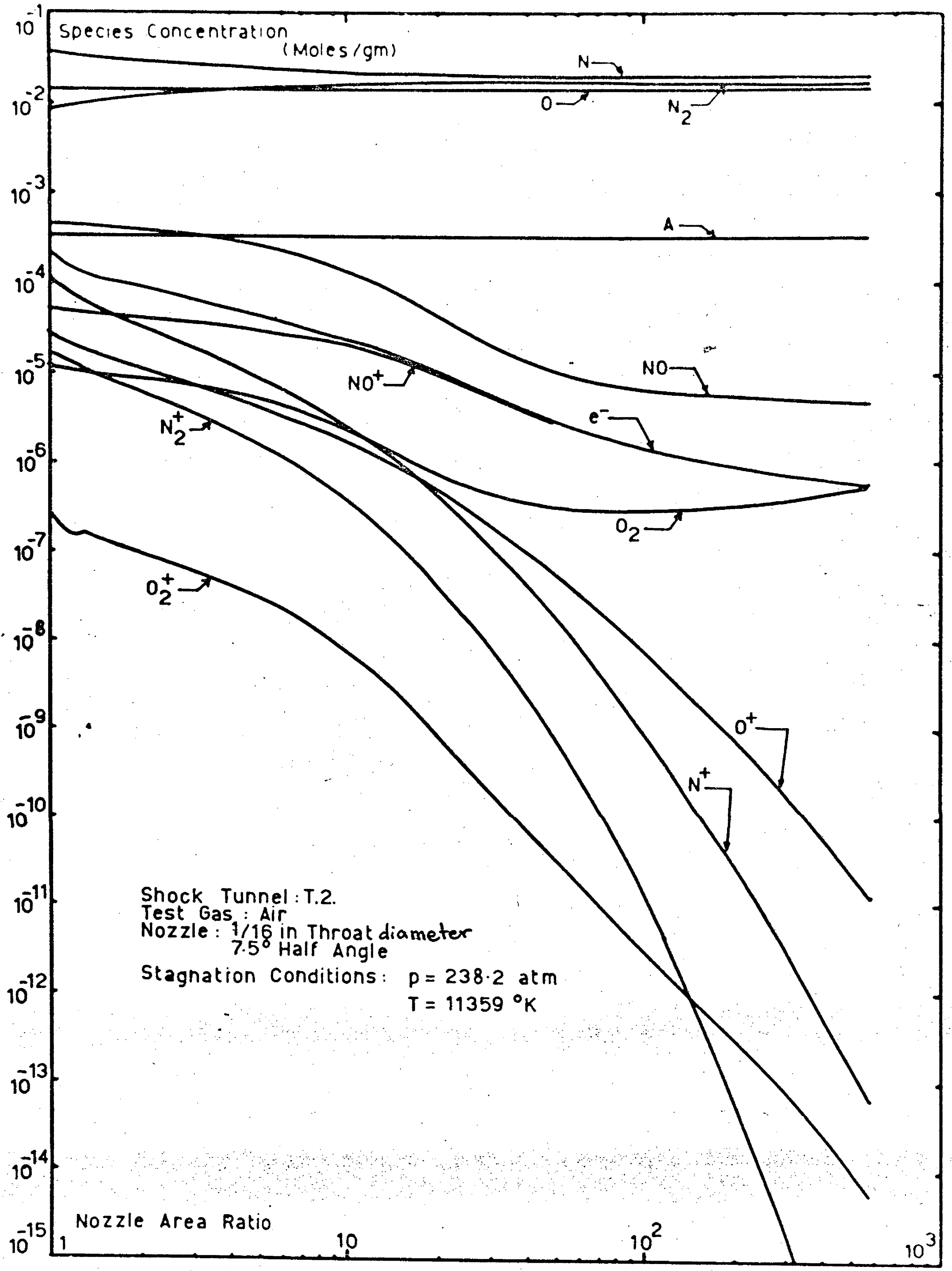

Figure No. 18 Species Concentrations in a Nozzle Expansion in Air in T.2

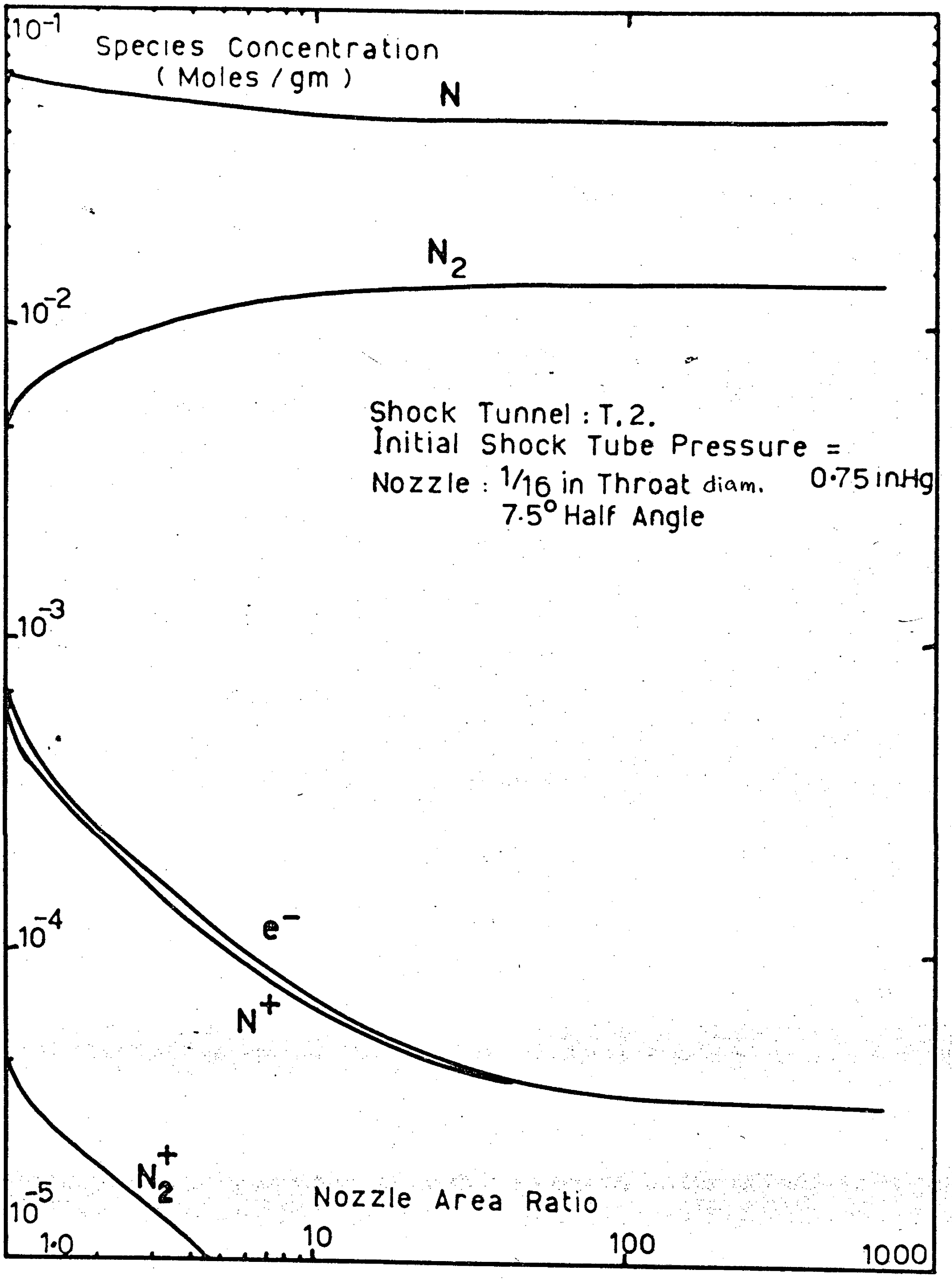

Figure 19 Species Concentrations in a Nozzle Expansion in Nitrogen in T.2

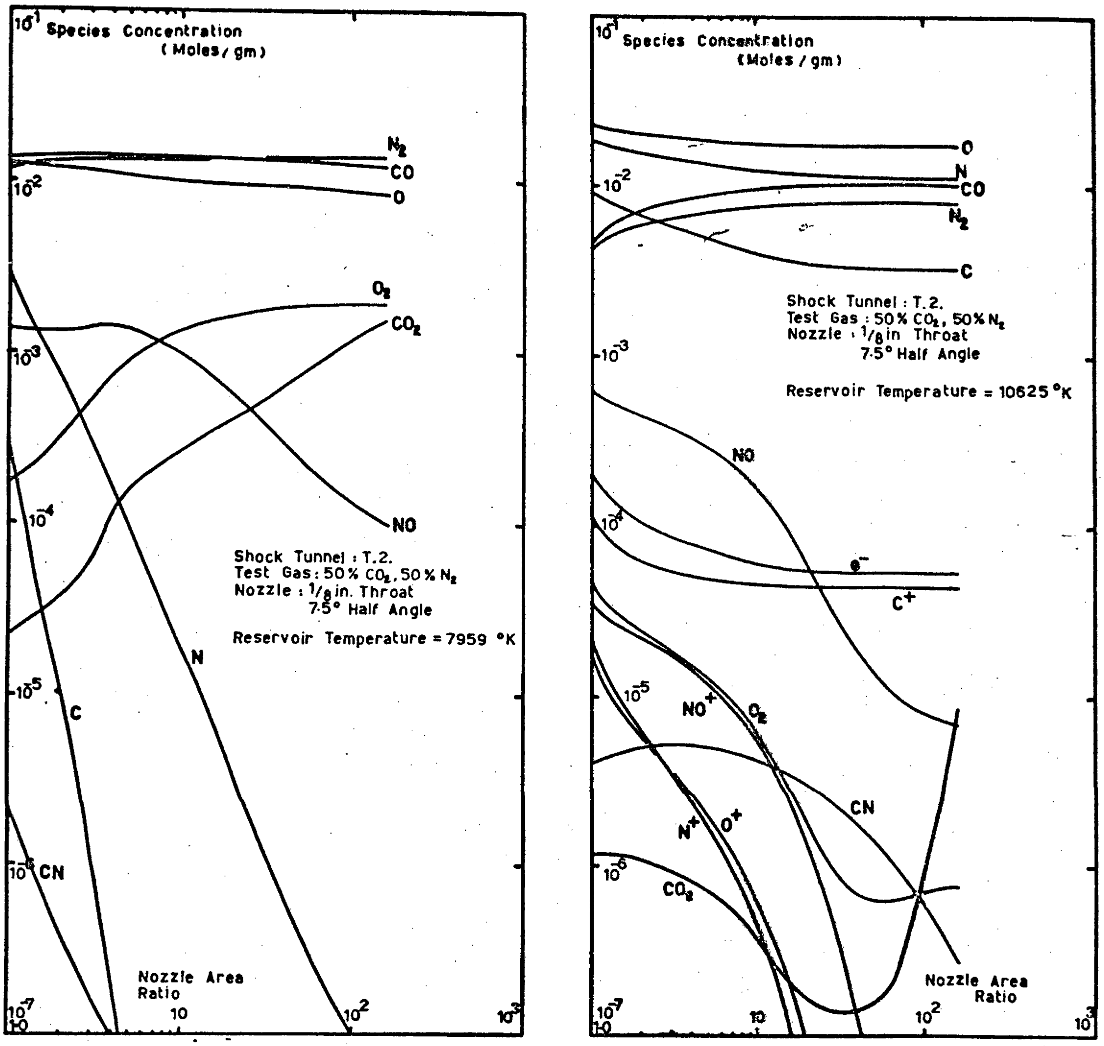

Figure No. 20. Species Concentrations in a Nozzle Expansion in 50% N_2, 50% CO_2 in T.2

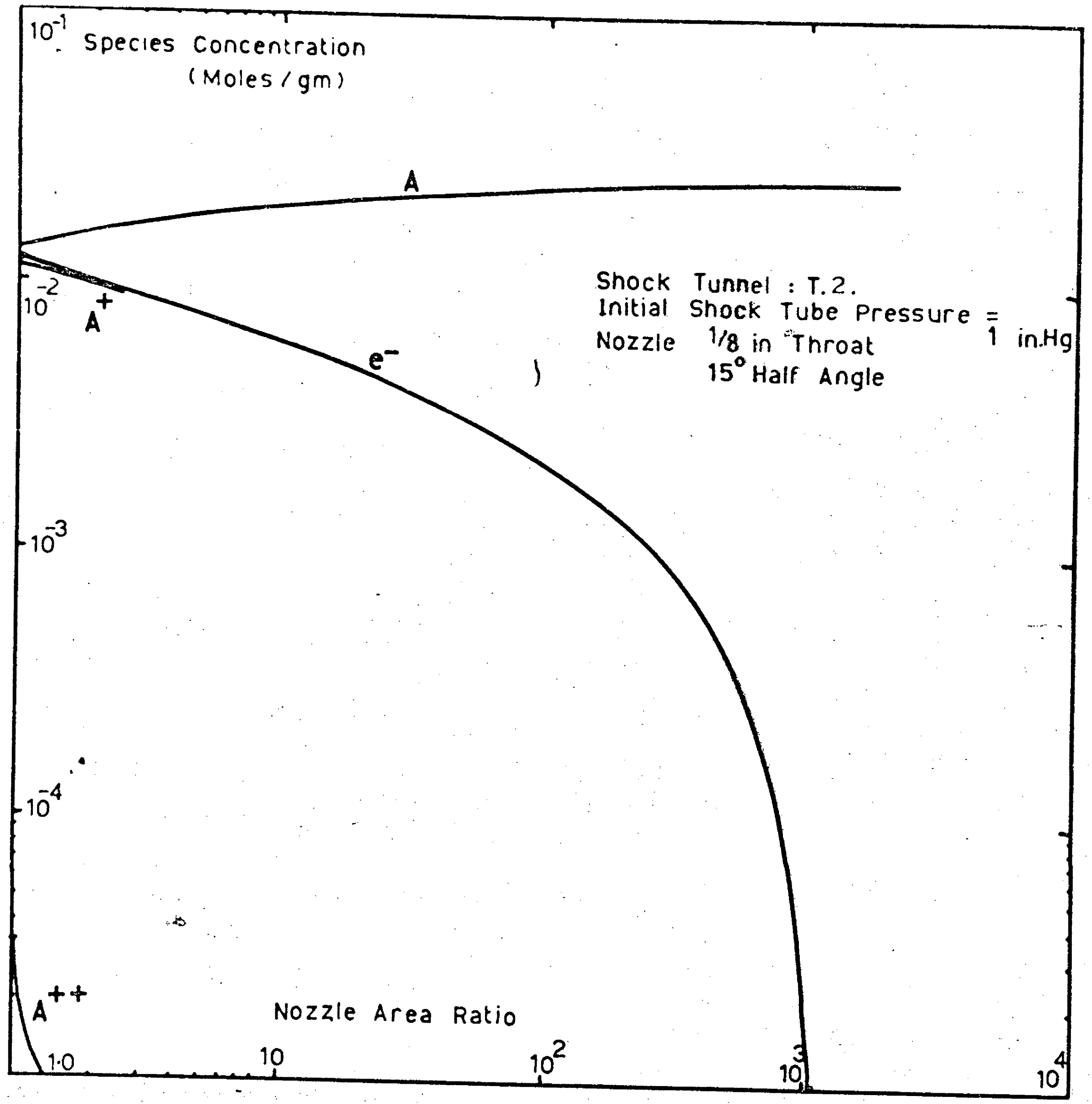

Figure No. 21. Species Concentrations in a Nozzle Expansion in Argon in T.2

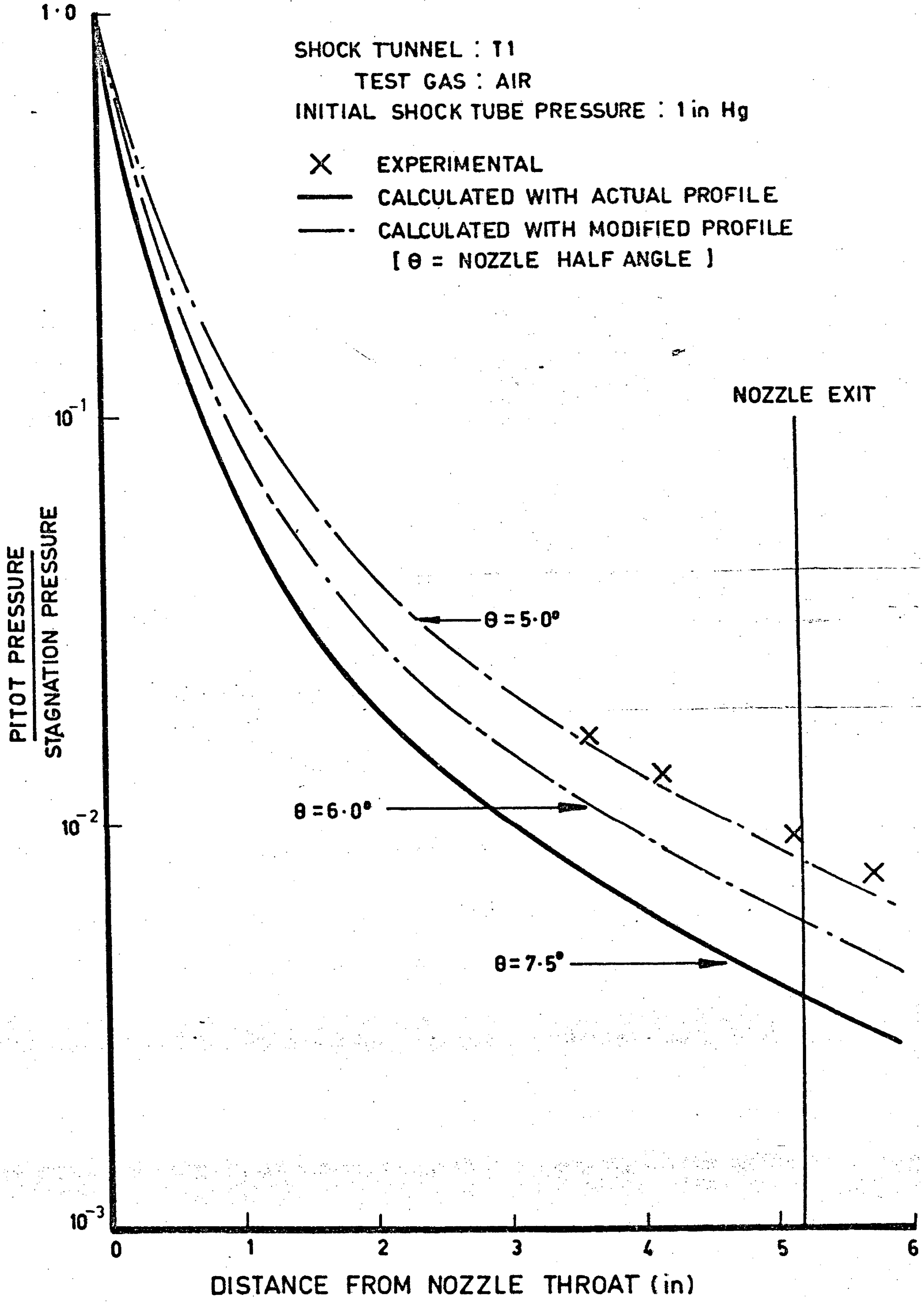

Figure No. 22 Axial Pitot Pressure Survey in T.1

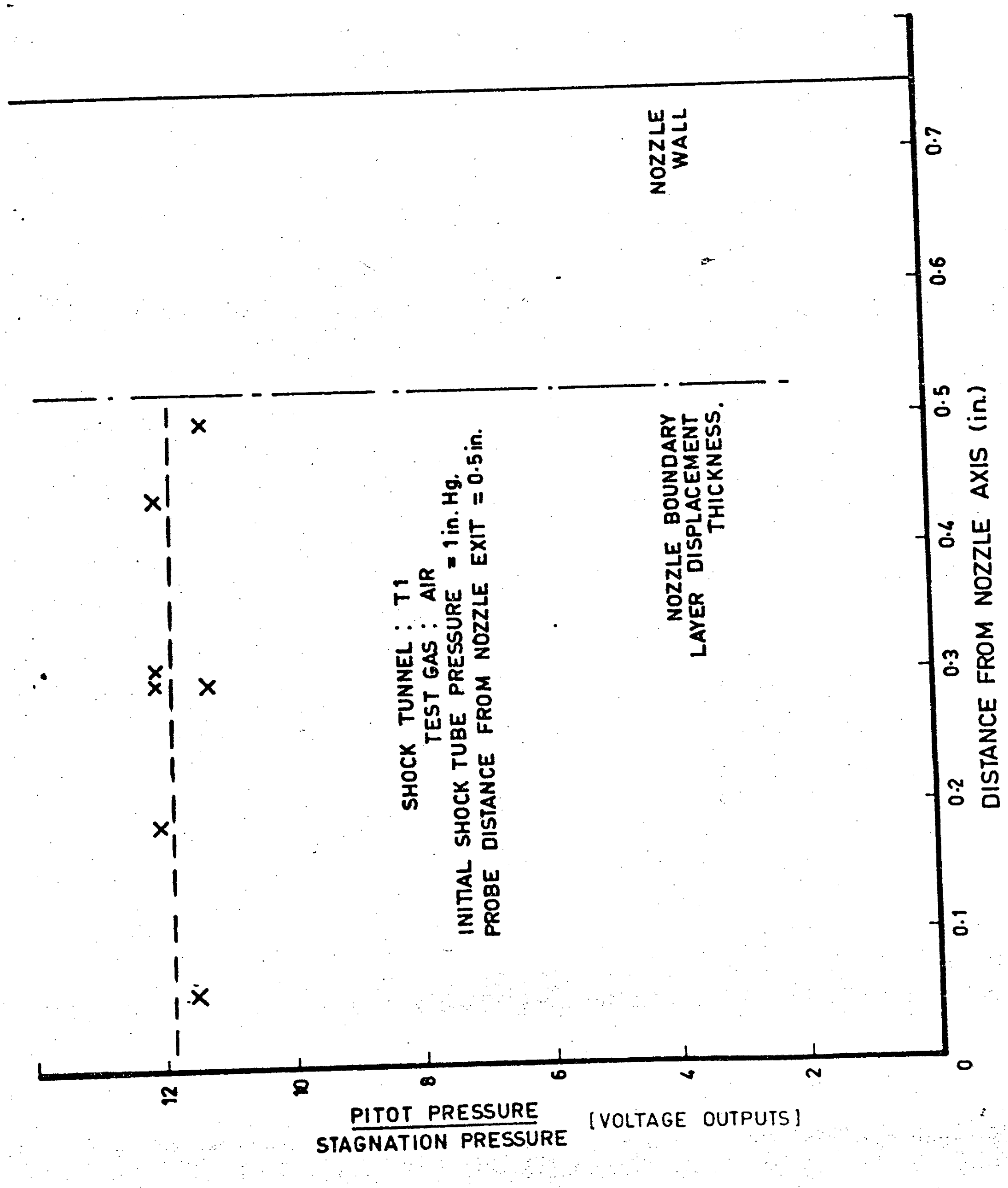

Figure No. 23 Radial Pitot Pressure Survey in T.1

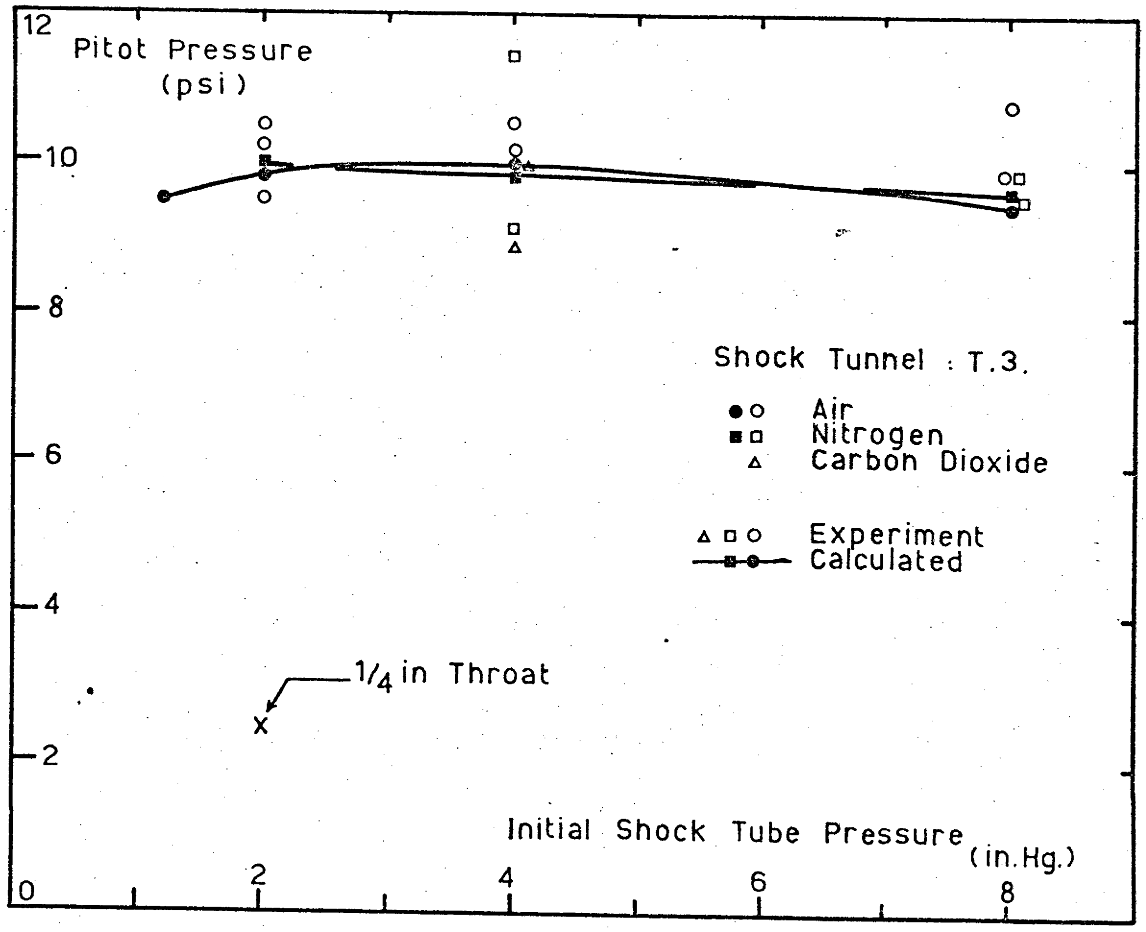

Figure No. 24. Pitot Pressure in T.3

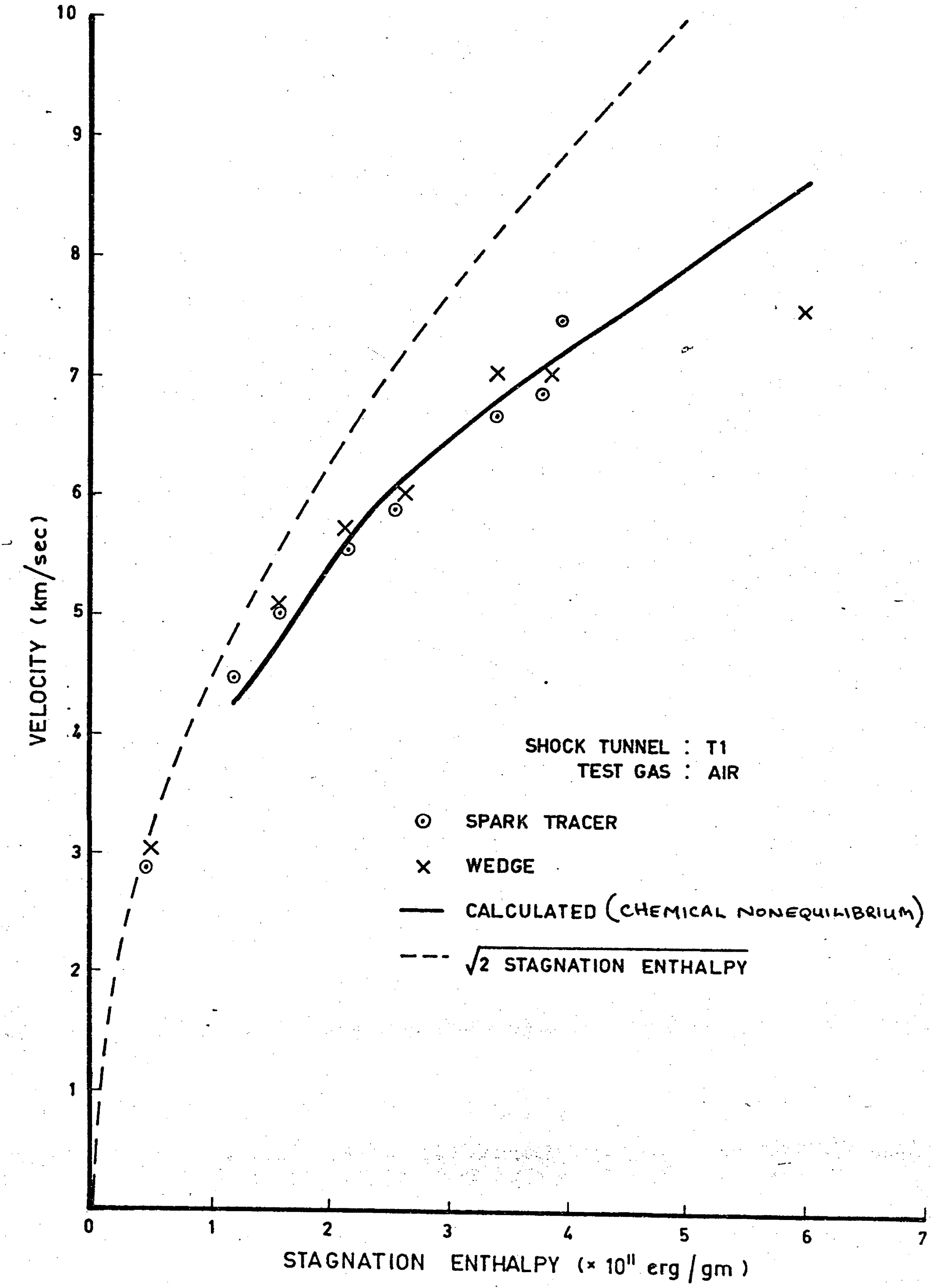

Figure No. 25. Free Stream Velocity in T.1

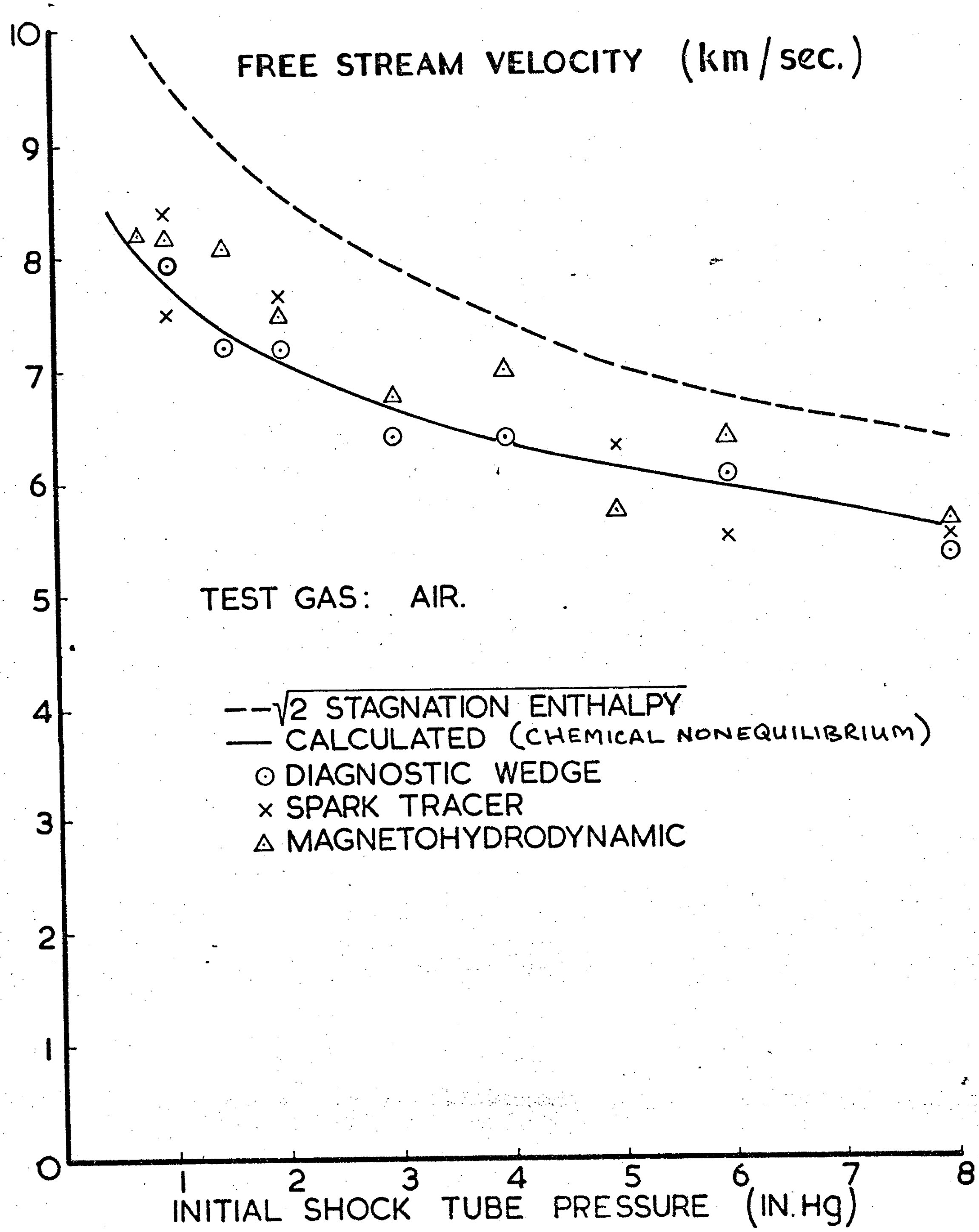

Figure No. 26. Free Stream Velocity in Air in T.2

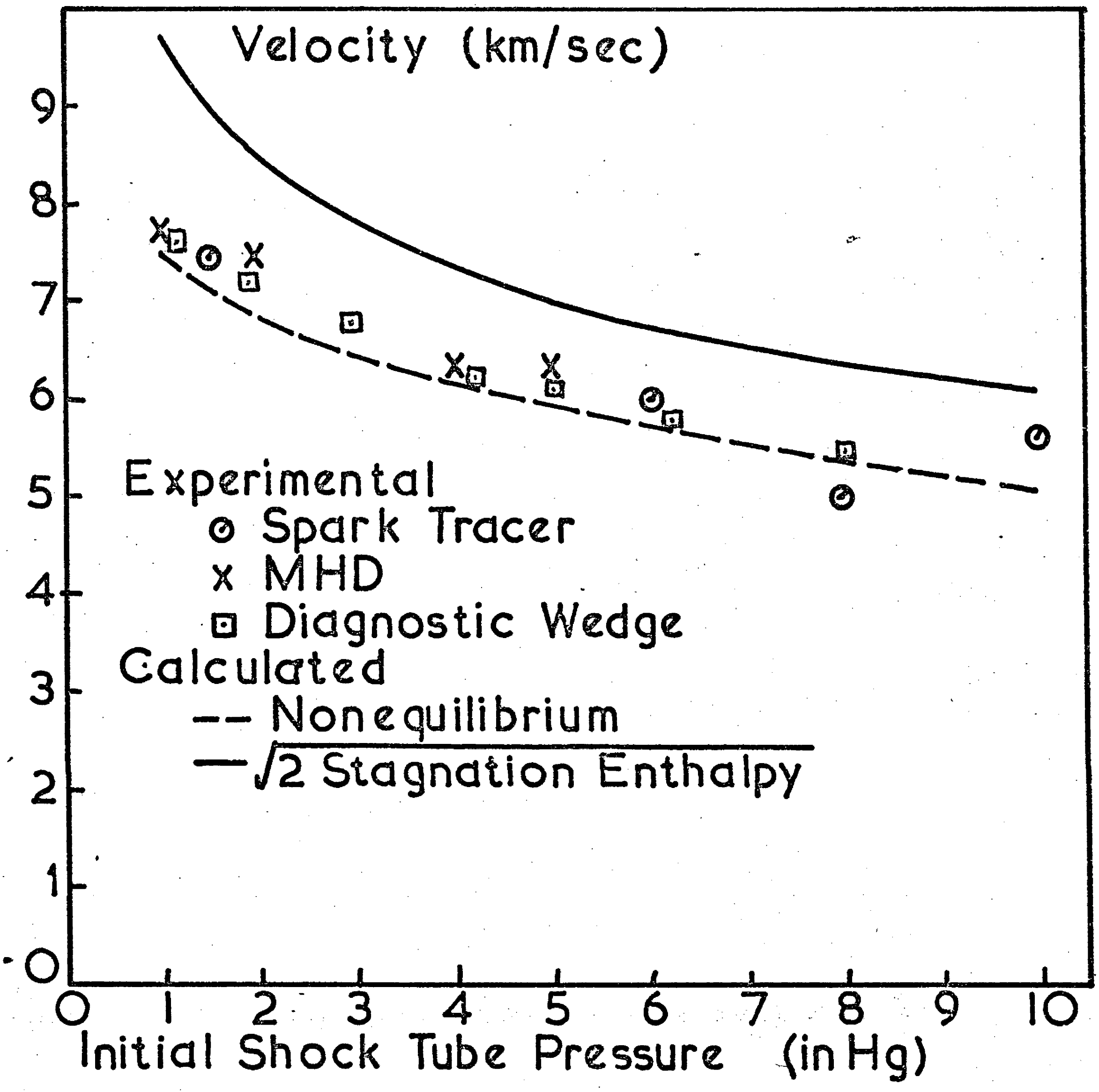

Figure No. 27 Free Stream Velocity in Nitrogen in T.2

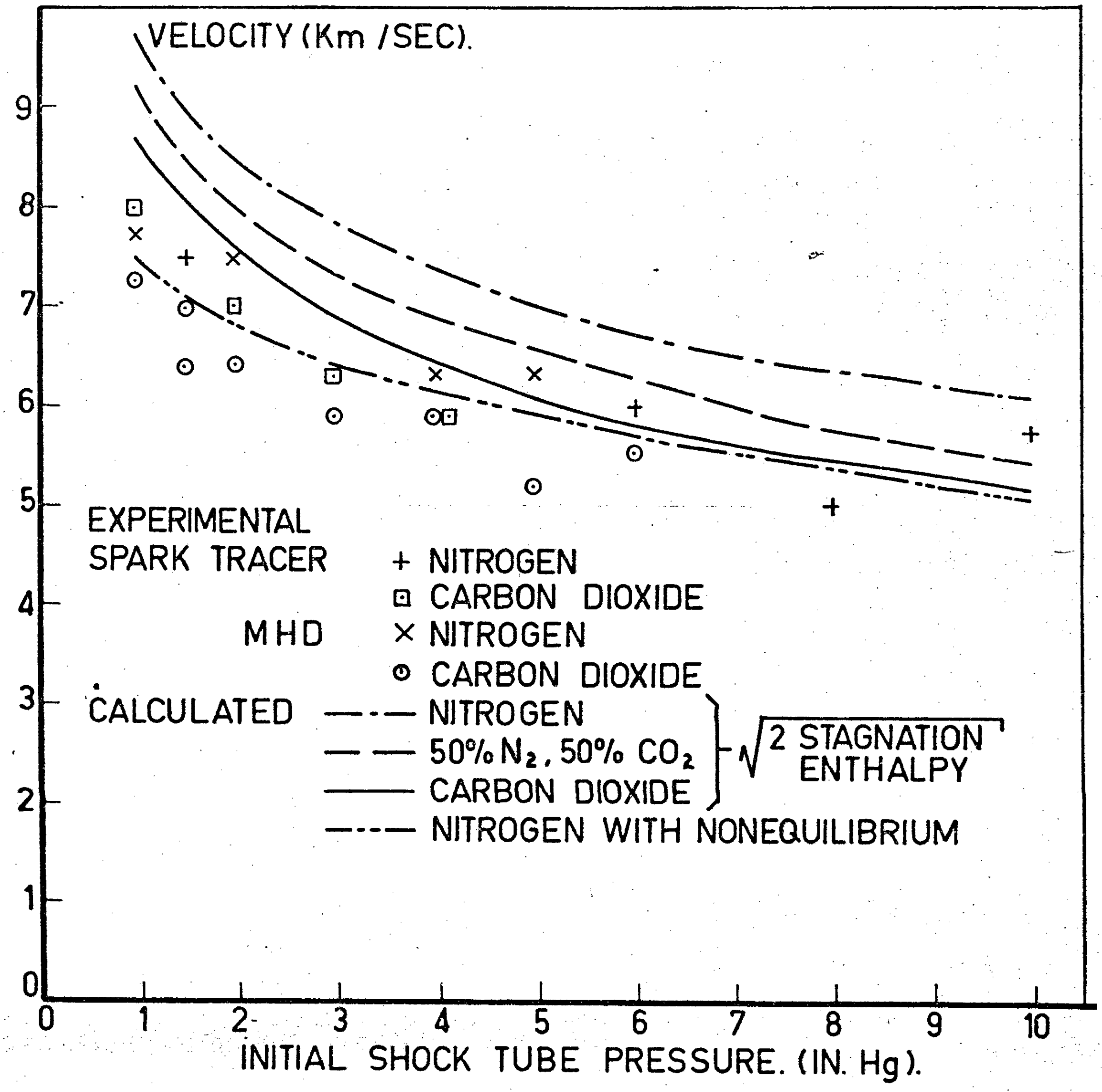

Figure No. 28 Free Stream Velocity in Carbon Dioxide in T.2

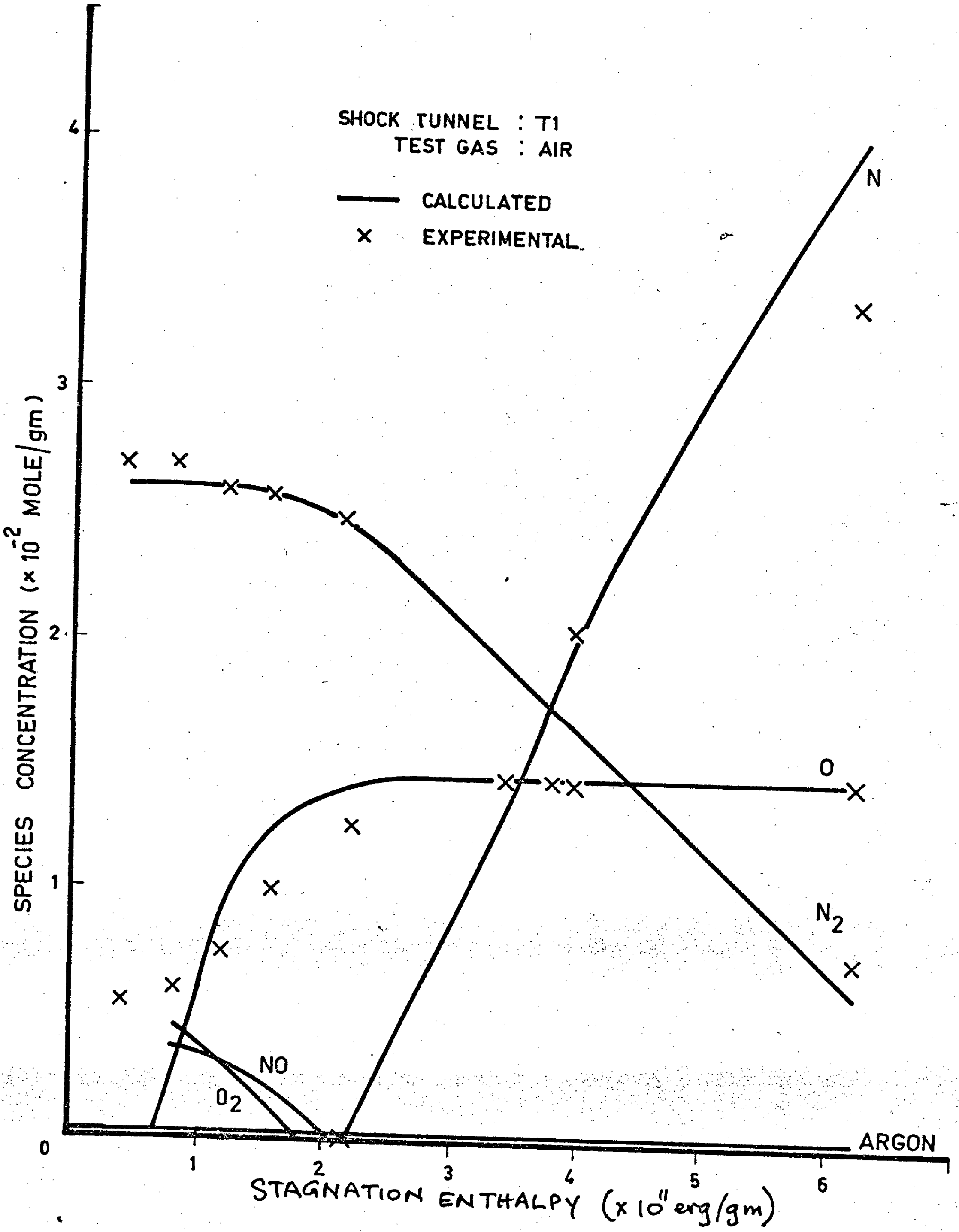

Figure No. 29 Free Stream Species Concentrations in T.1

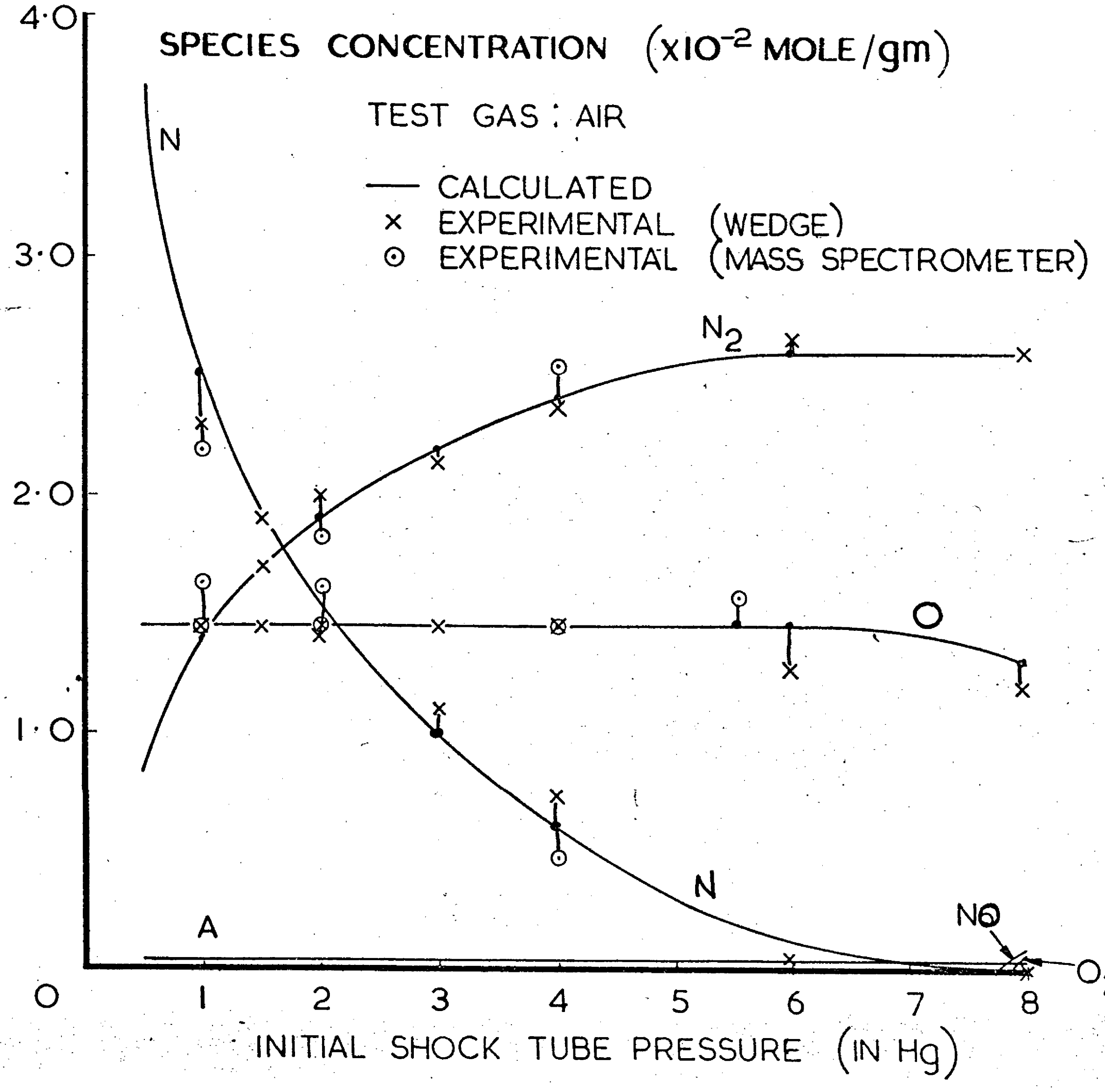

Vertical lines indicate relationship between experimental and calculated results

Figure No. 30 Free Stream Species Concentrations in Air in T.2

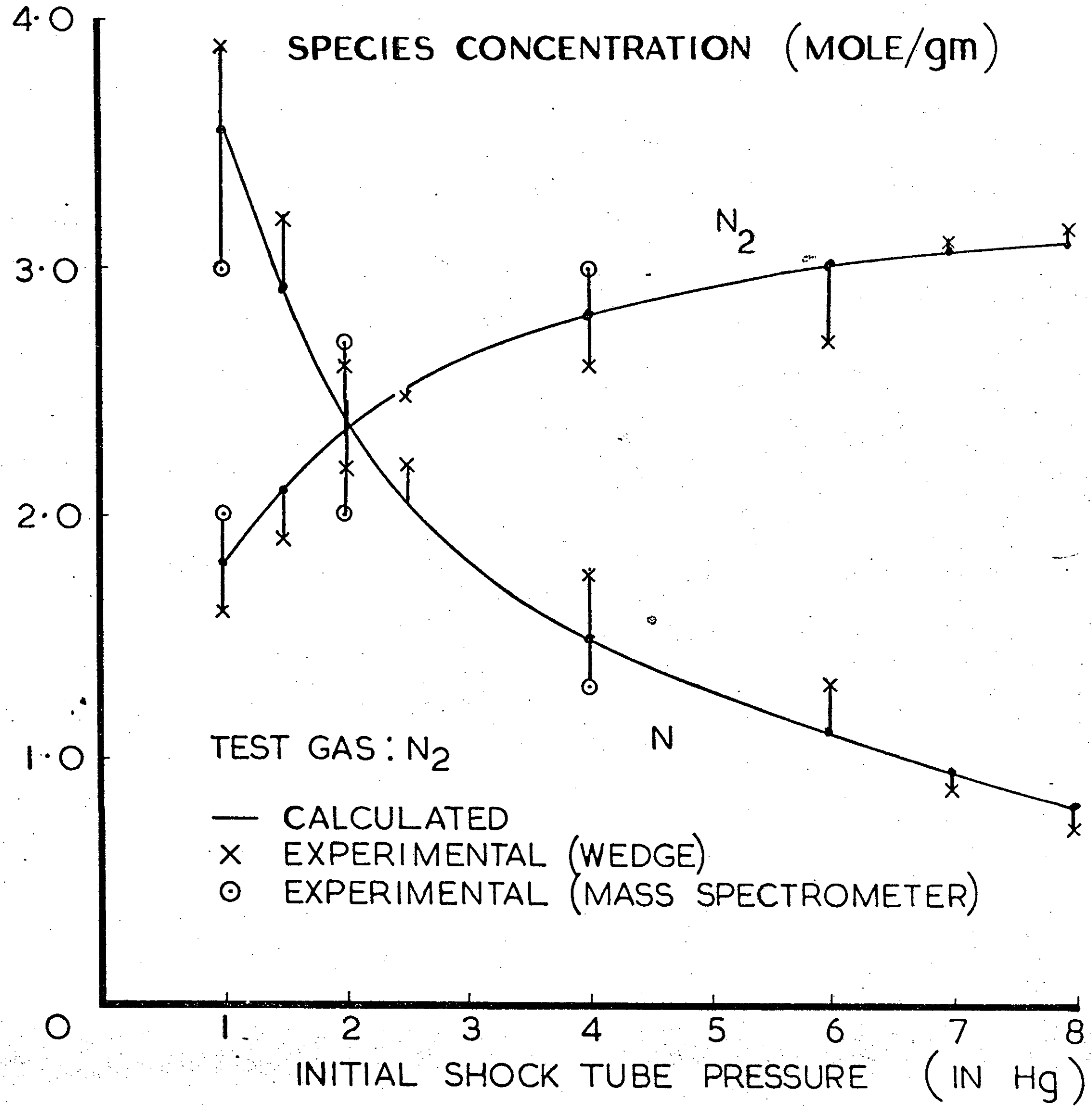

Figure No. 31 Free Stream Species Concentrations in Nitrogen in T.2

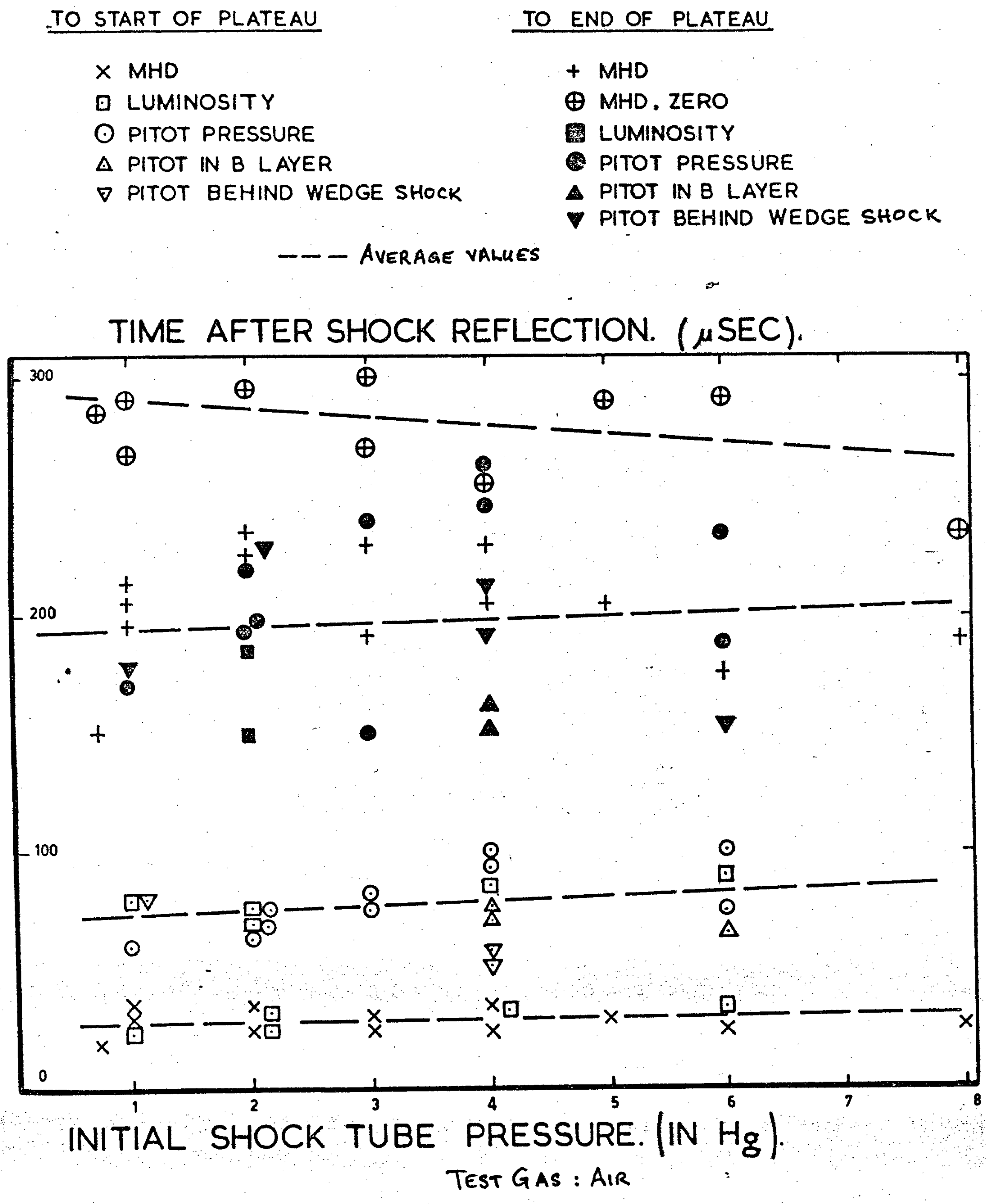

Figure No. 32 Test Time in T.2 with Large Nozzle Throat

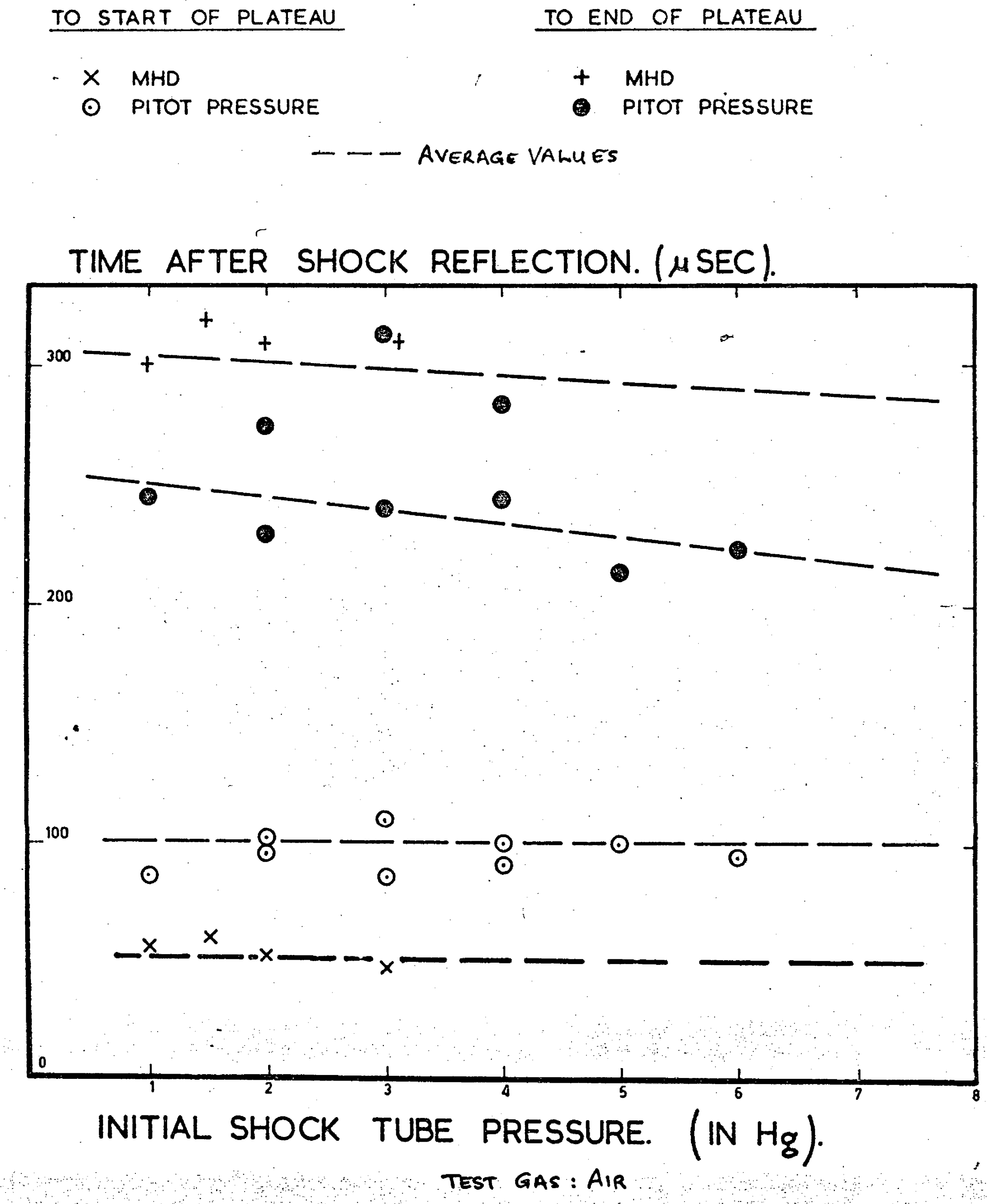

Figure No. 33 Test Time in T.2 with Small Nozzle Throat

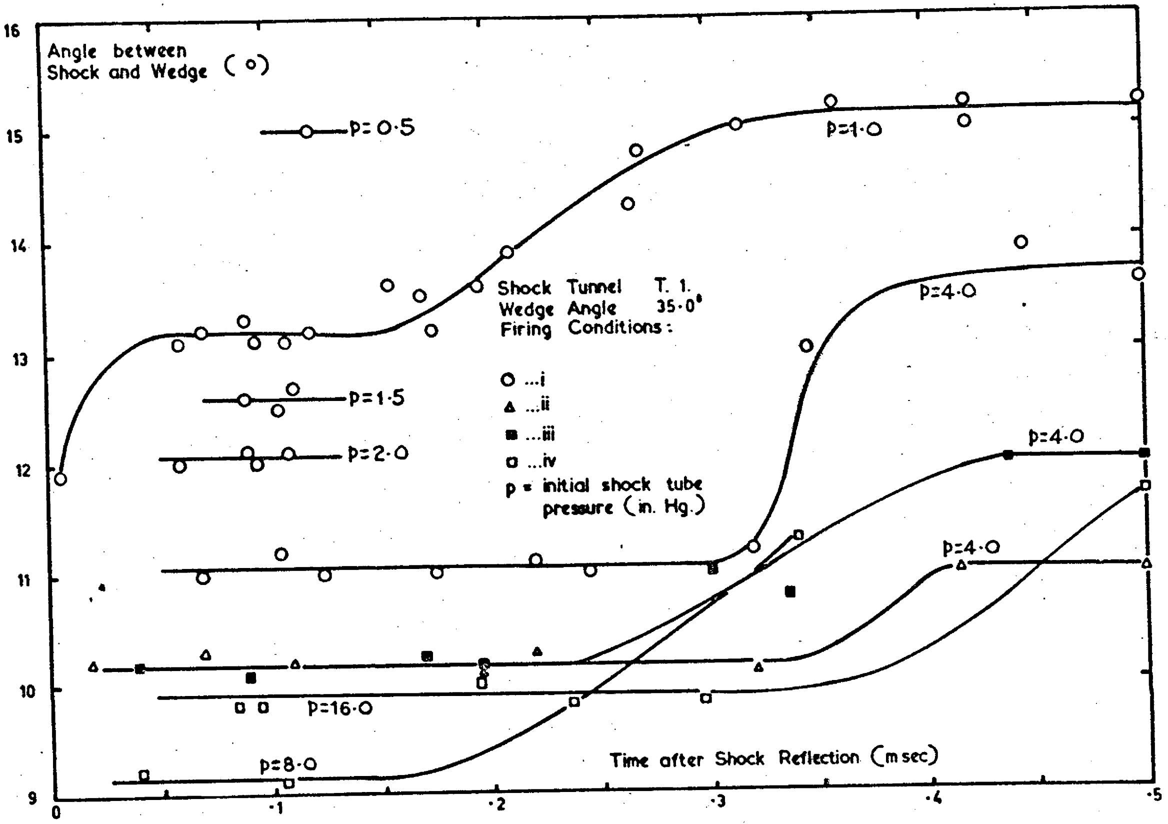

Figure No. 34 Time Resolved Wedge Shock Angles in T.1

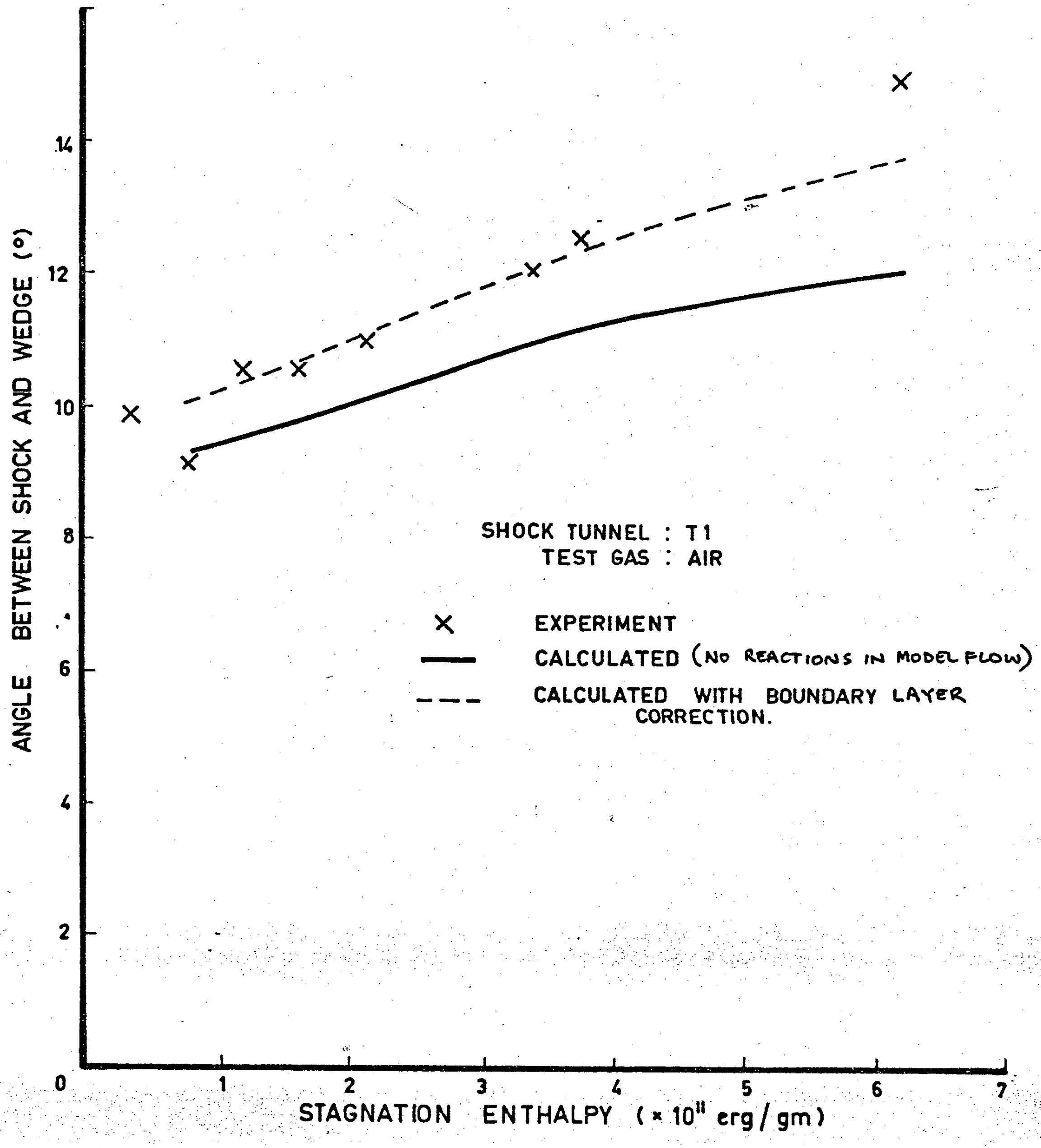

Figure No. 35   Wedge Shock Angles in T.1

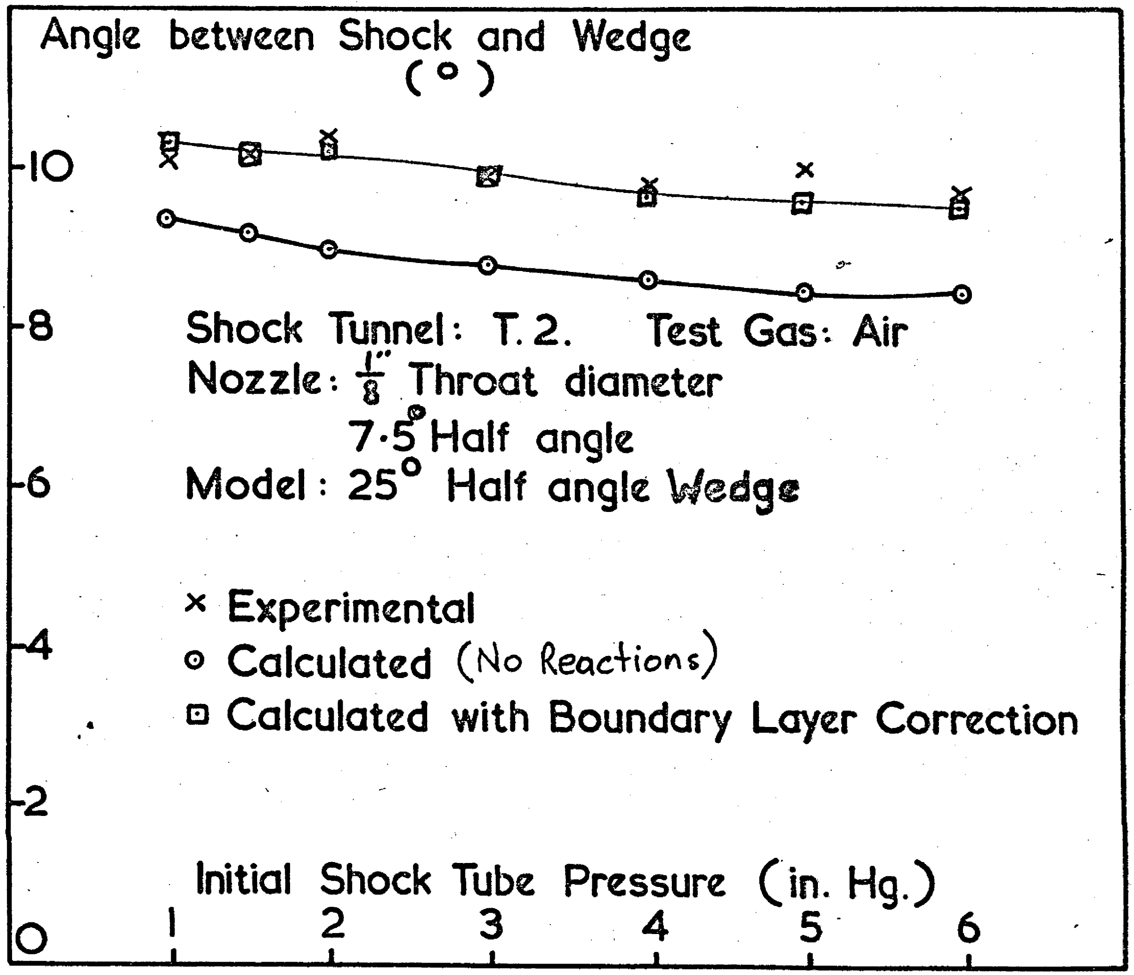

Figure No. 36 Shock Angles on a 25° Wedge in Air in T.2

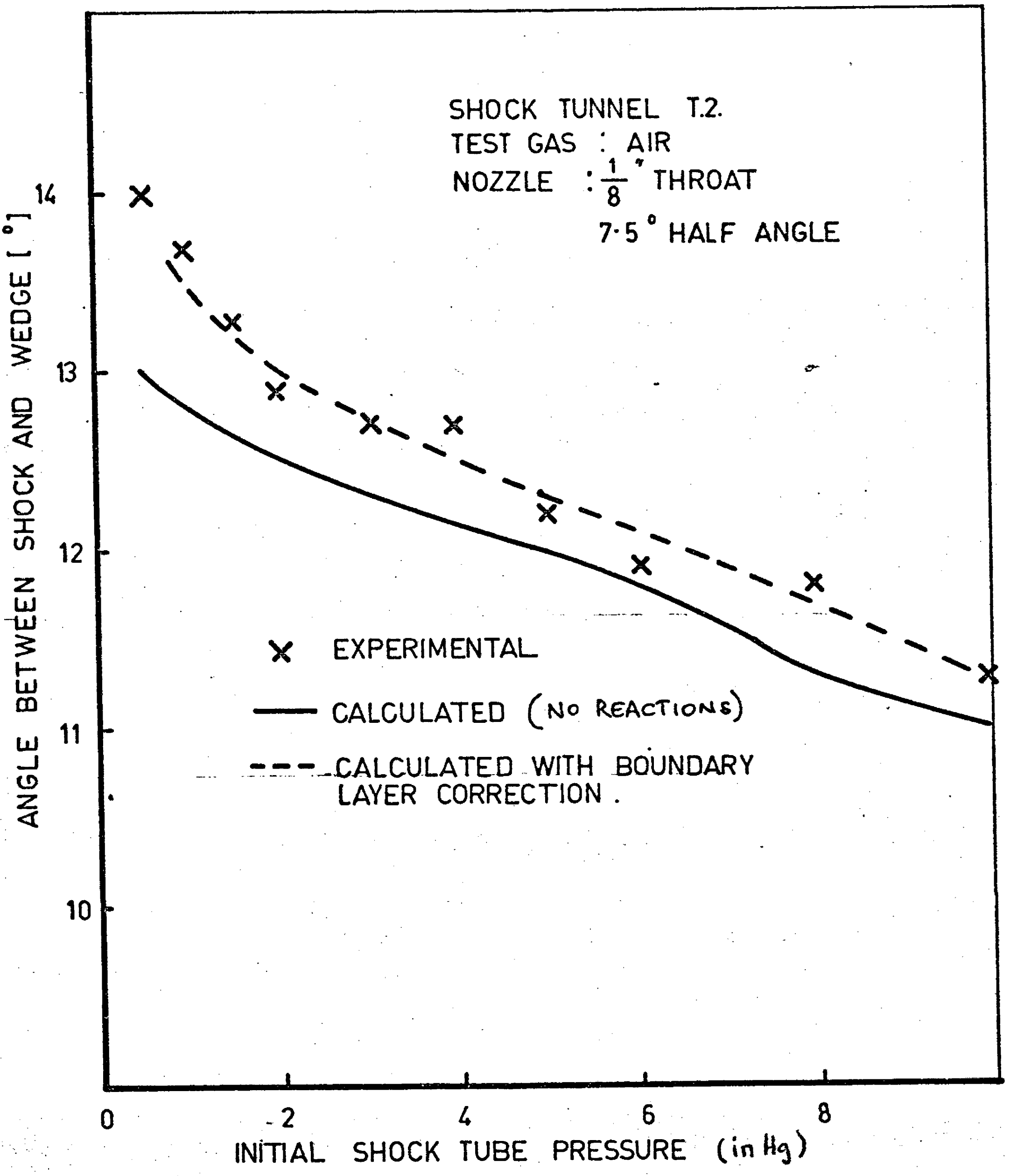

Figure No. 37 Shock Angles on a 35° Wedge in Air in T.2 with Small Nozzle Area Ratio

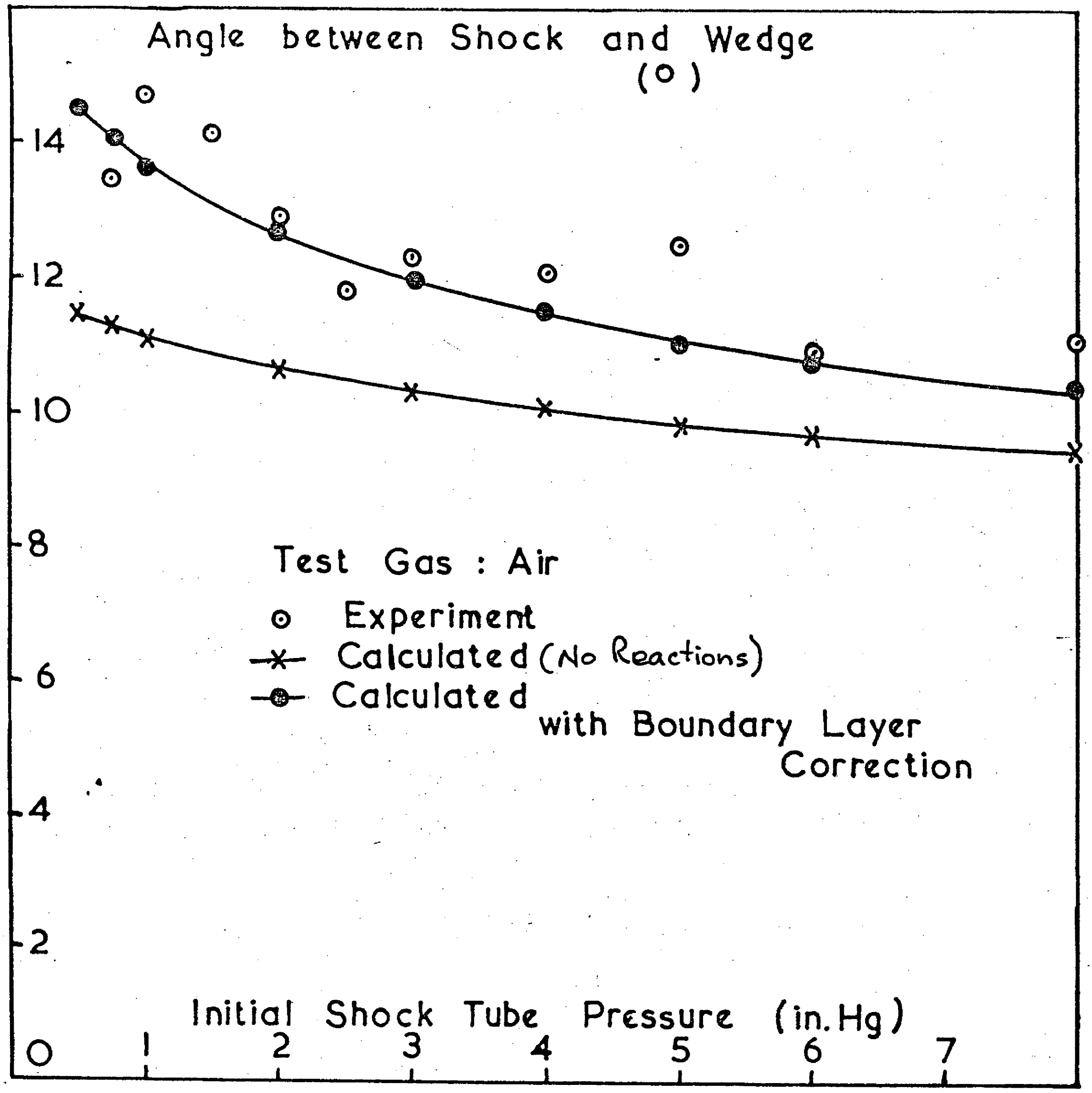

Figure No. 38 Shock Angles on a 35° Wedge in Air in T.2 with Large Nozzle Area

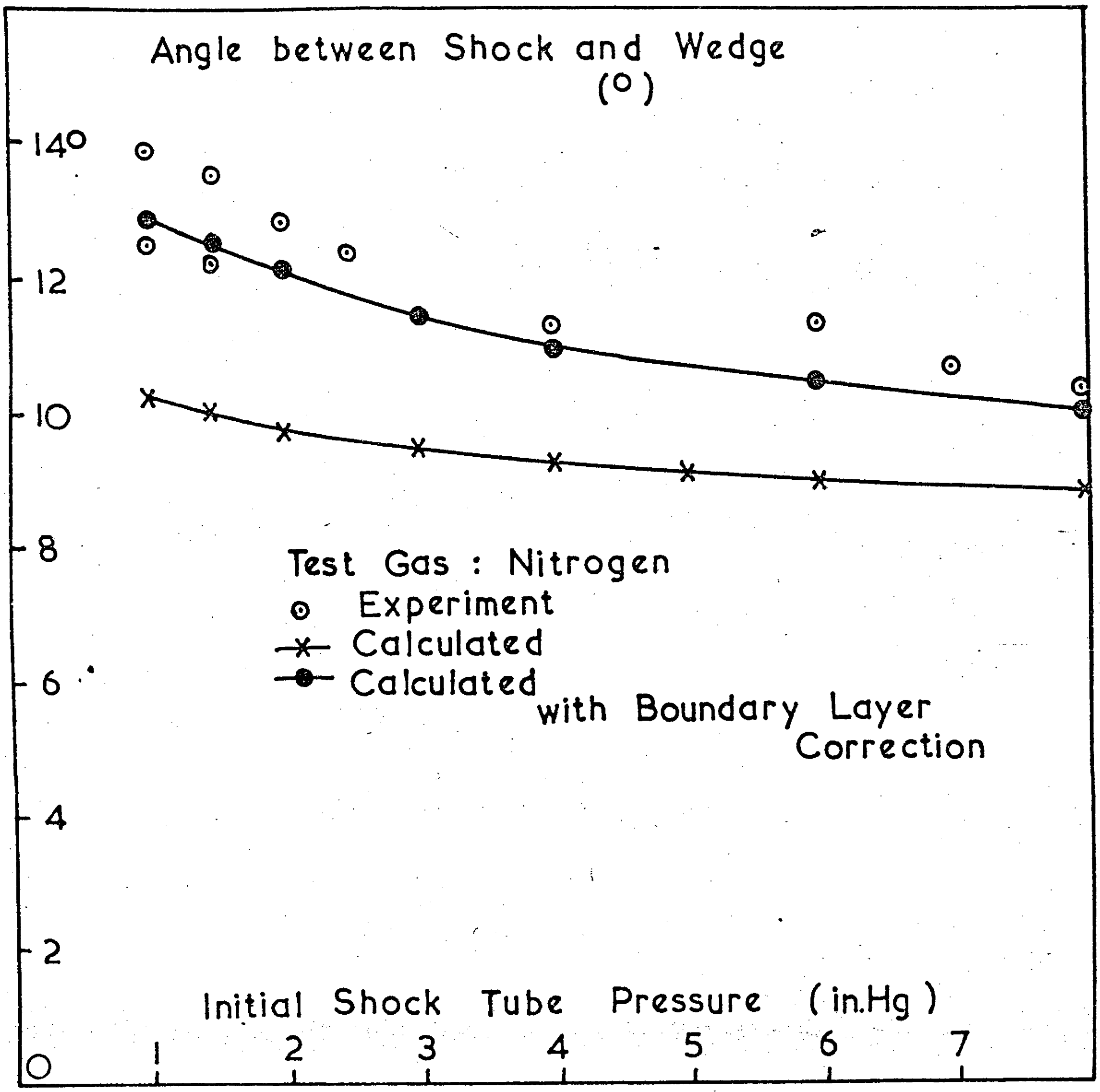

Figure No. 39 Shock angles on a 35° Wedge in Nitrogen in T.2 with Large Nozzle Area Ratio

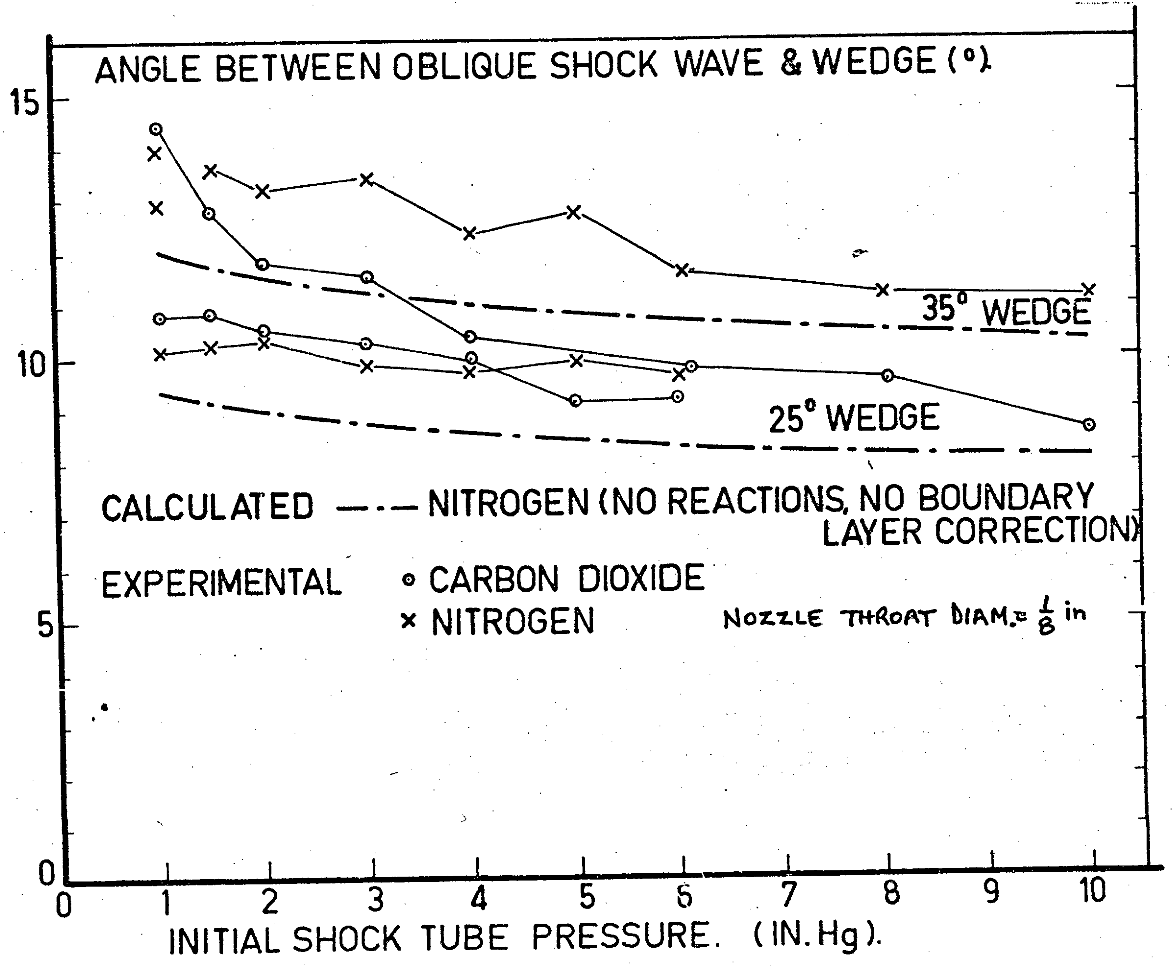

Figure No. 40 Wedge Shock Angles in Carbon Dioxide in T.2

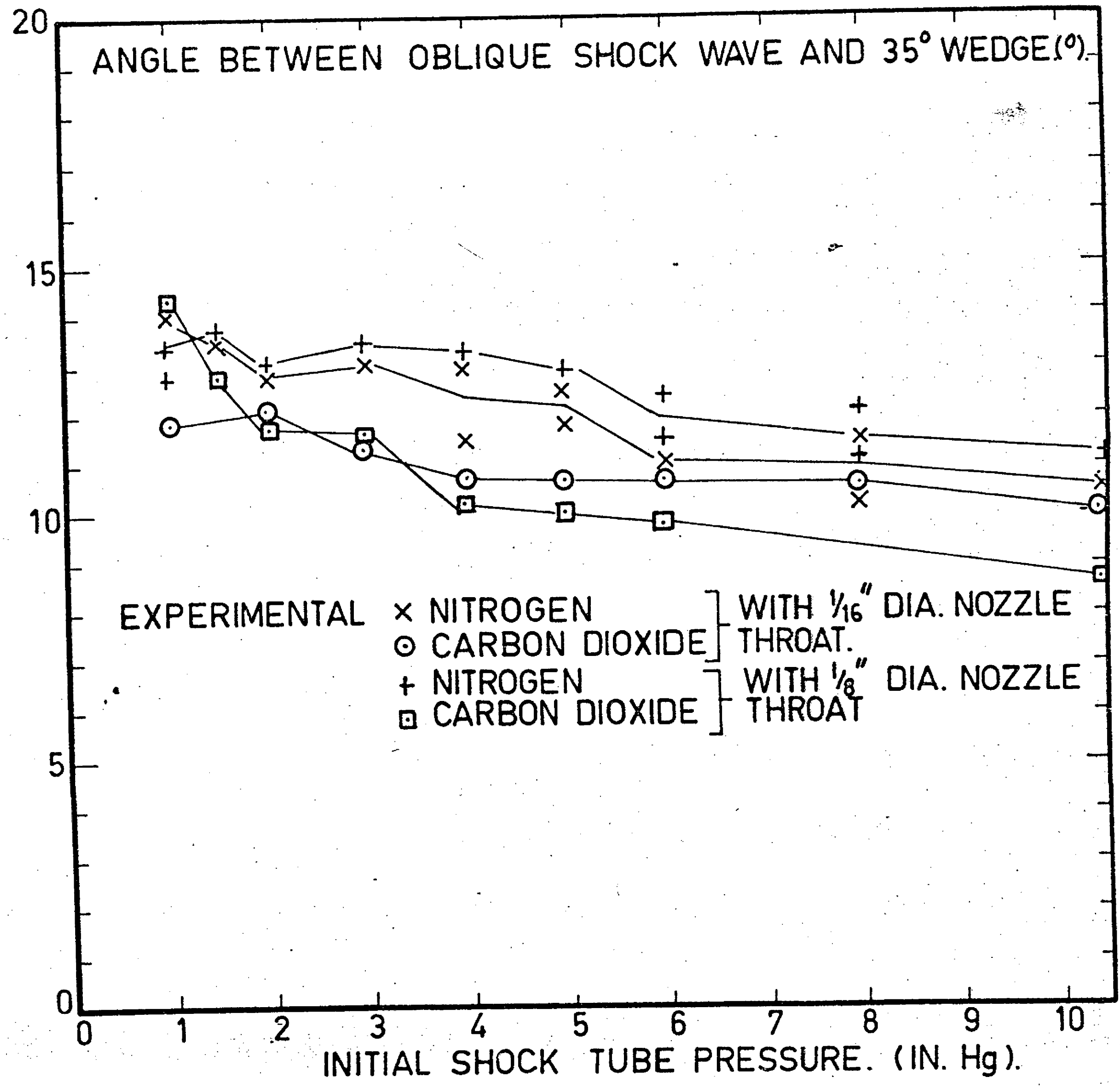

Figure No. 41 Shock Angles on a 35° Wedge in Carbon Dioxide in T.2

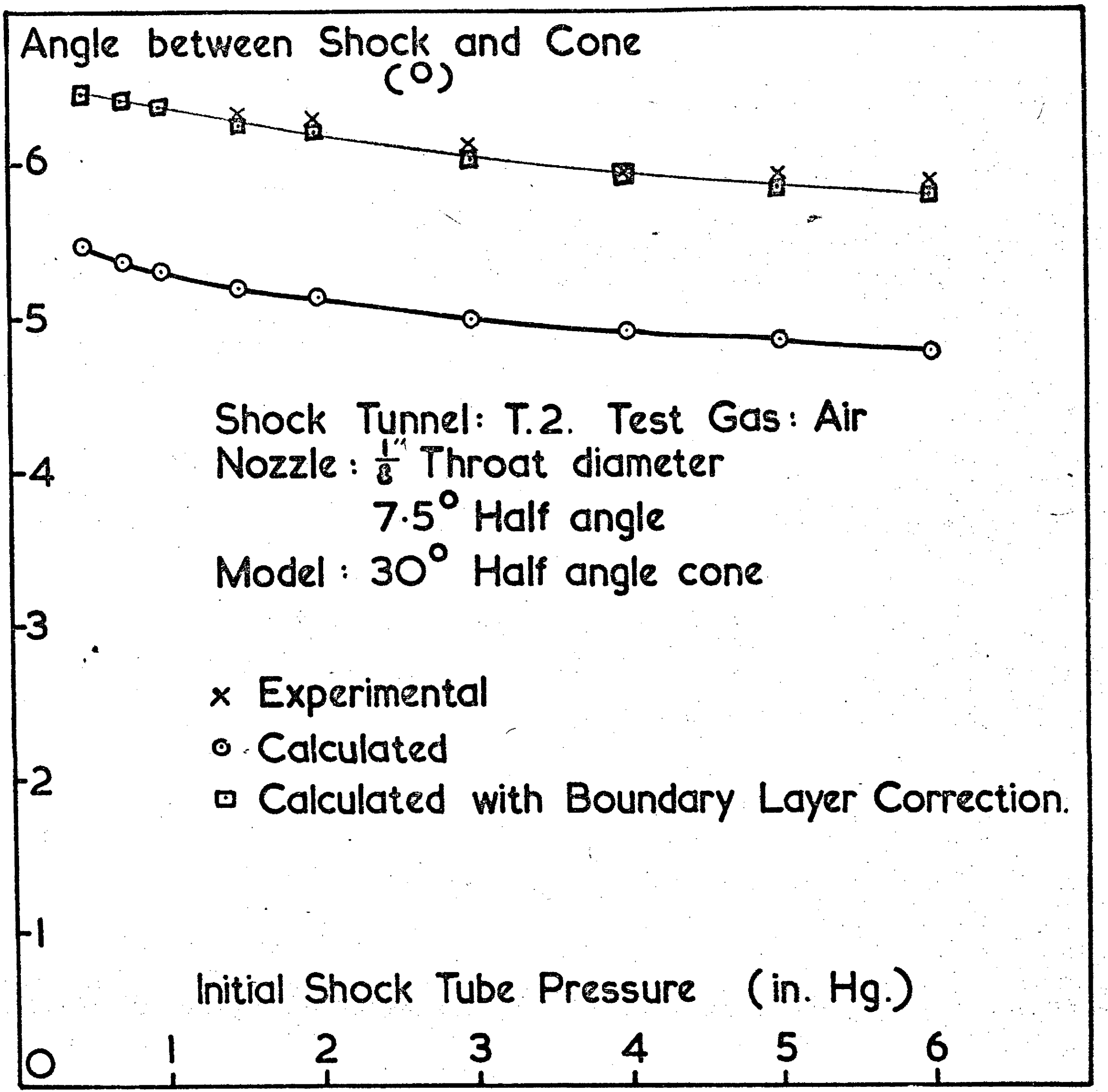

Figure No. 42 Cone Shock Angles in T.2

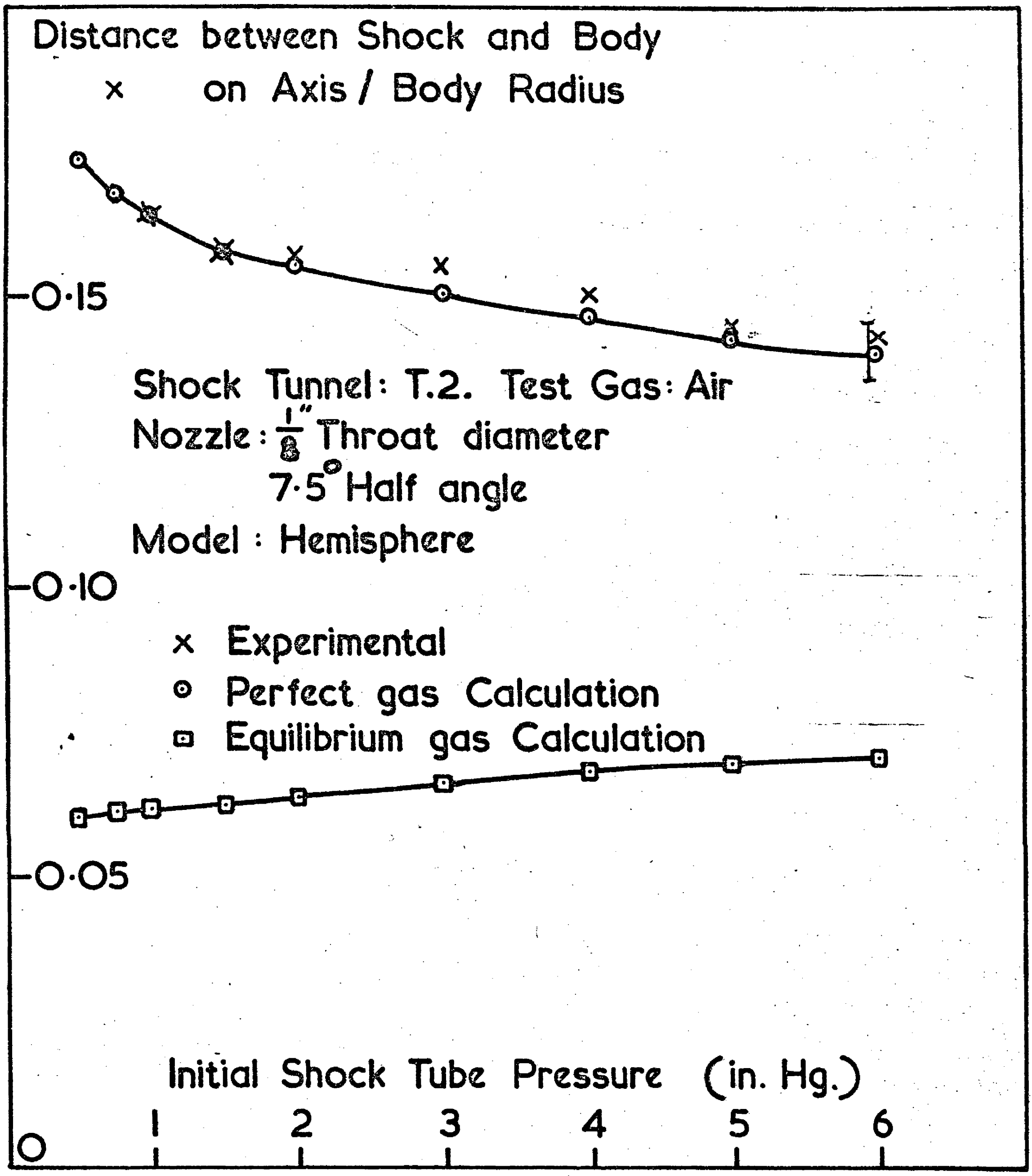

Figure No. 43 Shock Stand-off Distance on a Hemisphere in Air in T.2

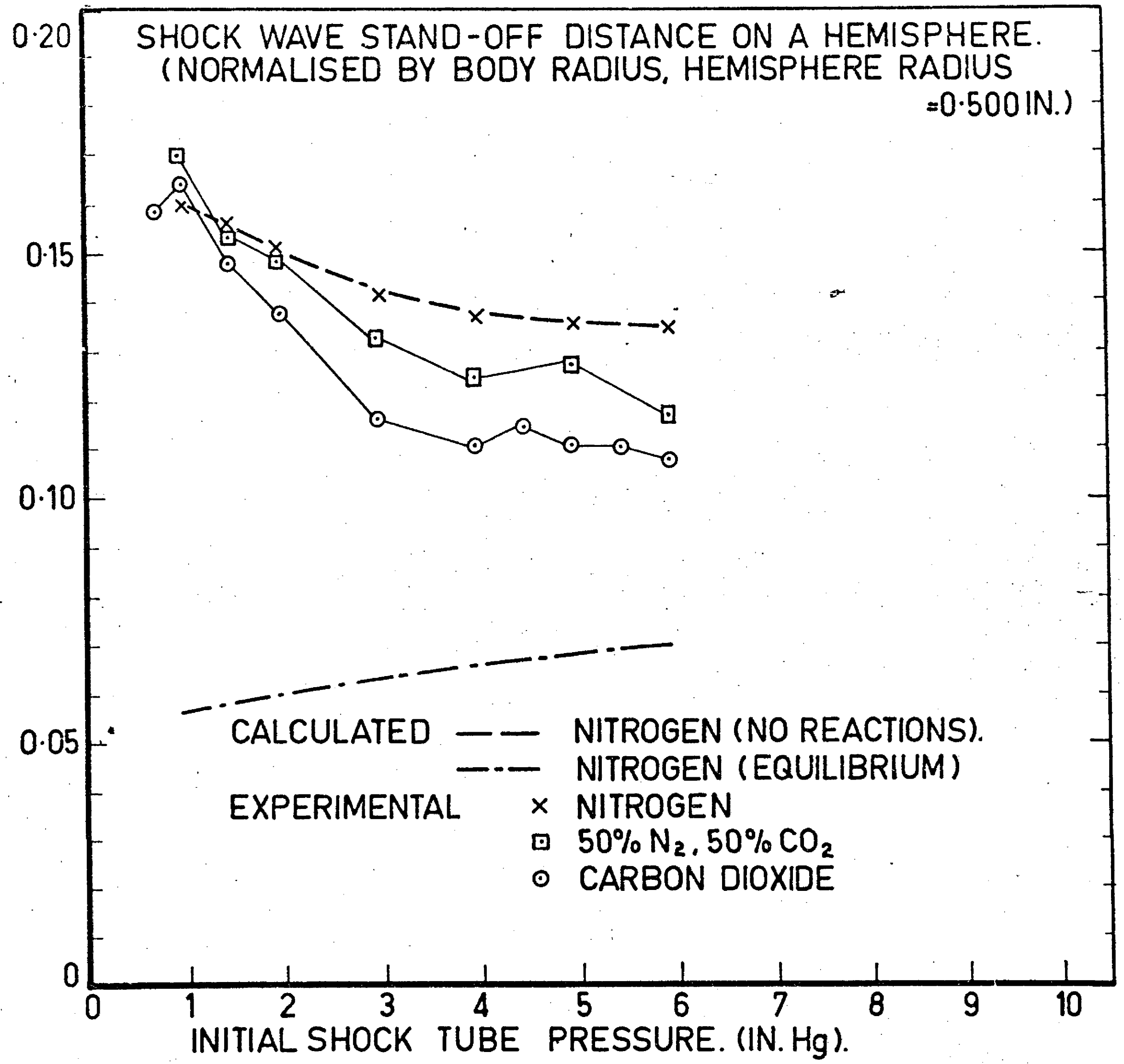

Figure No. 44 Shock Stand-off Distance on a Hemisphere in Carbon Dioxide in T.2

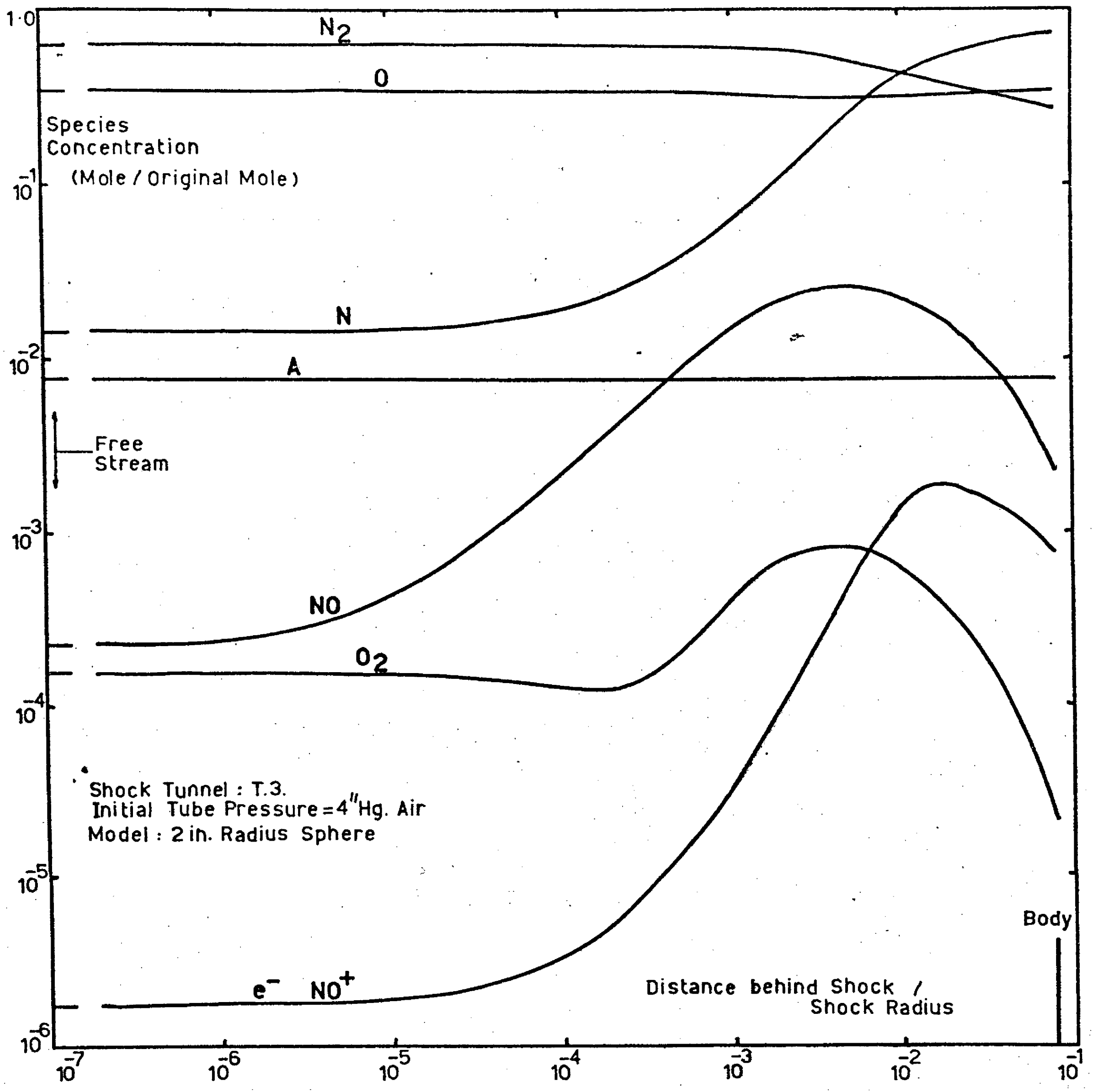

Figure No. 45 Species Concentrations behind the Shock Wave on a Hemisphere in Air

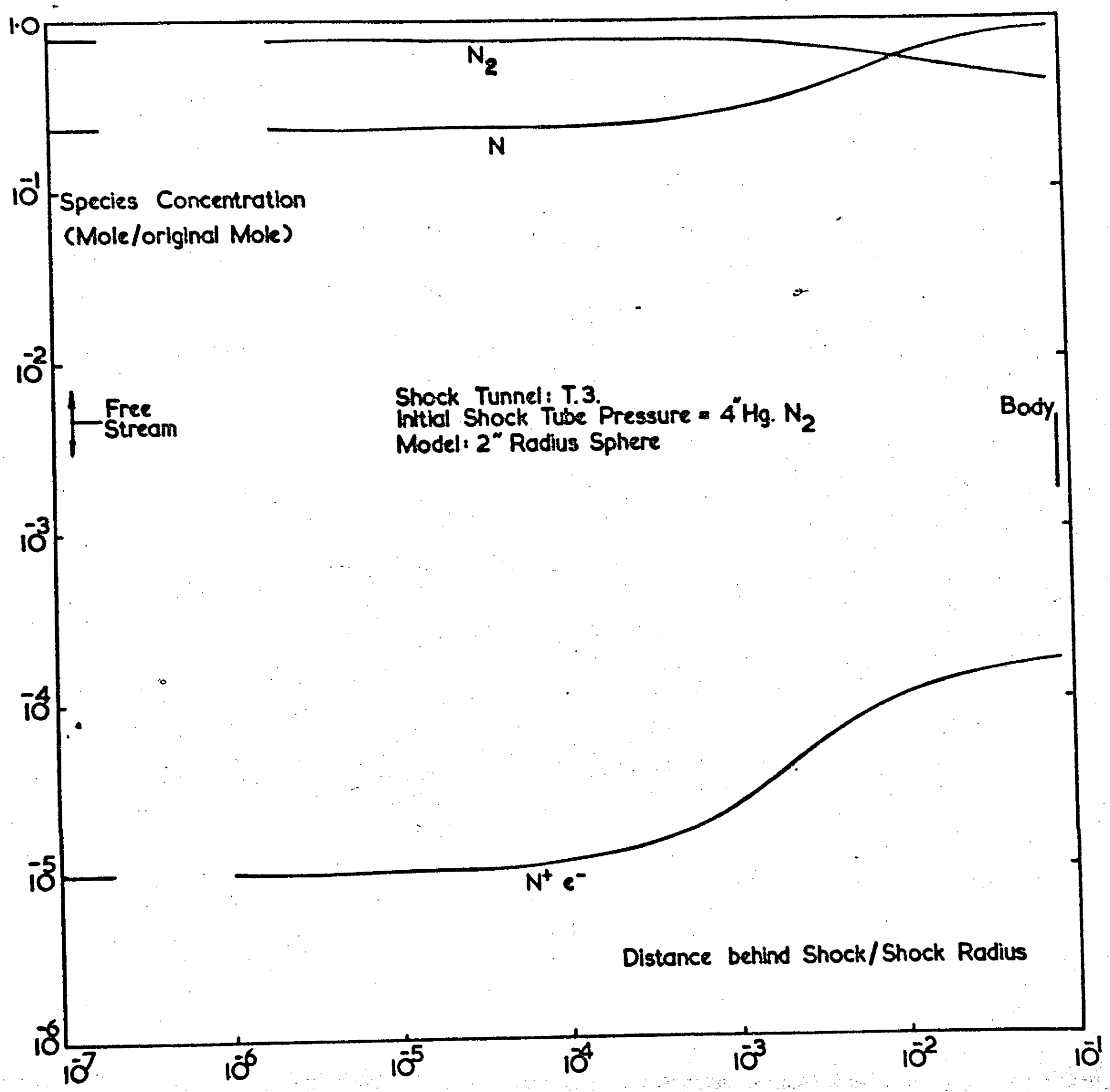

Figure No. 46 Species Concentrations behind the shock Wave on a Hemisphere in Nitrogen

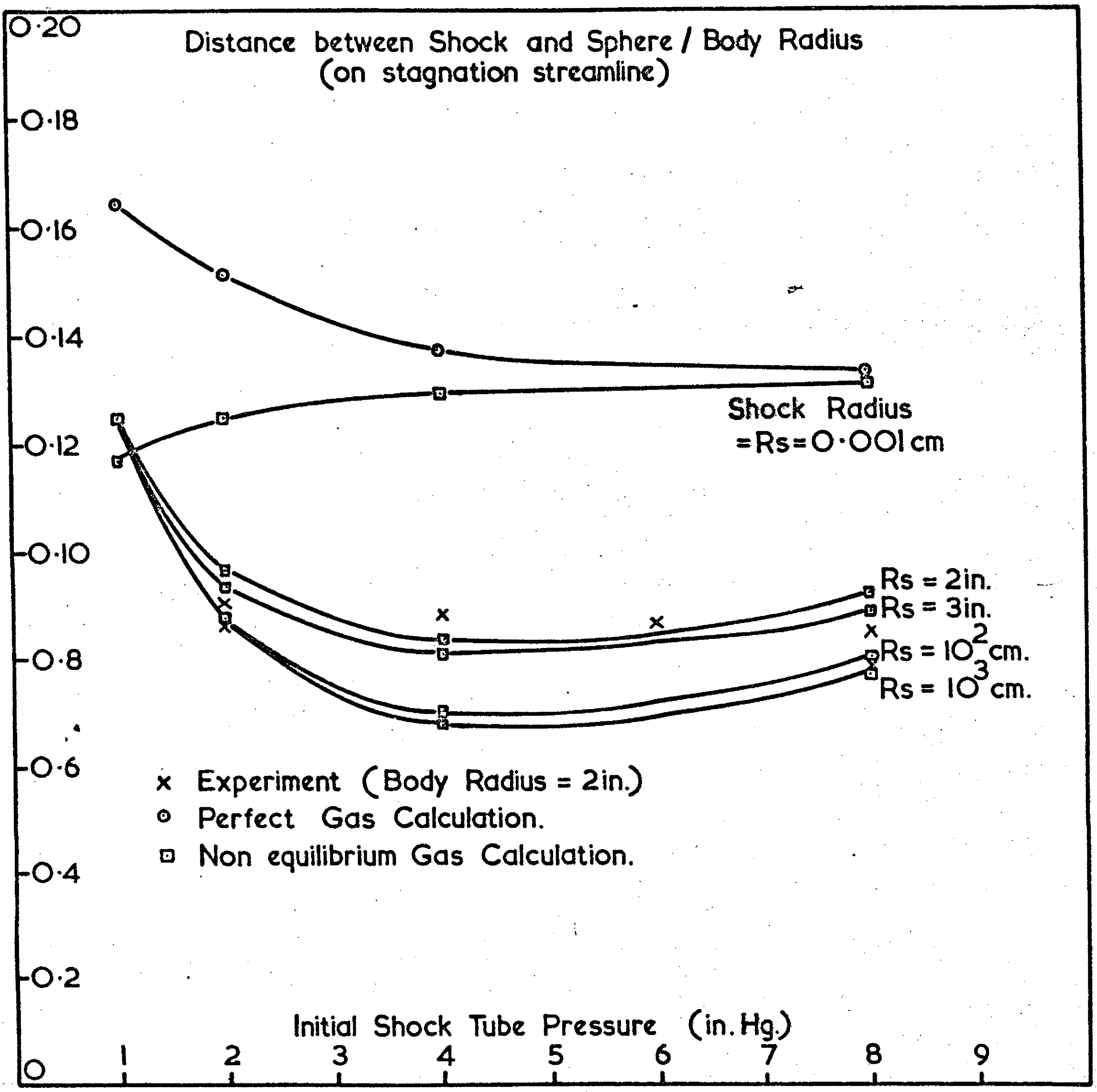

Figure No. 47 Shock Stand-off Distance on a Hemisphere in Air in T.3

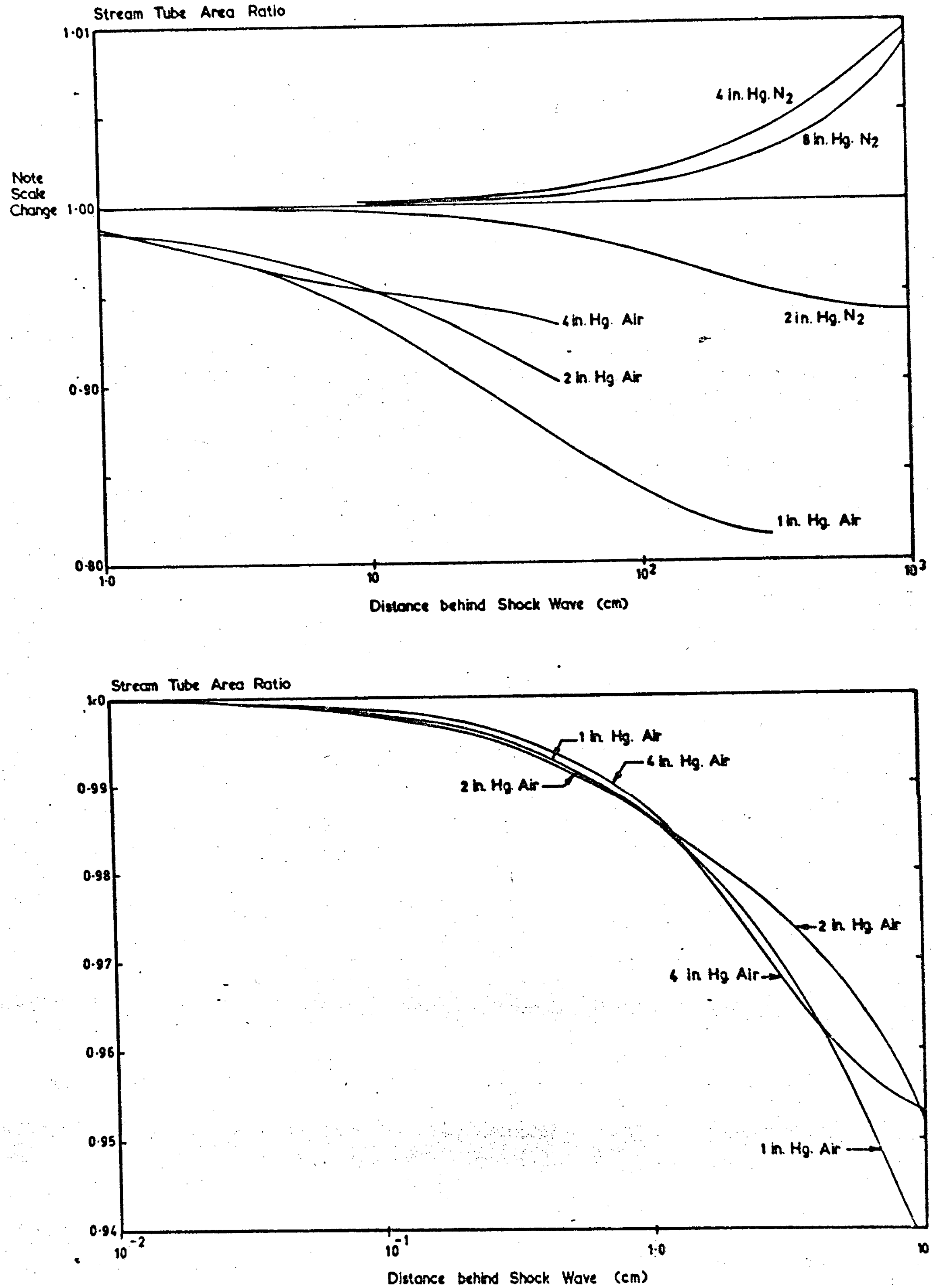

Wedge angle = 25°
Shock wave angles shown in figures 49,50
Calculations with chemical nonequilibrium, assuming constant pressure along stream line.

Figure No. 48 Stream Tube Cross-Sectional Areas Behind the Shock Waves on a Wedge in T.3.

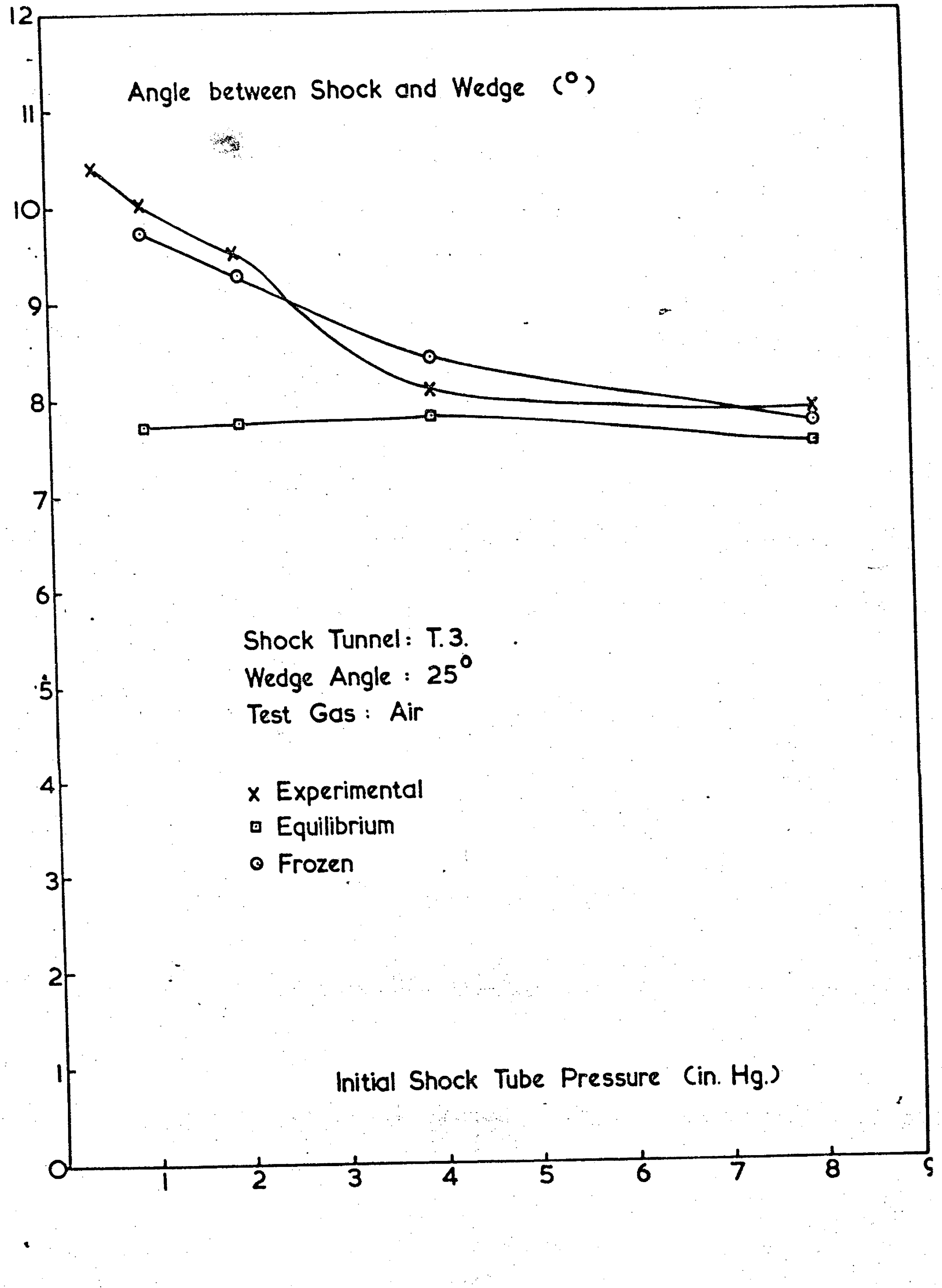

Figure No. 49 Shock Wave Angles on a Wedge in Air in T.3

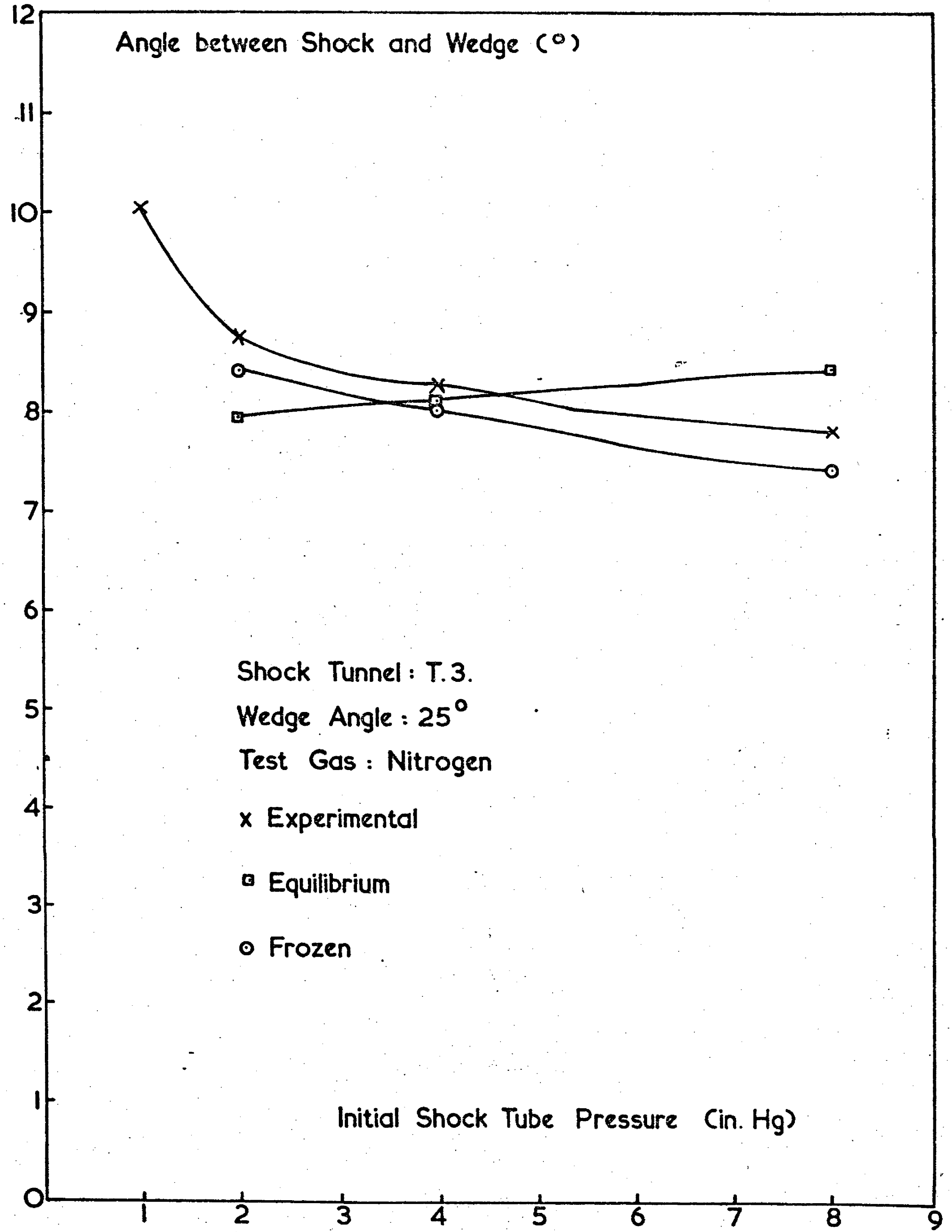

Figure No. 50 Shock Wave Angles on a Wedge in Nitrogen in T.3

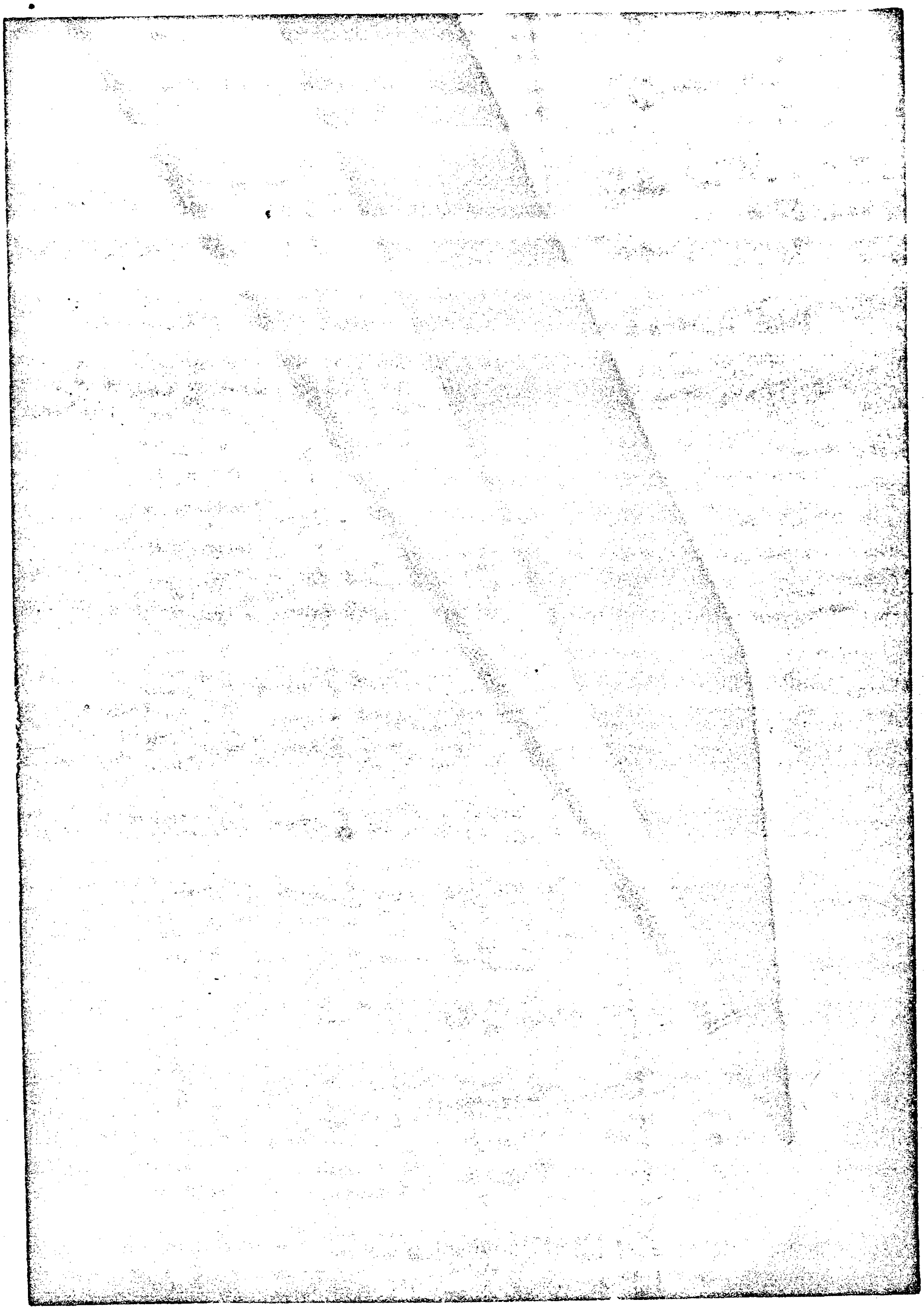

Figure No. 51 Schlieren Photograph of Wedge Flow in T.3

Figure No. 52 Schlieren Photograph of Flow over a Flared Hemisphere Cylinder

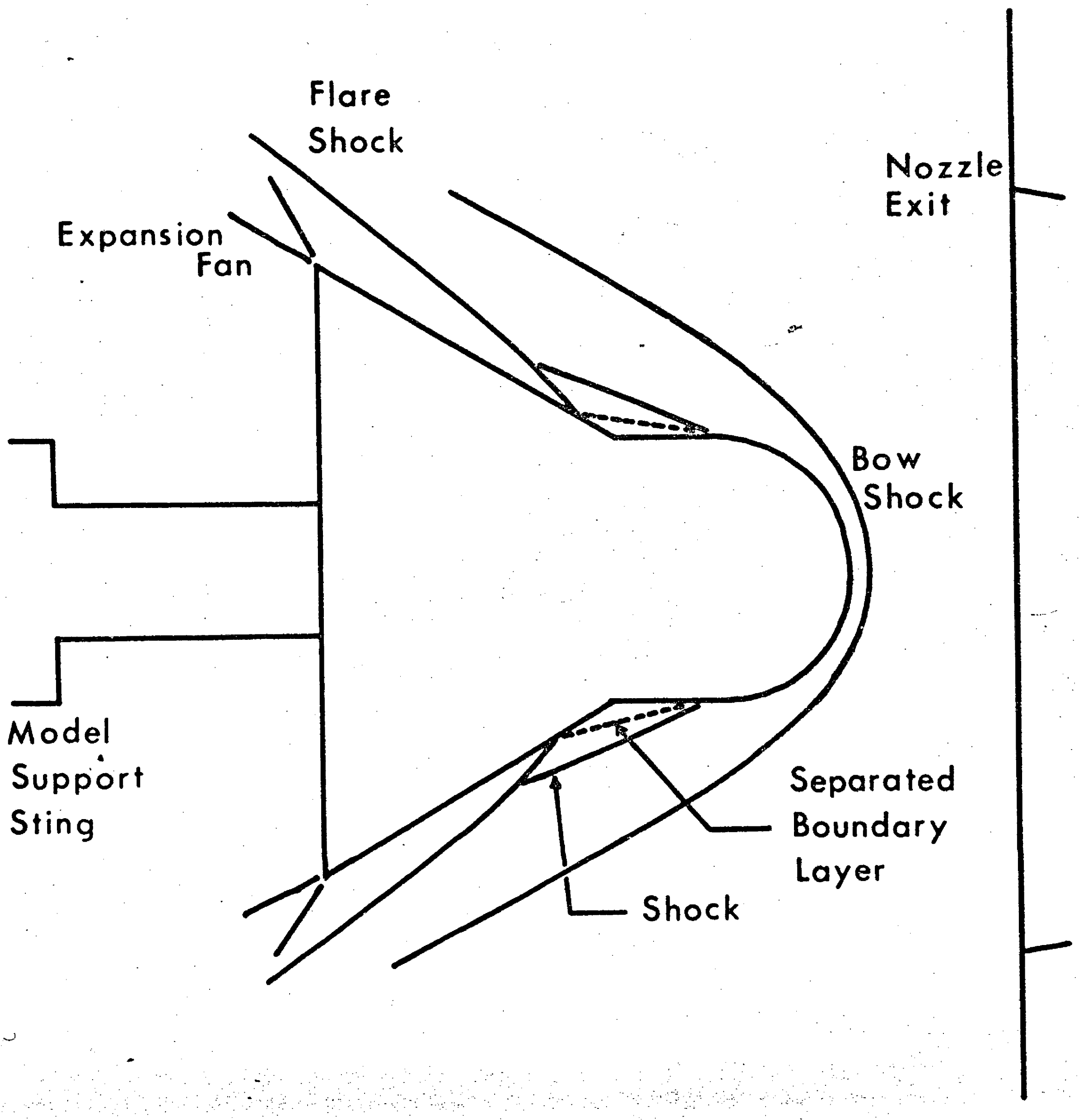

Figure No. 53 Interpretation of Flow over a Flared Hemisphere Cylinder

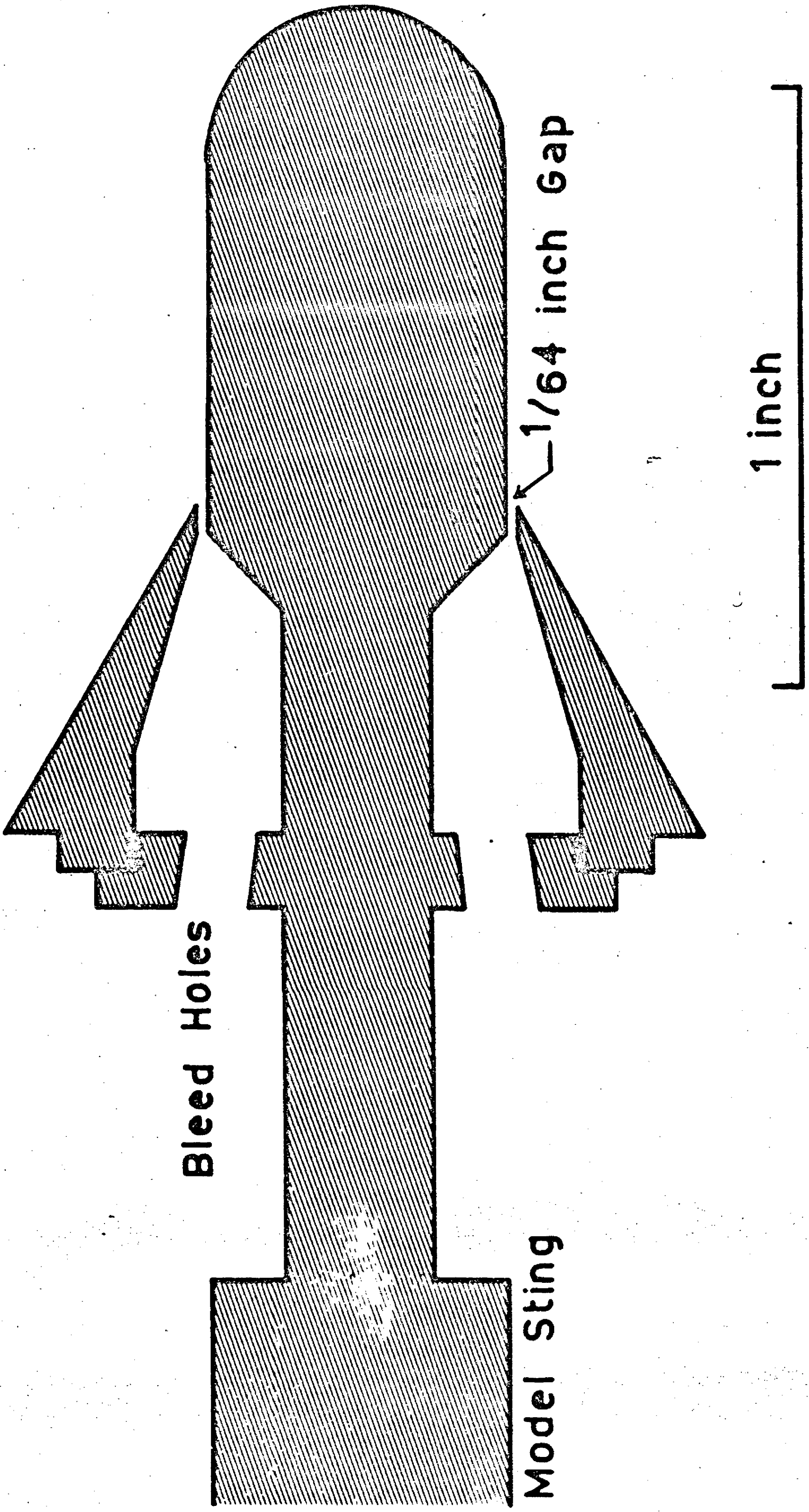

Figure No. 54 Flared Hemisphere Cylinder with Boundary Layer Bleed

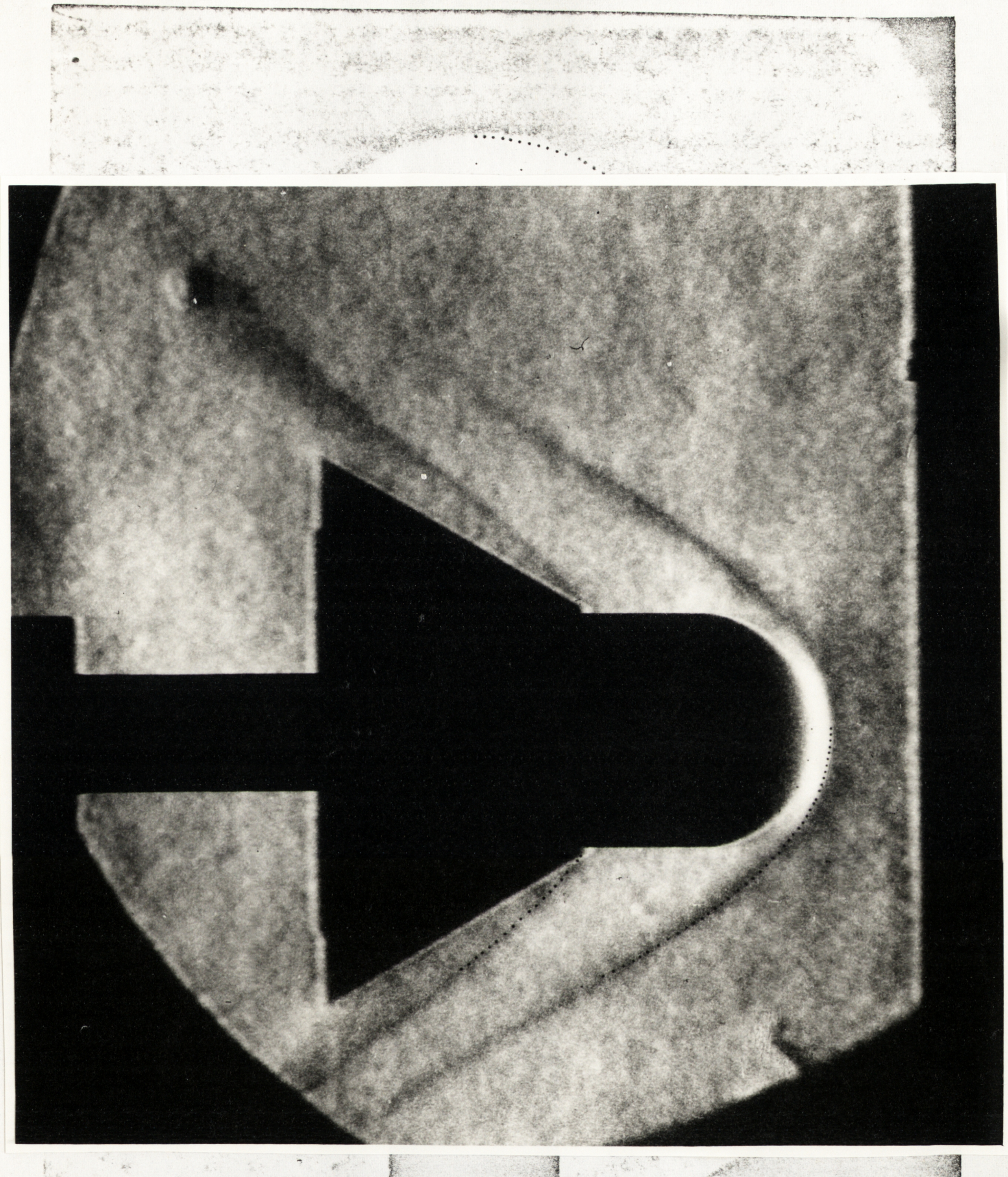

Figure No. 55 Calculated and Experimental Flow over a Flared Hemisphere Cylinder

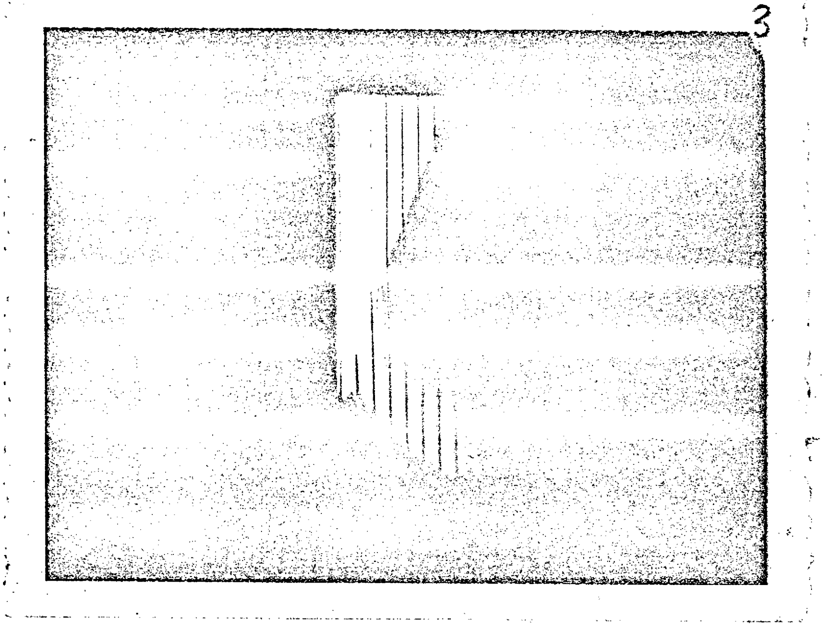

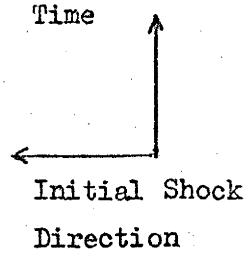

Initial Shock Tube Pressure = 2 in Hg of Air

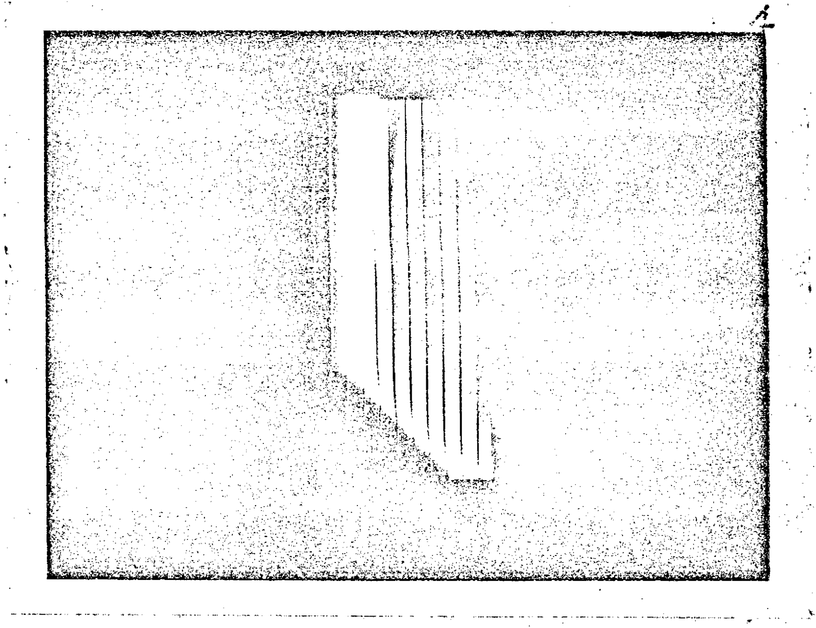

Initial Shock Tube Pressure = 2 in Hg of Argon

Shock Tunnel T.2

Distance between Markers = 1.0 cm

Sweep Duration = 50 microsec

Figure No. 56 Streak Photographs of Incident and Reflected Shock Waves

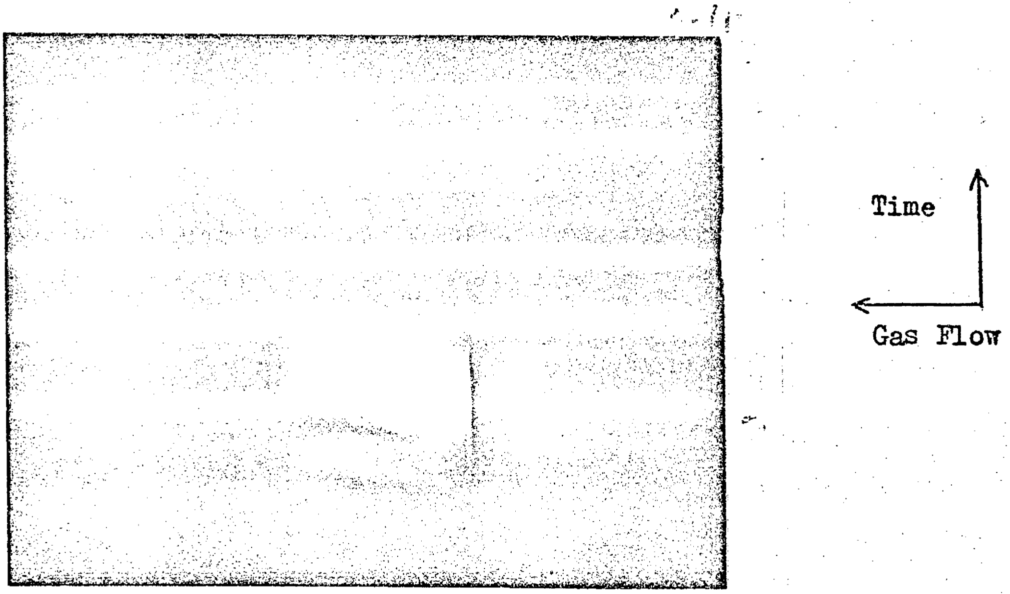

Initial Shock Tube Pressure = 1 Hg of Air

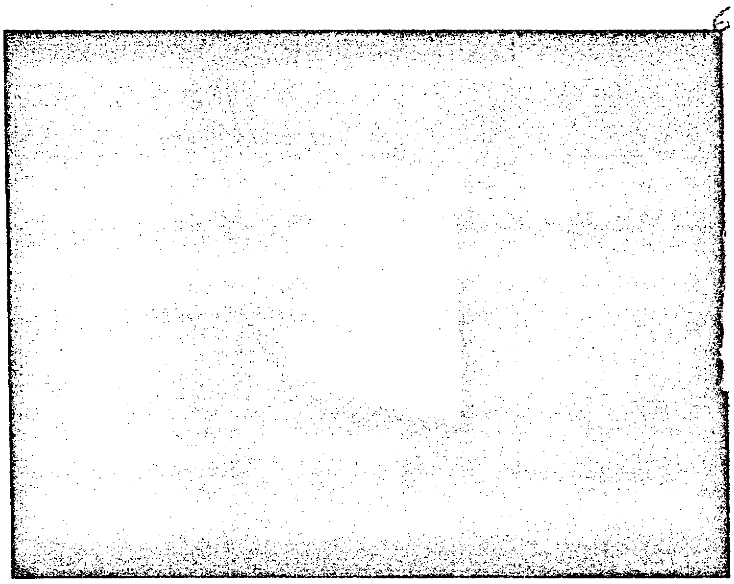

Initial Shock Tube Pressure = 2 in Hg of Air

Shock Tunnel T.2 Nozzle: $\frac{1}{8}$ in Throat

Length Swept = 8.8 cm 7.5° Half Angle

Sweep Duration = 200 microsec

Figure No. 57 Streak Photographs of Free Stream Gas Flow

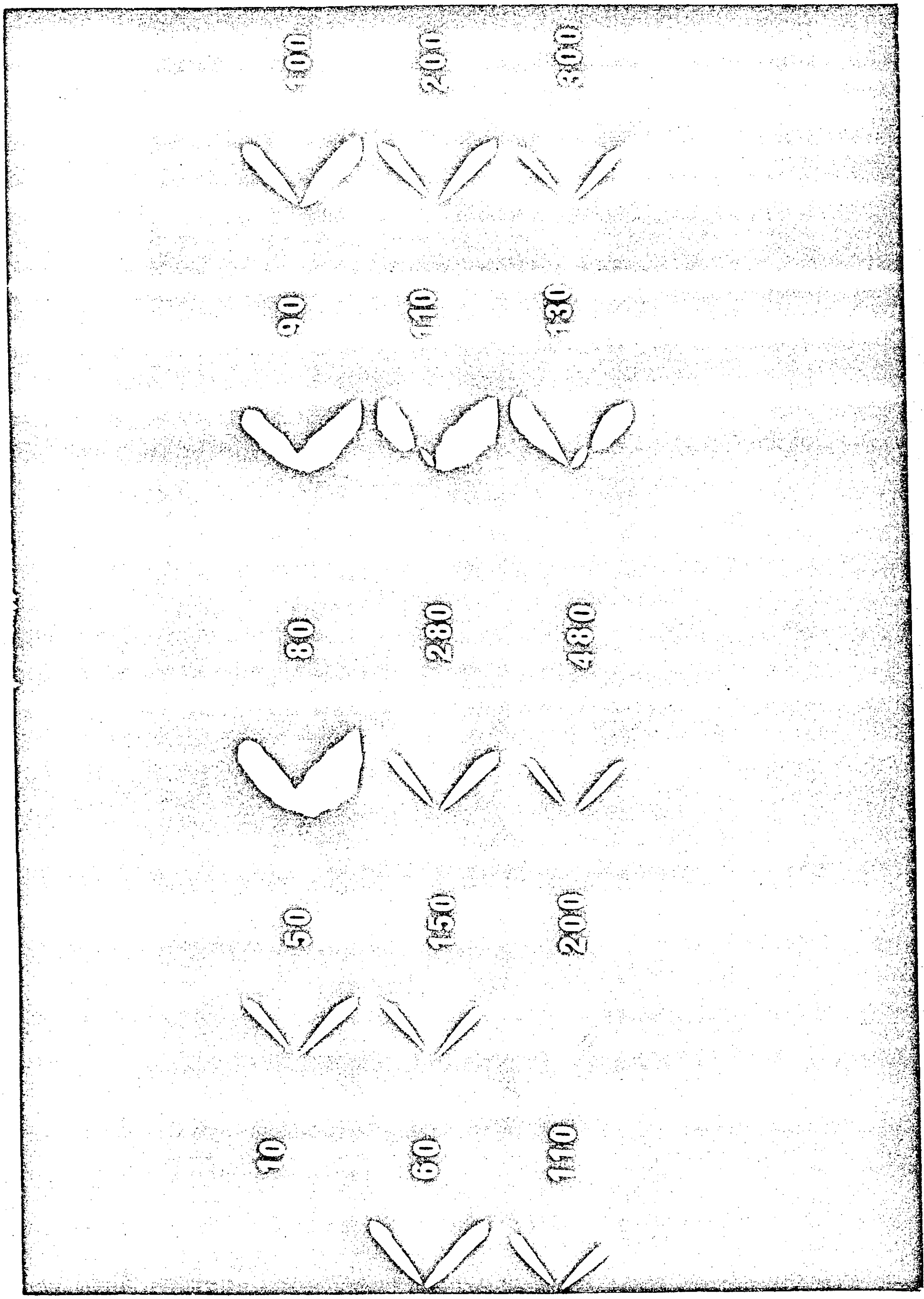

Numbers = time after shock reflection (μsec)

Figure No. 58 Framing Photograph of Shock Wave on Wedge

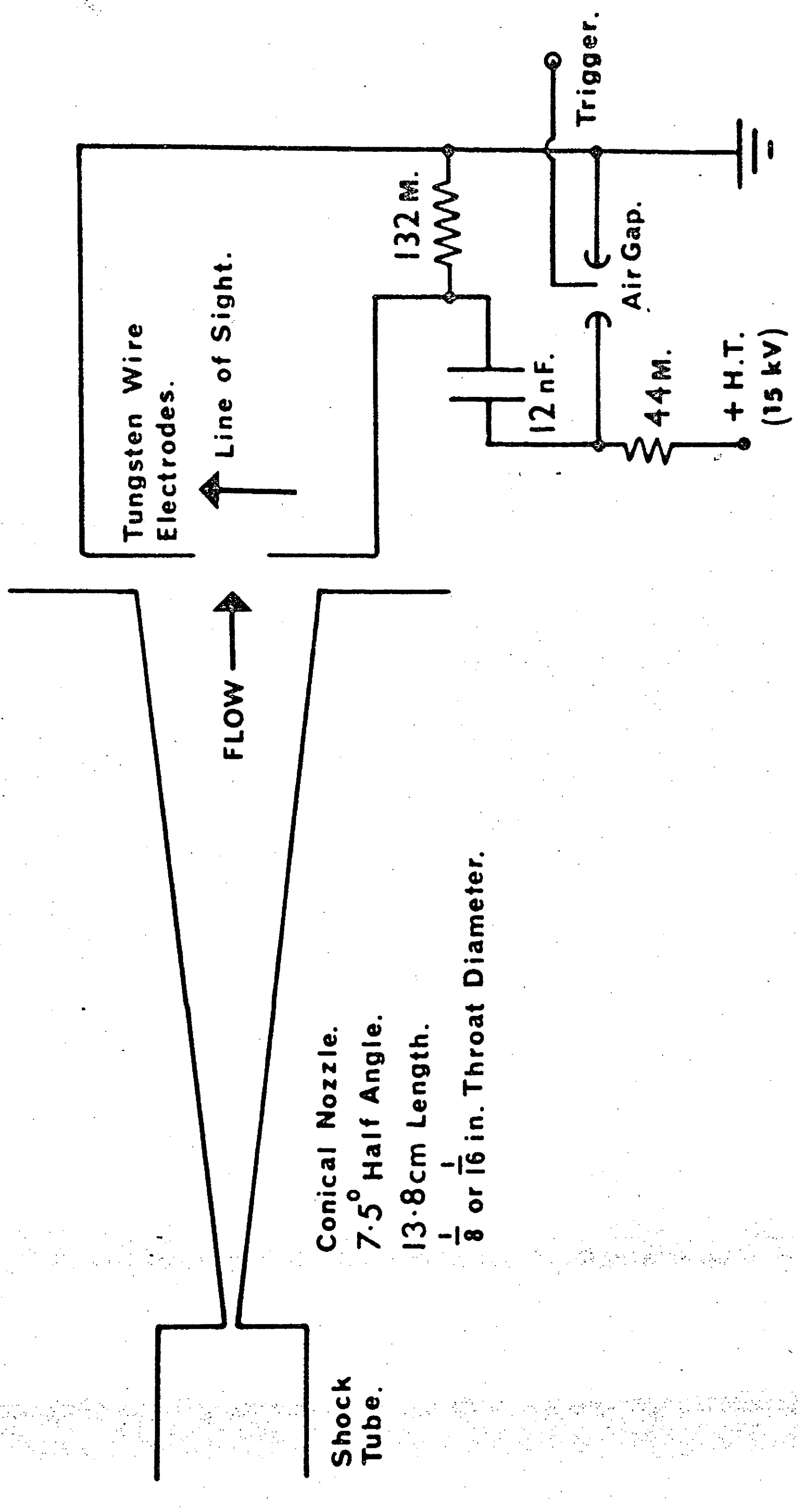

Figure No. 59 Spark Tracer Technique

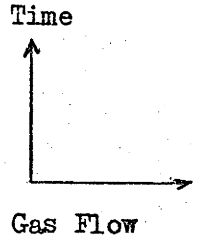

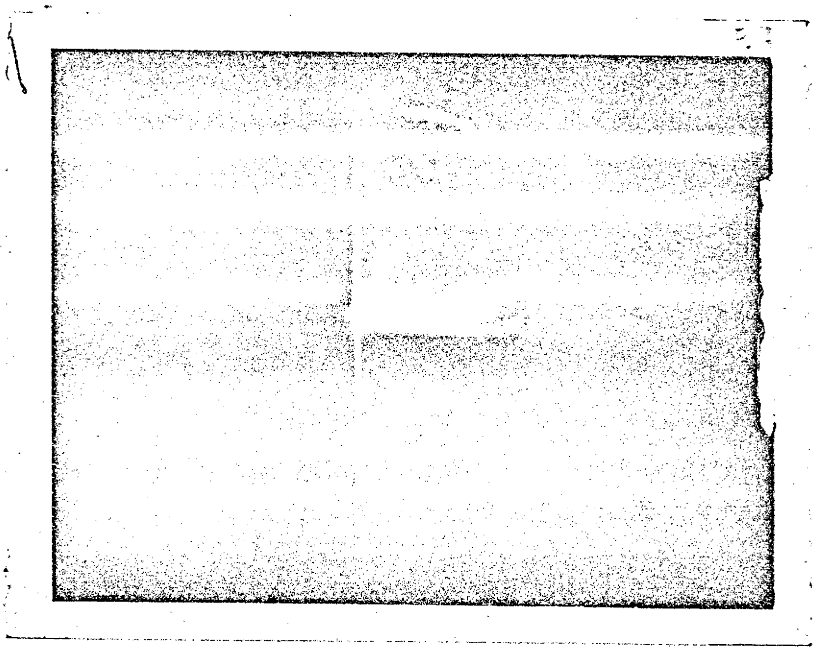

Time after Shock
Reflection = 125 microsec

Initial Shock Tube Pressure = 4 in Hg of Air

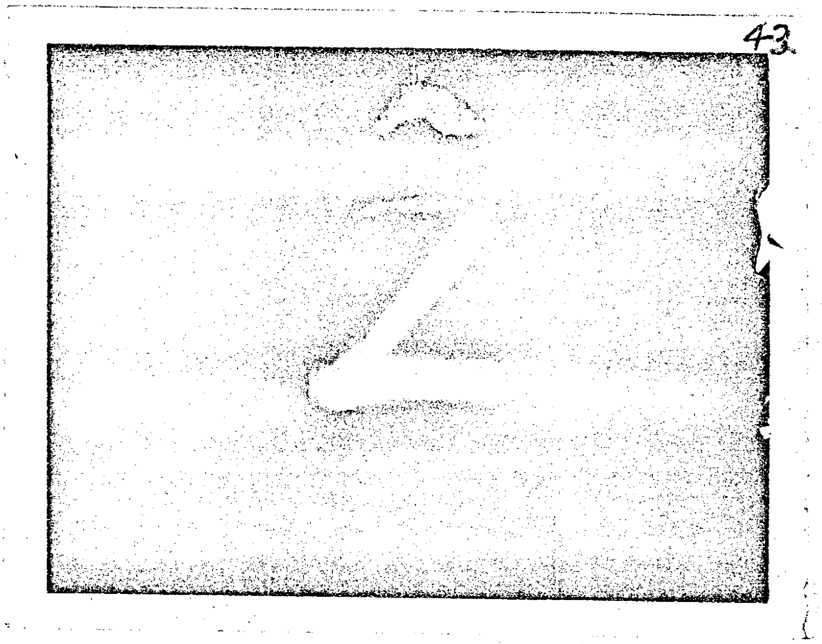

Time after Shock
Reflection = 150 microsec

Initial Shock Tube Pressure = 1 in Hg of Argon

Shock Tunnel T.2

Nozzle: 1/16 in Throat

7.5° Half Angle

Length Swept = 3.6 cm

Sweep Duration = 5 microsec

Figure No. 60 Streak Photographs of Spark Tracer

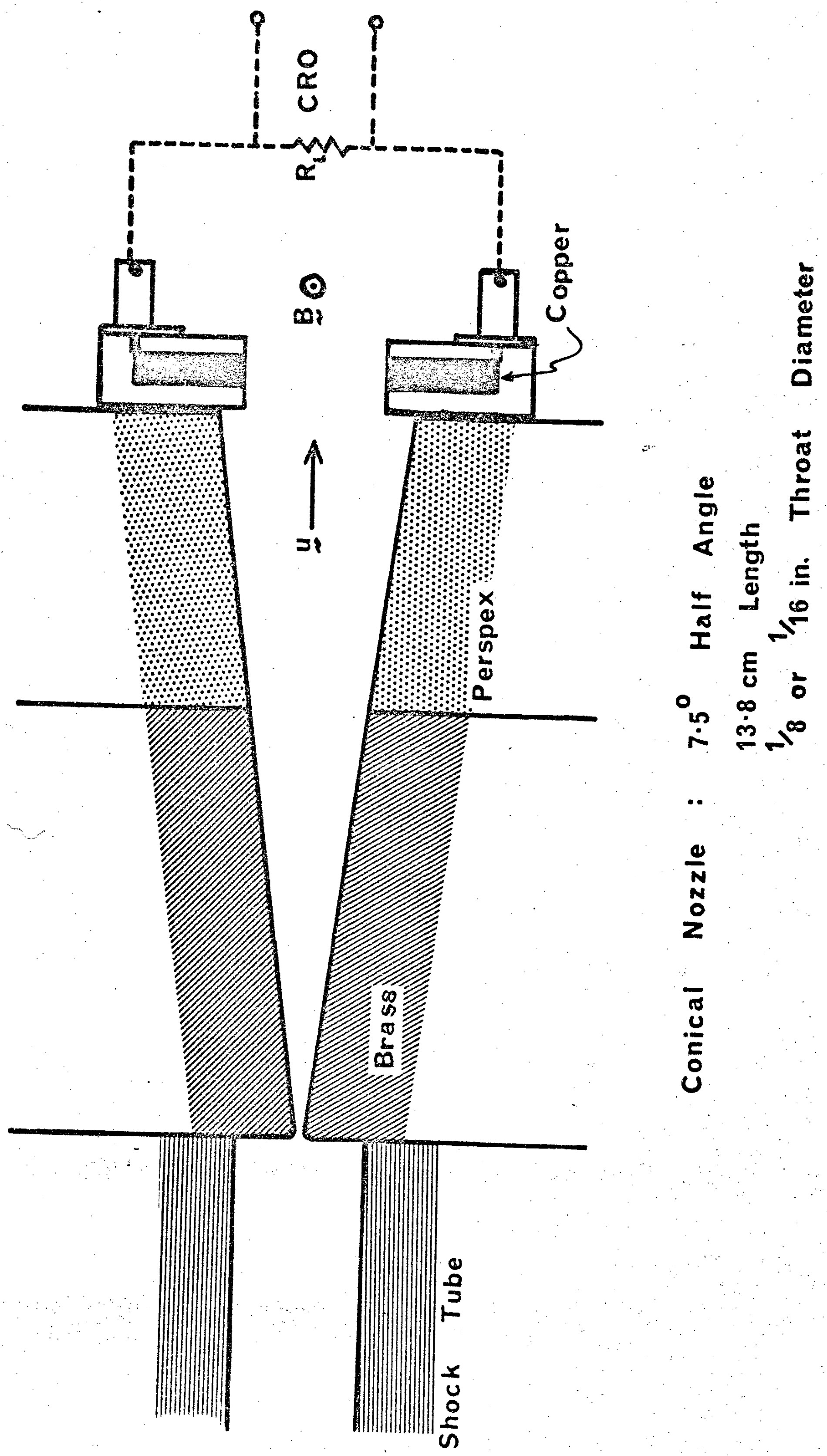

Figure No. 61 Magnetohydrodynamic Technique

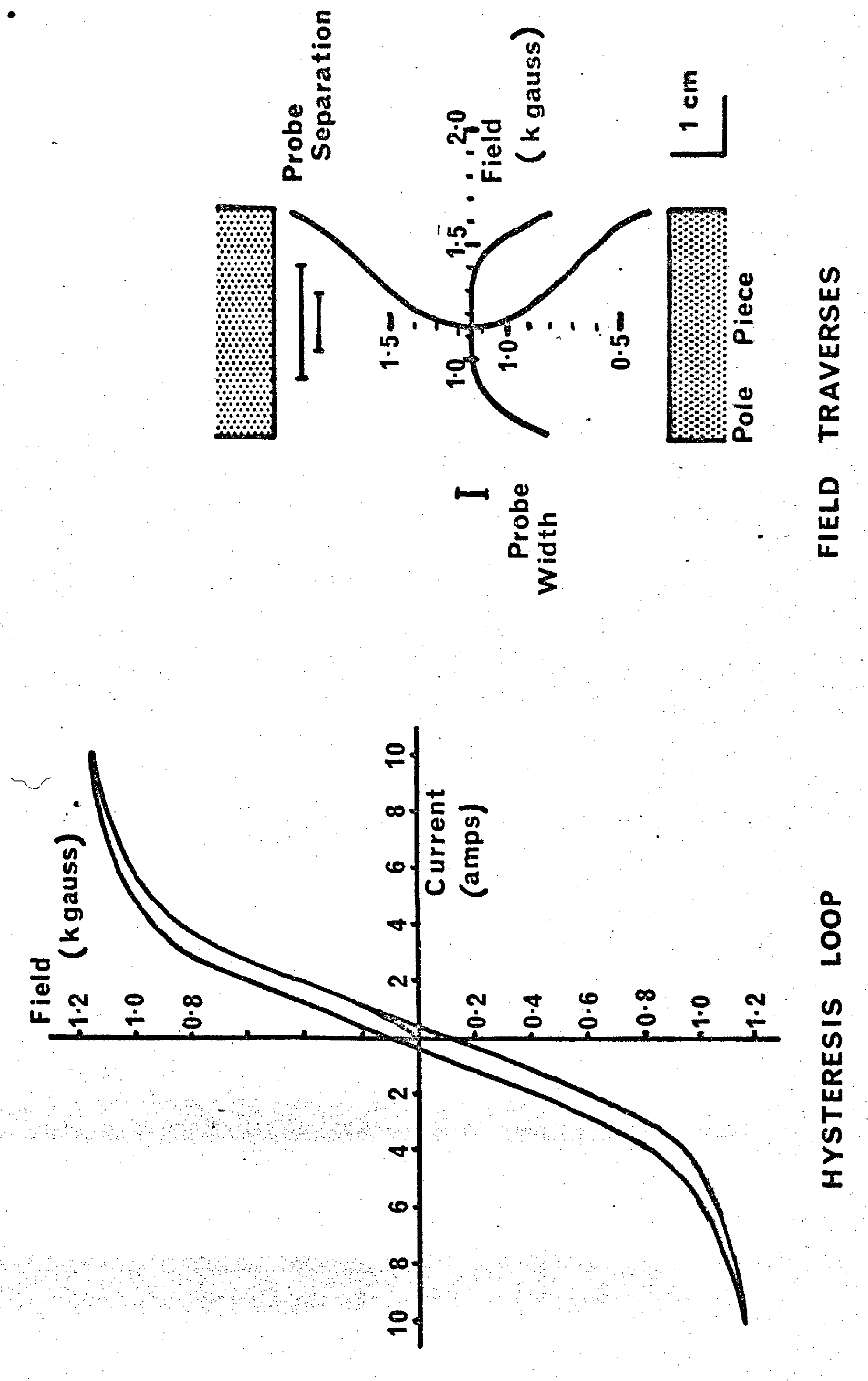

Figure No. 62 Magnetic Field Properties for the Magnetohydrodynamic Technique

← Flow Direction

Figure No. 63 Flow over the Magnetohydrodynamic Probes

15

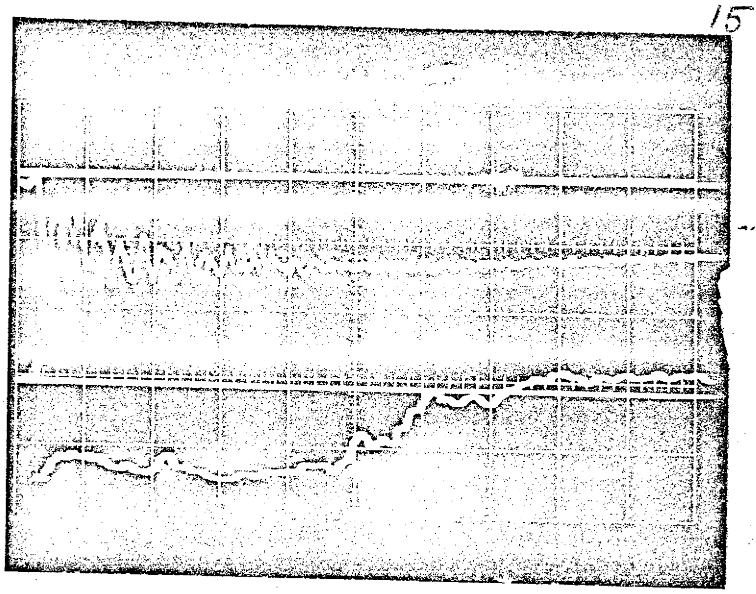

Nozzle Throat = $\frac{1}{8}$ in

Time Base

= 50 microsec/cm

Initial Shock Tube Pressure = 2 in Hg of Air

23

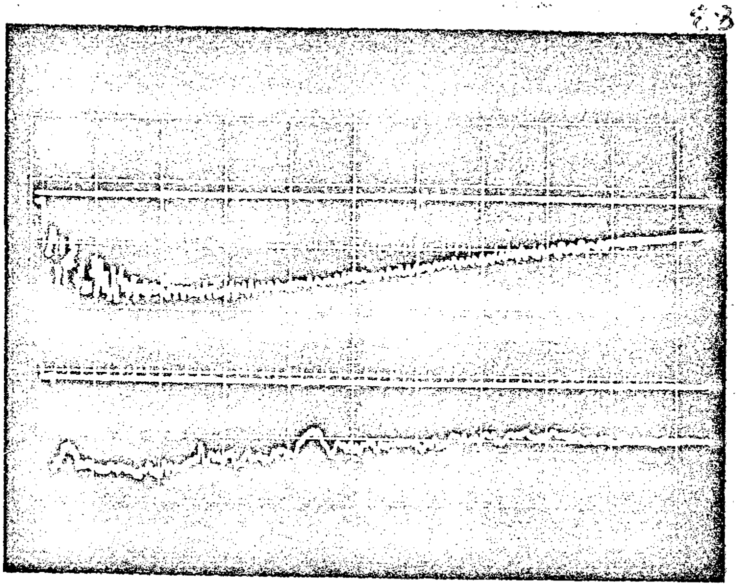

Nozzle Throat = 1/16 in

Time base = 100 microsec/cm

Initial Shock Tube Pressure = 1 in Hg of Air

Shock Tunnel: T.2 Nozzle: 7.5° half angle

Upper Trace: Nozzle Reservoir Pressure Transducer

Lower Trace: Magnetohydrodynamic Probe, 5 volts/cm

Figure No. 64 Oscilloscope Traces from the Magnetohydrodynamic Technique

37

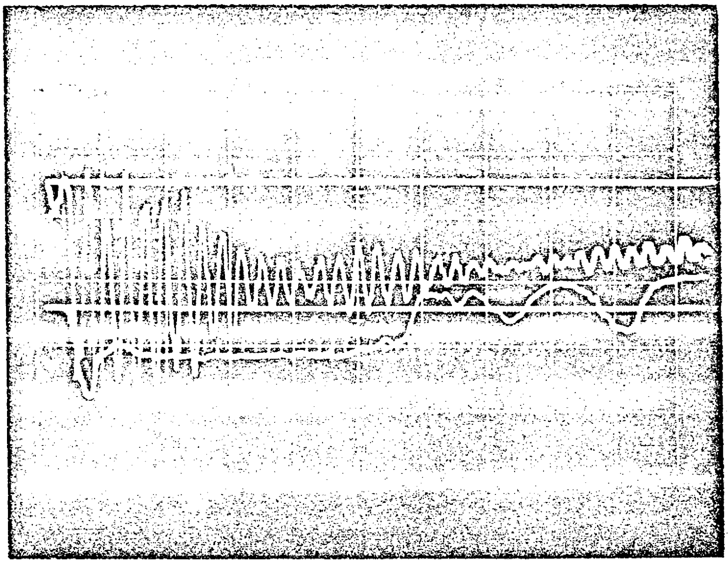

Initial Shock Tube Pressure = 5 in Hg of Carbon Dioxide

18

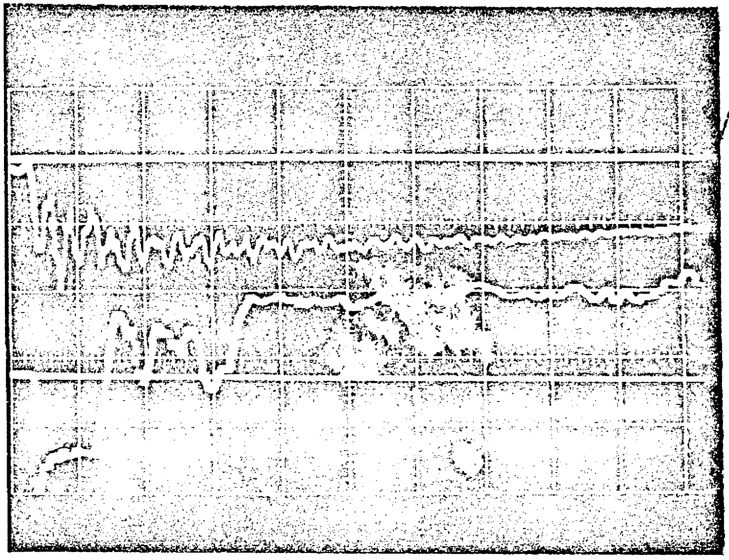

Initial Shock Tube Pressure = 2 in Hg of Argon

Shock Tunnel: T.2 Nozzle: $\frac{1}{8}$ in Throat
7.5 Half Angle

Upper Trace: Nozzle Reservoir Pressure Transducer

Lower Trace: Magnetohydrodynamic Probe, 5 volts/cm, 50 microsec/cm

Figure No. 64 (continued)

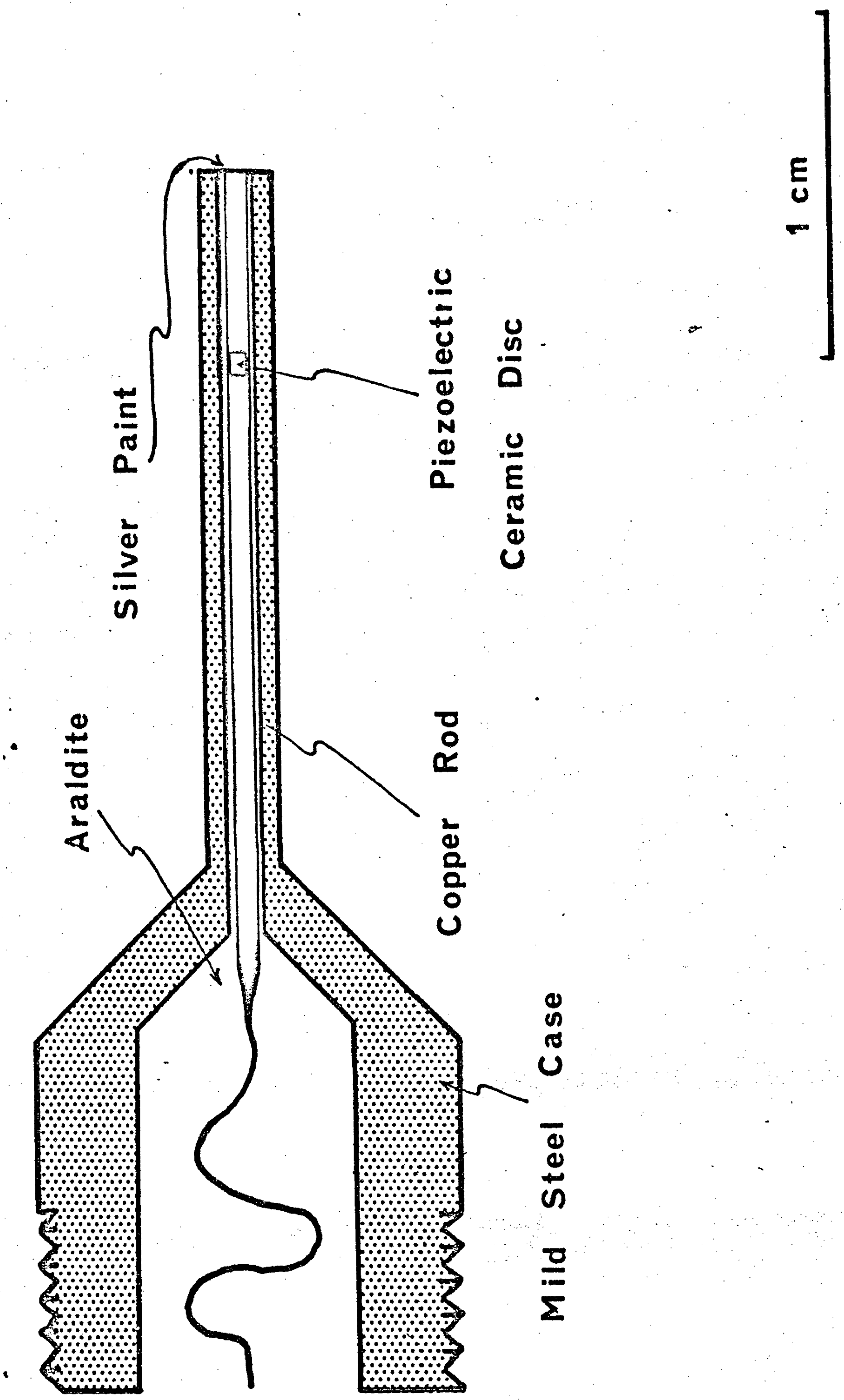

Figure No. 65 Pitot Pressure Probe

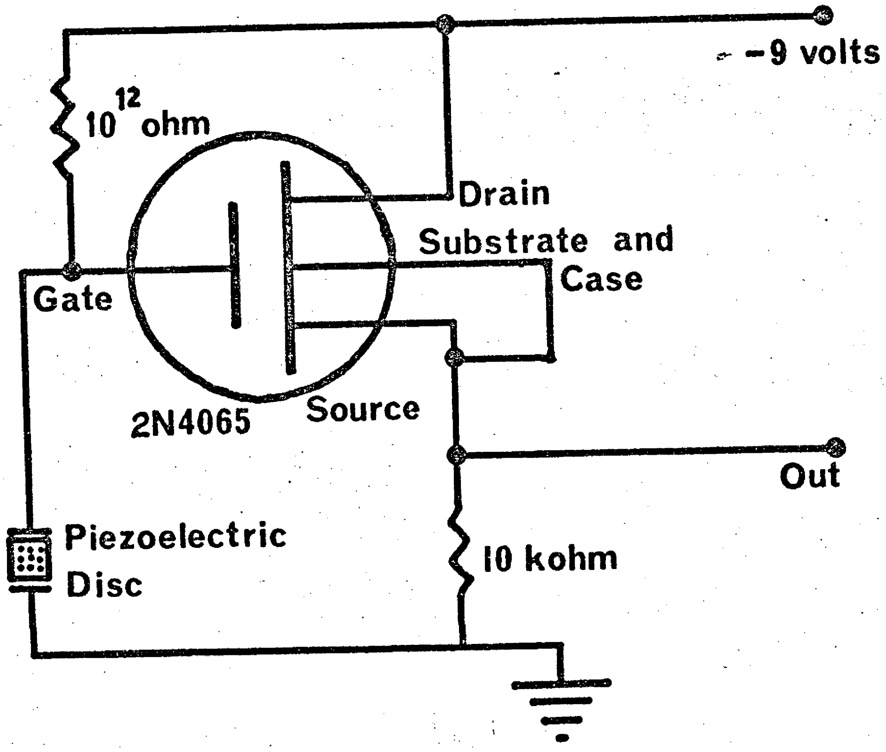

Figure No. 66 Pressure Transducer Converter Circuit

25

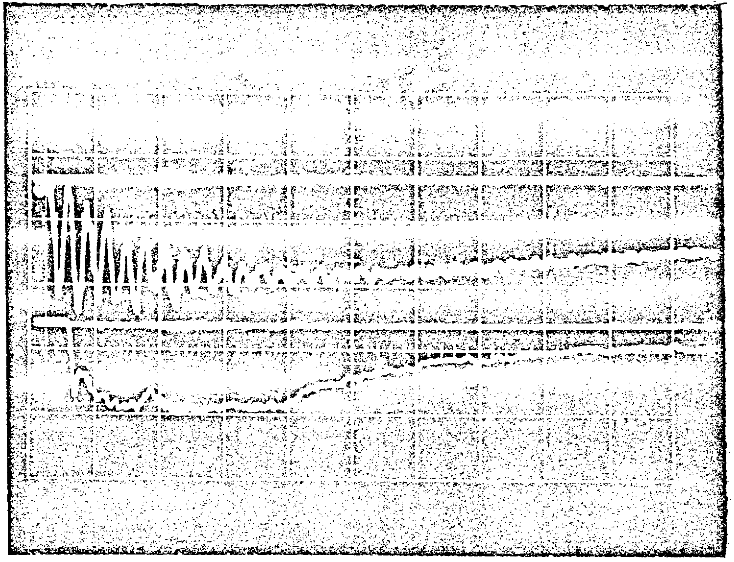

Initial Shock Tube Pressure = 2 in Hg of Air

10

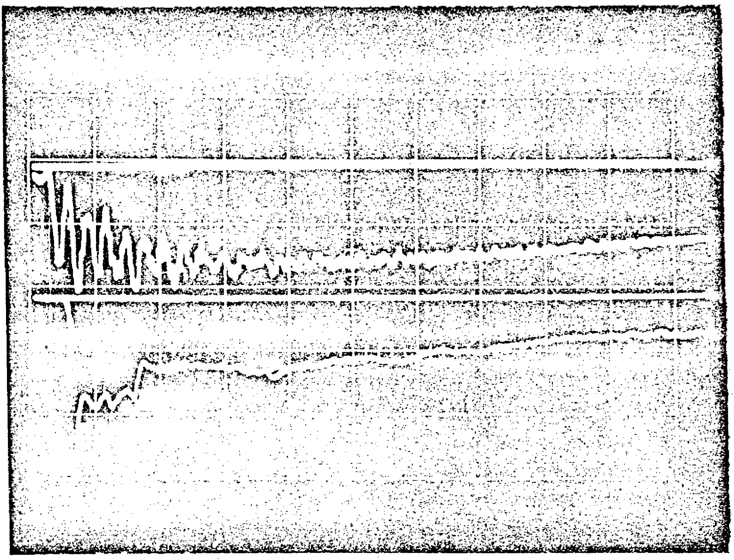

Initial Shock Tube Pressure = 2 in Hg of Air

Shock Tunnel: T.2 Nozzle: $\frac{1}{8}$ in Throat
7.5 Half Angle

Upper Trace: Nozzle Reservoir Pressure Transducer

Lower Trace: Pitor Pressure Probe, 1 volt/cm, 50 microsec/cm

Figure No. 67 Free Stream Pitot Pressure Traces

21

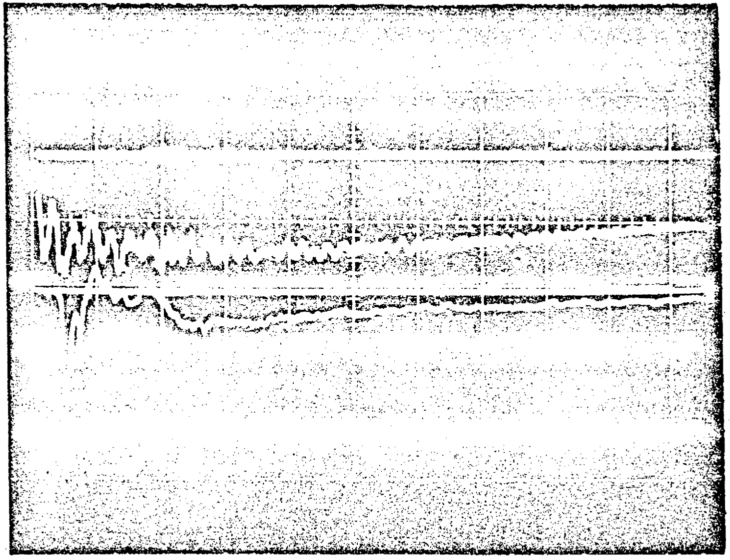

Initial Shock Tube Pressure = 2 in Hg of Argon

Shock Tunnel: T.2 Nozzle: $\frac{1}{8}$ in Throat
7.5° Half Angle

Upper Trace: Nozzle Reservoir Pressure Transducer

Lower Trace: Pitot Pressure Probe, 1 volt/cm, 50 microsec/cm

Figure 67 (continued)

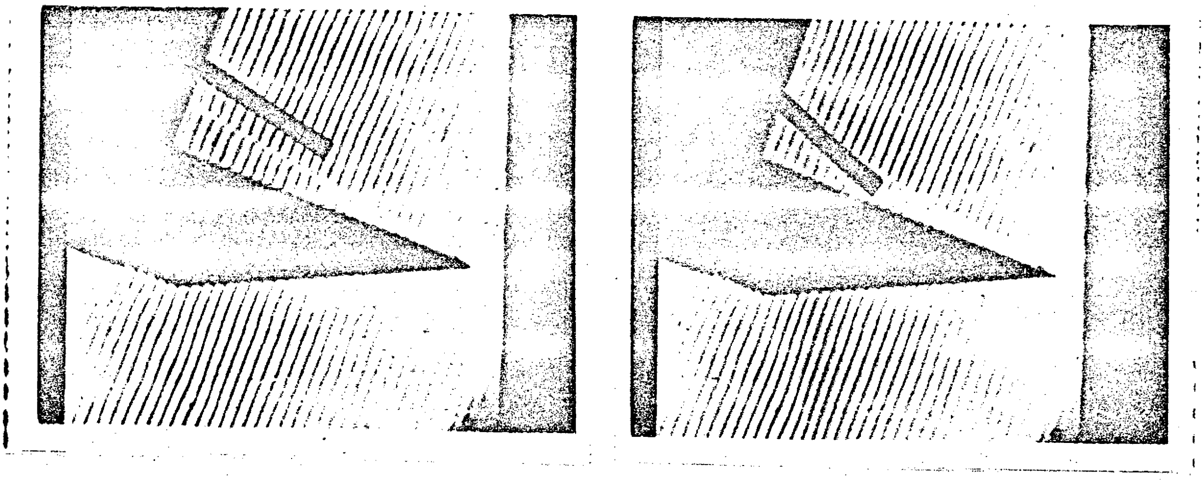

Finite Fringe Interferograms at 4330 Angstrom

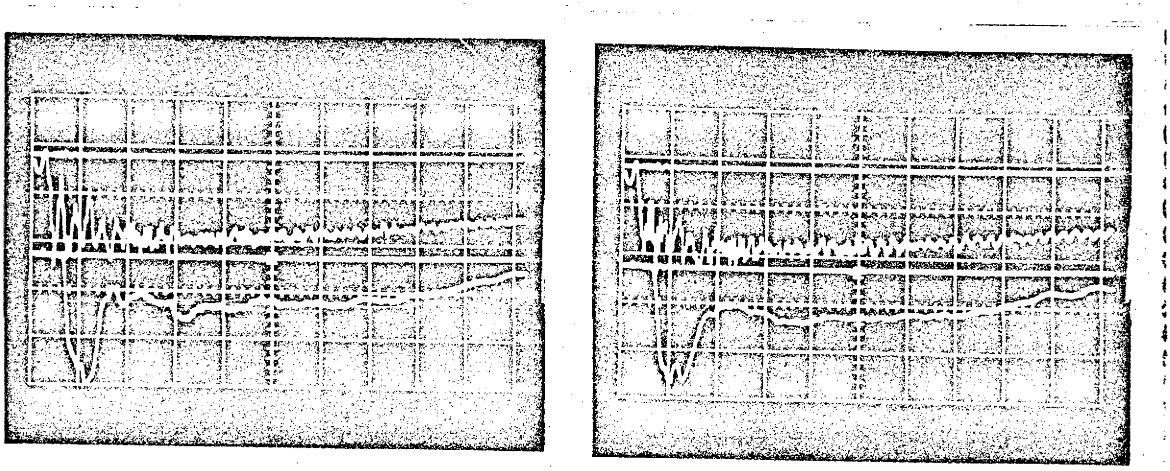

Initial Shock Tube Pressure = 4 in Hg of Air

Shock Tunnel: T.2 Nozzle: $\frac{1}{8}$ in Throat

7.5° half angle

Upper Trace: Nozzle Reservoir Pressure Transducer

Lower Trace: Pitot Pressure Probe, 50 microsec/cm,

Left: 0.2 volt/cm, Right; 0.5 volt/cm

Figure 68 Pitot Pressure behind an Oblique Shock Wave.

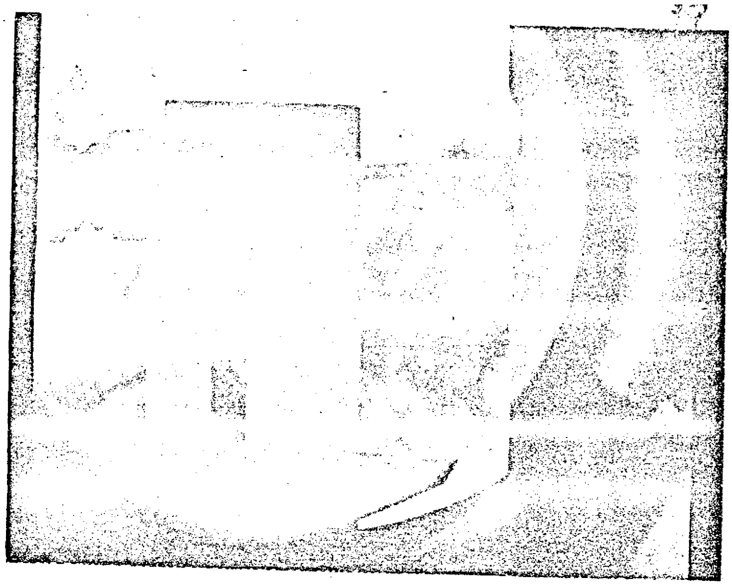

Interferogram at 5000 Angstrom Infinite Fringe

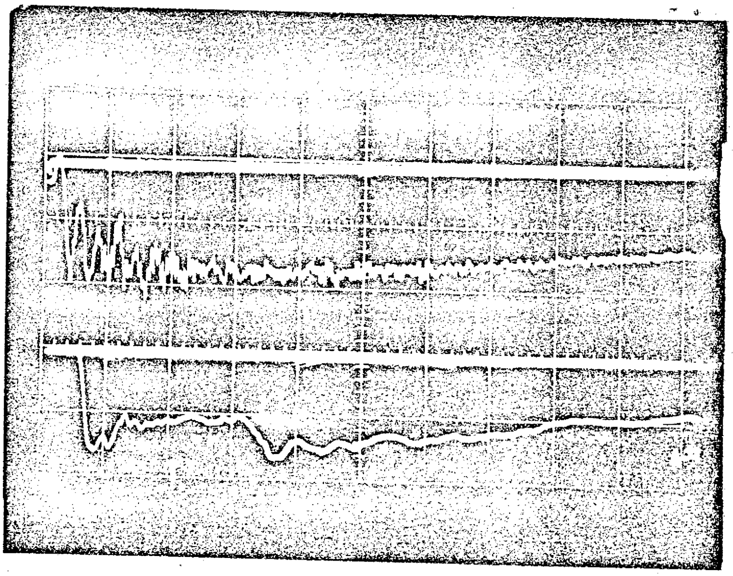

Initial Shock Tube Pressure = 4 in Hg of Air

Shock Tunnel: T.2 Nozzle: $\frac{1}{8}$ in Throat
7.5 Half Angle

Upper Trace: Nozzle Reservoir Pressure Transducer

Lower Trace: Pitot Pressure Probe, 0.5 volt/cm, 50 microsec/cm

Figure 69 Pitot Pressure in the Nozzle Boundary Layer

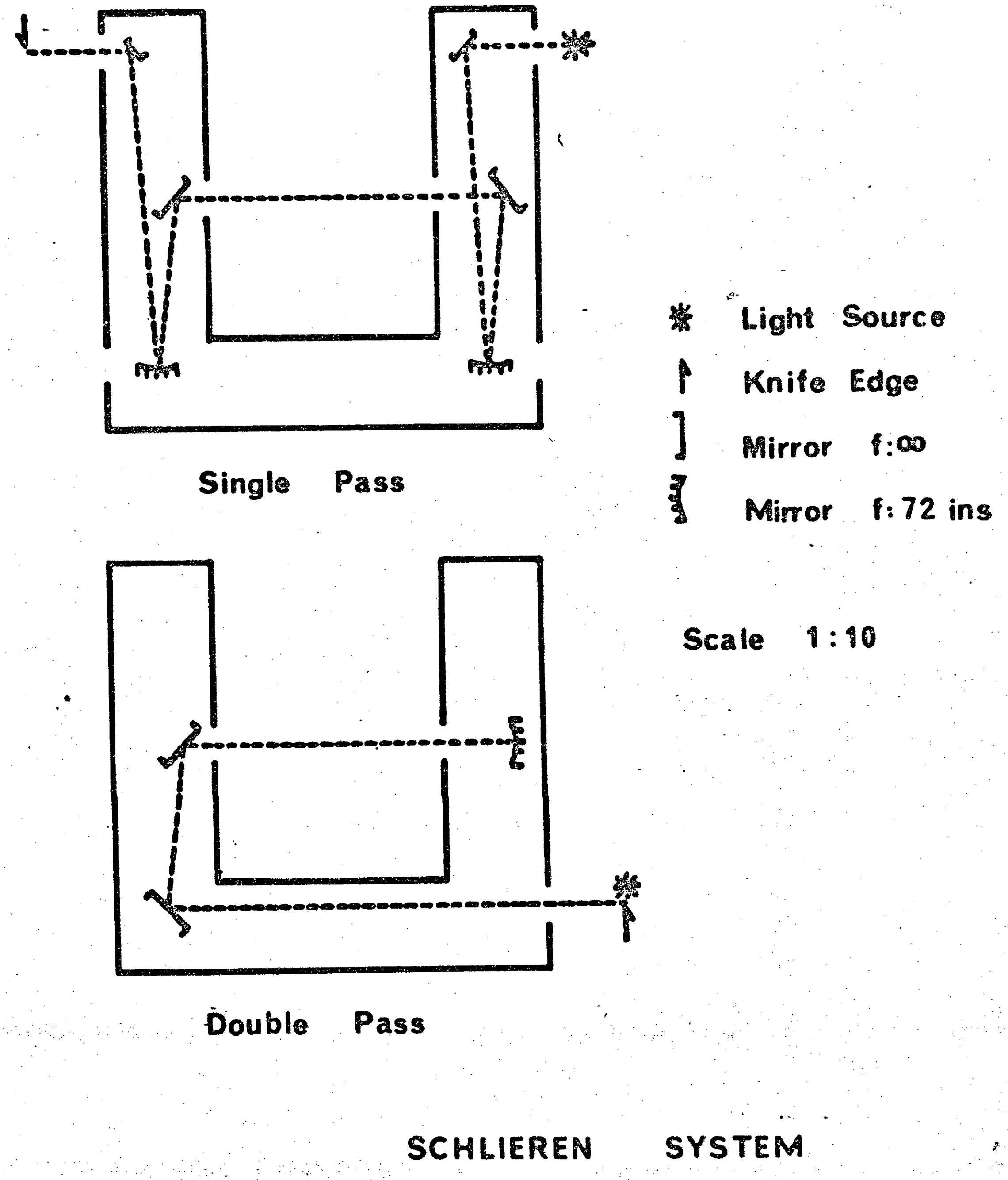

Figure No. 70 The Single or Double Pass Schlieren System

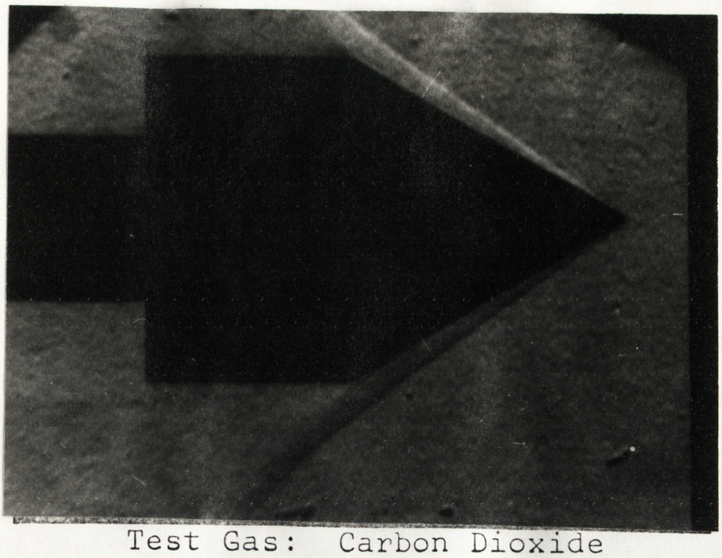

Filter: Wratten 35
Time = 125 μsec
Knife Edge: Horizontal

Test Gas: Carbon Dioxide
Initial Shock Tube Pressure = 5 in Hg
Nozzle: 1/8 in Throat
7.5° Half Angle
Model: 30° Included Angle Cone

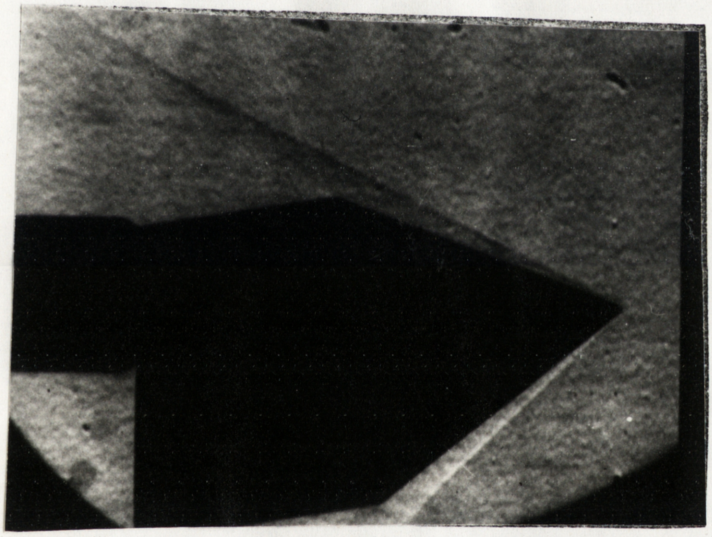

Filter: Wratten 35
Time = 125 μsec
Knife Edge: Horizontal

Test Gas: Carbon Dioxide
Initial Shock Tube Pressure = 5 in Hg
Nozzle: 1/8 in Throat
7.5° Half Angle
Model: 30° Included Angle Cone at 10° yaw

Figure No. 71 Schlieren Photographs in T.2

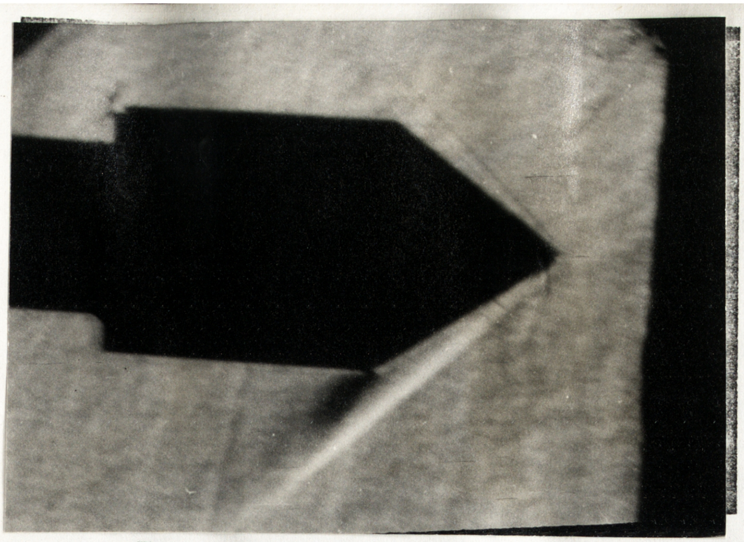

Double Pass System
(Proto type)
Filter: Wratten 47
Time = 150 μsec
Knife Edge: Parallel to Shock

Test Gas: Carbon Dioxide
Initial Shock Tube Pressure = 10 in Hg
Nozzle: 1/16 in Throat
7.5° Half Angle
Model: 35° Half Angle Wedge

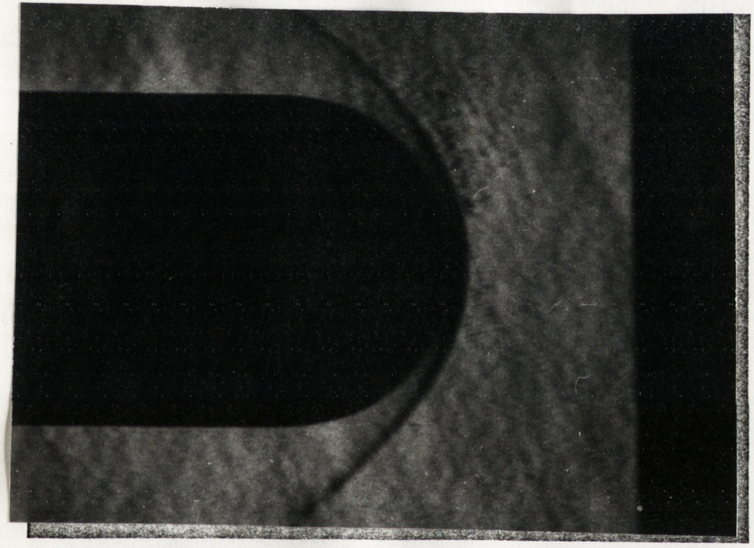

Single Pass System
Filter: Wratten 47
Time = 125 μsec
Knife Edge: Vertical

Test Gas: Carbon Dioxide
Initial Shock Tube Pressure = 6 in Hg
Nozzle: 1/8 in Throat
7.5° Half Angle
Model: Hemisphere Cylinder (R_b = 0.5 in)

Figure No. 71 (Contd)

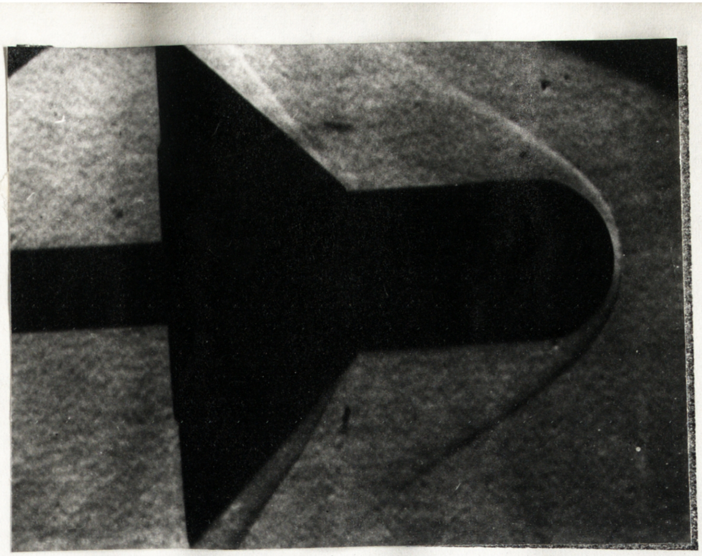

Filter: Wratten 47

Time: 125 μsec.

Knife Edge: Horizontal

Test Gas: Air

Initial Shock Tube Pressure = 5 in Hg

Nozzle: 1/8 in Throat
7.5^0 Half Angle

Model: Flanged Hemisphere Cylinder with Boundary Layer Bleed (R_b = 0.5 cm)

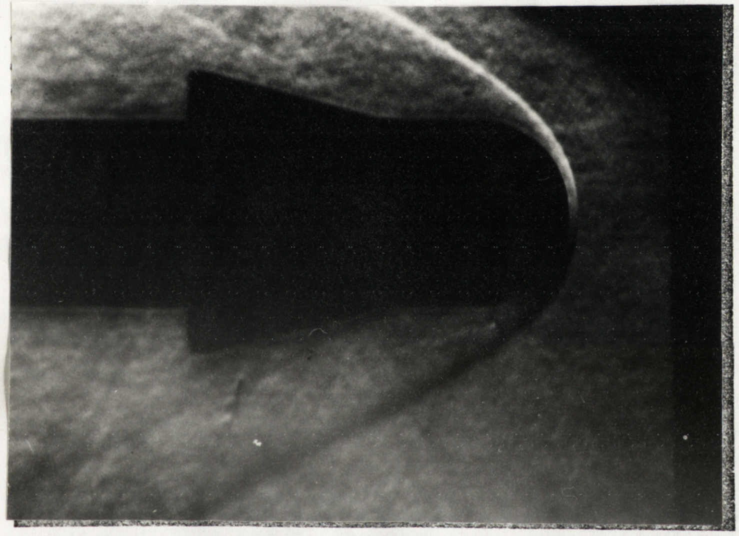

Filter: Wratten 47

Time = 125 μsec

Knife Edge: Horizontal

Test Gas: Carbon Dioxide

Initial Shock Tube Pressure = 6 in Hg

Nozzle: 1/8 in Throat
7.5^0 Half Angle

Model: Flanged Hemisphere Cylinder (R_b = 0.25 in Flare Angle = 15^0)

Figure No. 71 (Contd)

Double Pass System

Filter: Wratten 47

Time = 300 μsec

Knife Edge: Vertical

Test Gas: Nitrogen

Initial Shock Tube Pressure = 10 in Hg

Nozzle: 1/8 in Throat

15° Half Angle

Model: 45° Half Angle Wedge

Figure No. 71 (Contd)

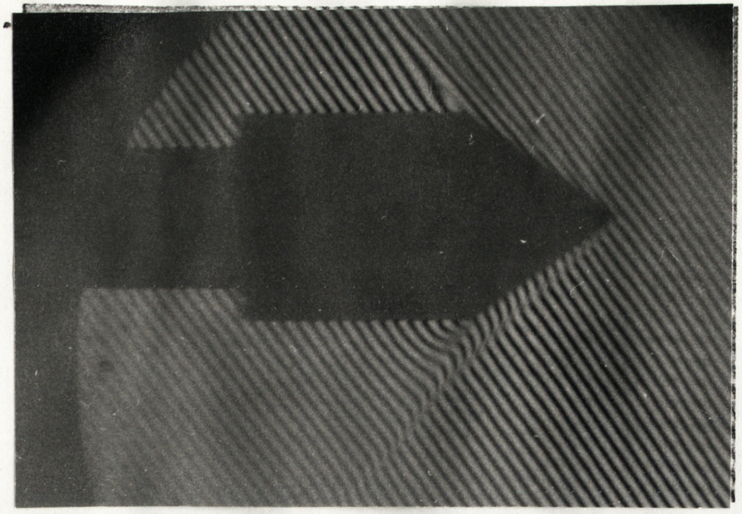

Filter: 4330 Å

Time = 150 μsec

Test Gas: Carbon Dioxide

Initial Shock Tube Pressure = 3 in Hg

Nozzle: 1/8 in Throat
7.5° Half Angle

Model: 35° Half Angle Wedge

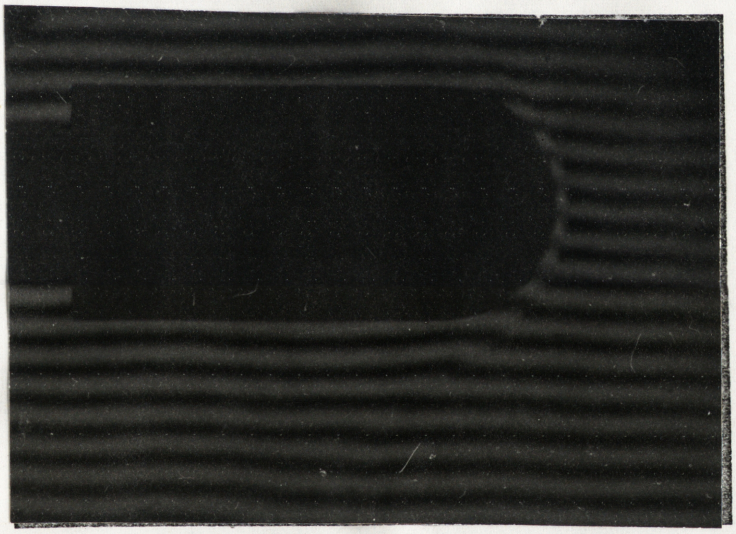

Filter: 4330 Å

Time = 130 μsec

Test Gas: Carbon Dioxide

Initial Shock Tube Pressure = 6 in Hg

Nozzle: 1/16 in Throat
7.5° Half Angle

Model: Hemisphere Cylinder (R_b = 0.5 in)

Figure No. 72 Mach Zehnder Interferograms in T.2

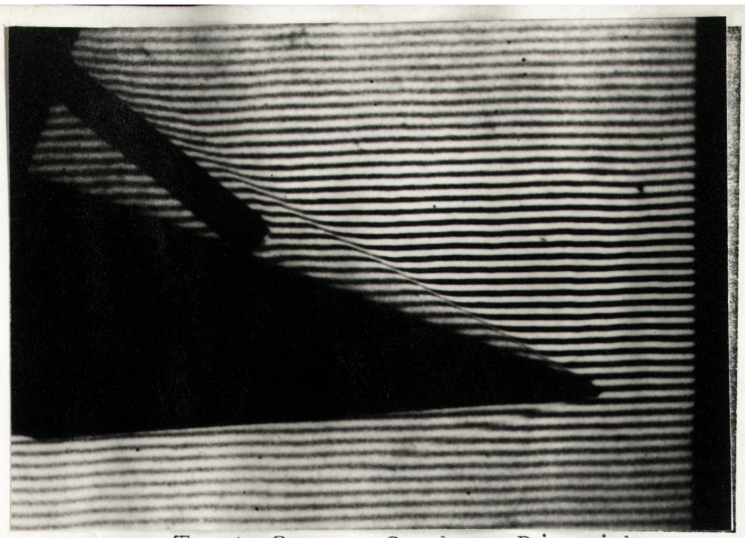

Filter: 4330 Å

Time = 75 μsec

Test Gas: Carbon Dioxide

Initial Shock Tube Pressure = 6 in Hg

Nozzle: 1/8 in Throat

7.5° Half Angle

Model: Wedge (20° Angle to Flow) with Pitot Probe

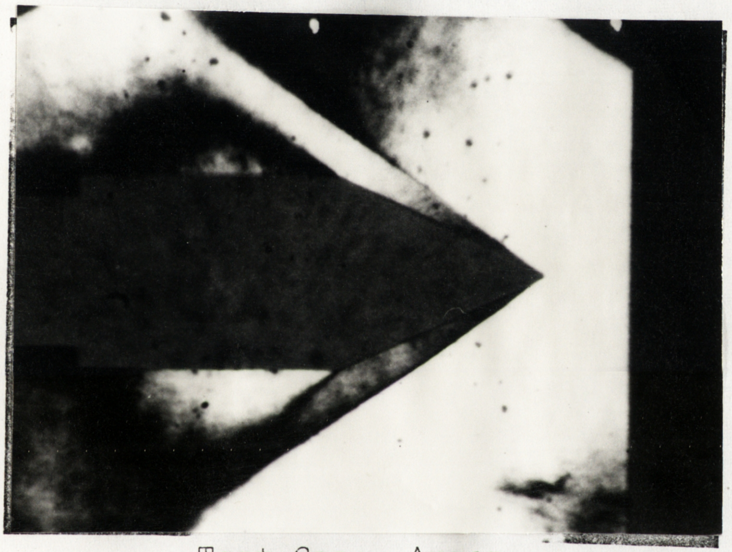

Infinite (Vertical) Fringes

Filter: None

Time: 175 μsec

Test Gas: Argon

Initial Shock Tube Pressure = 4 in Hg

Nozzle: 1/8 in Throat

7.5° Half Angle

Model: 25° Half Angle Wedge

Figure No. 72 (Contd)

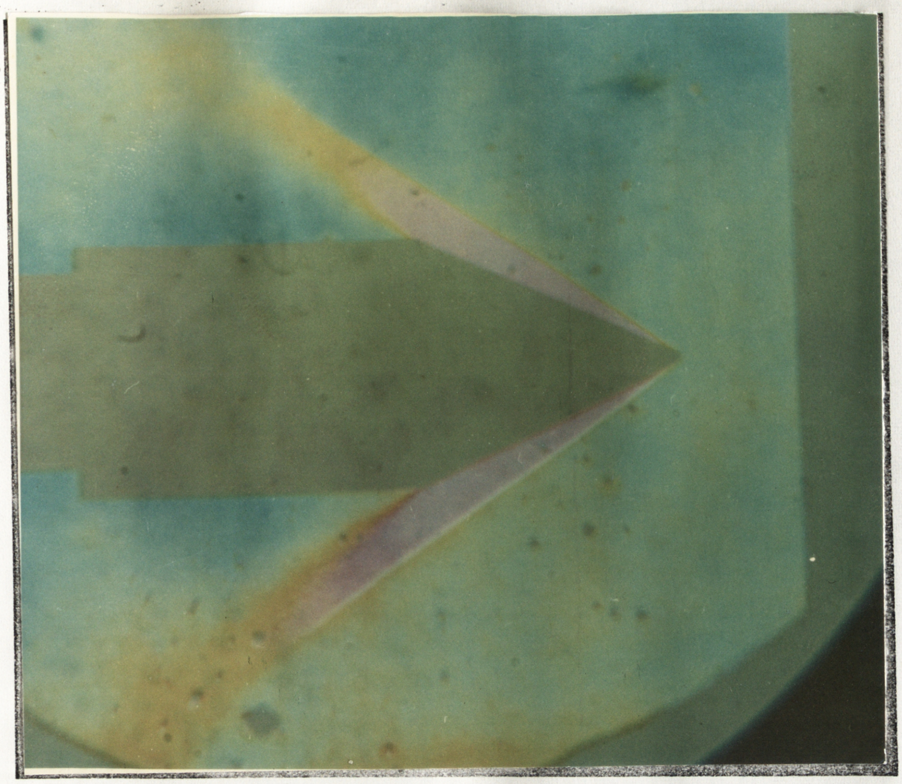

Infinite (Vertical) Fringes

No Filter

Xenon Flashtube Light Source

Time = 150 μsec

Test Gas: Air

Initial Shock Tube Pressure = 5 in Hg

Nozzle: 1/8 in Throat

7.5° Half Angle

Model: 25° Half Angle Wedge

Figure No. 72 (Contd)